N O T I C E

THIS DOCUMENT HAS BEEN REPRODUCED FROM MICROFICHE. ALTHOUGH IT IS RECOGNIZED THAT CERTAIN PORTIONS ARE ILLEGIBLE, IT IS BEING RELEASED IN THE INTEREST OF MAKING AVAILABLE AS MUCH INFORMATION AS POSSIBLE

NASA CR-135251

QUIET CLEAN SHORT-HAUL EXPERIMENTAL ENGINE (QCSEE)

Under-the-Wing (UTW) Engine Boilerplate Nacelle Test Report

VOLUME III

Mechanical Performance

DECEMBER 1977

by

Advanced Engineering and Technology Programs Department
GENERAL ELECTRIC COMPANY

(NASA-CR-135251) QUIET CLEAN SHORT-HAUL EXPERIMENTAL ENGINE (QCSEE). UNDER-THE-WING (UTW) ENGINE BOILERPLATE NACELLE TEST REPORT. VOLUME 3: MECHANICAL PERFORMANCE (General Electric Co.) 128 p HC A07/MF A01 G3/07 N80-15097 Unclas 33477

Prepared For

National Aeronautics and Space Administration

NASA Lewis Research Center
NAS3-18021

1. Report No.	2. Government Accession No.	3. Recipient's Catalog No.
NASA CR-135251		

4. Title and Subtitle	5. Report Date
QCSEE UNDER-THE-WING (UTW) ENGINE BOILERPLATE NACELLE TEST REPORT - VOLUME III, MECHANICAL PERFORMANCE	December 31, 1977
	6. Performing Organization Code
7. Author(s) Advanced Engineering and Technology Programs Department Group Engineering Division	8. Performing Organization Report No. R77AEG212-3
	10. Work Unit No.
9. Performing Organization Name and Address General Electric Company Aircraft Engine Group Cincinnati, Ohio 45215	11. Contract or Grant No. NAS3-18021
	13. Type of Report and Period Covered Contractor Report
12. Sponsoring Agency Name and Address National Aeronautics and Space Administration Washington, D.C. 20546	14. Sponsoring Agency Code

15. Supplementary Notes

Experimental Report, Project Manager, C.C. Ciepluch, QCSEE Project Office
Technical Adviser, N.E. Samanich, NASA-Lewis Research Center, Cleveland, Ohio 44135

16. Abstract

The Quiet Clean Short-Haul Experimental Engine (QCSEE) Program includes the design and testing of high bypass geared turbofan engines with nacelles forming the propulsion systems for short-haul passenger aircraft. These flight systems contain the technology required for externally blown-flap-type aircraft for introduction into passenger service in the 1980's.

This report covers the initial phase of testing of the Under-the-Wing (UTW) engine and boilerplate nacelle components. The report consists of three volumes and an appendix as follows:

Volume I -	Summary Report	CR-135249
Volume II -	Aerodynamics and Performance	CR-135250
Volume III -	Mechanical Performance	CR-135251
Appendix -	Detailed Engine Performance	CR-For Government Use Only

17. Key Words (Suggested by Author(s))

Aircraft Propulsion Power
Integrated Engine/Nacelle Structure
Variable-Pitch Fans
Propulsion System Testing

19. Security Classif. (of this report)	20. Security Classif. (of this page)	21. No. of Pages	22. Price*
UNCLASSIFIED	UNCLASSIFIED	128	

*For sale by the National Technical Information Service, Springfield, Virginia 22151

NASA-C-168 (Rev. 6-71)

TABLE OF CONTENTS

Section		Page
1.0	SUMMARY	1
	1.1 System Dynamics	1
	1.2 Composite Fan Blades	1
	1.3 Reduction Gear	1
	1.4 Lube and Accessory Drive System	1
	1.5 Fan Frame	2
	1.6 Inlet	2
	1.7 Core Cowl Cooling	2
	1.8 Fan Exhaust Nozzle	2
	1.9 Digital Control System	3
2.0	INTRODUCTION	4
3.0	SYSTEM DYNAMICS	5
4.0	COMPOSITE FAN BLADES	8
	4.1 Blade Description	8
	4.2 Pretest Predictions	10
	4.3 Blade Instrumentation and Scope Limits	19
	4.4 Test Results	23
	4.5 Conclusions	34
5.0	MAIN REDUCTION GEAR	36
	5.1 Test Results	36
	5.2 Posttest Inspection	36
	5.2.1 Gears	36
	5.2.2 Bearings	41
6.0	LUBRICATION AND ACCESSORY DRIVE SYSTEM	44
	6.1 System Description	44
	6.2 Instrumentation	44
	6.3 Test Experience	45
	6.3.1 Main Shaft Bearings	45
	6.3.2 Lube Supply and Scavenge System	49
	6.3.3 Engine Heat Rejection	49
	6.3.4 Lube System Problems	53
	6.3.5 Posttest Inspection	55
7.0	FAN FRAME	56

PRECEDING PAGE BLANK NOT FILMED

TABLE OF CONTENTS (Concluded)

Section		Page
8.0	NACELLE COMPONENTS	62
	8.1 Inlet	62
	8.2 Core Cowl Cooling	62
	8.3 Fan Exhaust Nozzle	64
9.0	DIGITAL CONTROL SYSTEM	70
	9.1 General System Description	70
	9.2 Manual Control Modes	76
	9.3 Failure Detection and Correction	80
	9.4 Monitoring Control and Engine Variables	81
	9.5 Fan Pitch Angle (β_F) and Fan Exhaust Nozzle Calibration	81
	9.5.1 Fan Pitch Angle Calibration	81
	9.5.2 Fan Exhaust Nozzle (A18) Calibration	82
	9.6 Engine/Control System Testing	87
	9.6.1 Fuel Control System	87
	9.6.2 Nozzle Control System	97
	9.6.3 Fan Pitch Control System	102
10.0	VARIABLE-PITCH ACTUATION SYSTEM	111
	10.1 Engine Test Results	111
	10.2 Discussion of Test Results	111
11.0	REFERENCES	119

LIST OF ILLUSTRATIONS

Figure		Page
1.	QCSEE UTW Composite Blade with Platform.	9
2.	Platform Construction.	11
3.	Composite Blade Configuration.	12
4.	Calculated Blade Radial Stress.	13
5.	Calculated Blade Relative Radial Stresses for First Flexural Mode.	14
6.	Calculated Blade Relative Radial Stresses for Second Flexural Mode.	15
7.	Calculated Blade Relative Radial Stresses for First Torsional Mode.	16
8.	Fatigue S-N Curve for QCSEE Blade.	17
9.	Allowable Stress-Range Diagram, Blade Radial Stress.	18
10.	Locations of Fan Blade Instrumentation.	20
11.	Locations of Fan Blade Instrumentation.	21
12.	Locations of Fan Blade Instrumentation.	22
13.	Steady-State Stresses, Forward Mode.	26
14.	Steady-State Stresses, Reverse Mode.	27
15.	Campbell Diagram.	29
16.	Dynamic Stress Response.	33
17.	Main Reduction Gear Configuration.	37
18.	Dynamic Ring Gear Stress Response.	39
19.	Ring Gear Allowable Stress.	40
20.	QCSEE UTW Bearing Inner Race Skidding Distress.	42
21.	QCSEE UTW Outer Race Debris Damage.	43

LIST OF ILLUSTRATIONS (Continued)

Figure		Page
22.	Outer Race Temperature Versus Fan Speed.	46
23.	Outer Race Temperature Versus LP Turbine Speed.	47
24.	Outer Race Temperature Versus Core Speed.	48
25.	Lube Supply Pressure Versus Core Speed.	50
26.	Lube Scavenge Pressure Versus Core Speed.	51
27.	Engine Heat Rejection Versus Fan Speed.	52
28.	Heat Rejection Data.	54
29.	Strain Gage Locations for UTW Fan Frame, Mount Area.	57
30.	Strain Gage Locations for UTW Fan Frame, Bypass Vanes.	58
31.	Natural Frequencies of QCSEE Bypass Vanes.	59
32.	Inlet Decoupling Joint.	62
33.	Core Cowl Assembly and Cooling Air System.	65
34.	Flare Nozzle Flap Schematic.	67
35.	Fan Nozzle Mounting Ring Installations.	68
36.	System Interconnection Schematic.	71
37.	Digital Control Photograph.	72
38.	Control Room Elements of QCSEE Digital Control.	74
39.	Sensed Engine and Control Variables.	75
40.	Manual Fuel Control System.	77
41.	β_F Manual Control System.	78
42.	A18 Manual Control System.	79
43.	β_F Position Versus Demand Potentiometer Setting.	83
44.	Fan Pitch Angle Versus Digital Readout.	84

LIST OF ILLUSTRATIONS (Continued)

Figure		Page
45.	Fan Nozzle Area Versus Demand Potentiometer Setting.	85
46.	Fan Nozzle Area Versus Digital Readout.	86
47.	QCSEE UTW Typical Start.	88
48.	Core Idle Speed Ranges.	89
49.	Fan Speed Versus Power Demand.	90
50.	QCSEE UTW Power Change, Idle to 12,000 RPM.	91
51.	T41C Calculated Temperature Comparison.	94
52.	Fuel Flow Comparison.	95
53.	QCSEE UTW Core Stator Schedule.	96
54.	Fan Nozzle Closure on Start.	98
55.	QCSEE UTW Fan Nozzle Oscillations.	99
56.	Experimental Mach Number Data.	100
57.	Inlet Mach Number Comparison.	101
58.	Inlet Mach Number Variation.	103
59.	Fan Nozzle Load Data.	104
60.	Fan Pitch Movement in Forward.	105
61.	Fan Pitch Closure.	109
62.	Fan Pitch Closure.	110
63.	QCSEE UTW Build 1 Variable-Pitch Actuation System.	112
64.	Spherical Cam Gear Ratio Effect.	113
65.	Breakaway Motor Pressure Drops.	114
66.	Hydraulic Motor Pressure Drop Versus Torque Motor Current.	115

LIST OF ILLUSTRATIONS (Concluded)

Figure		Page
67.	Description of V-P Mechanism Used in Analysis.	117
68.	Predicted UTW Blade Loads.	118

LIST OF TABLES

Table		Page
1.	Maximum Synchronous Vibration Response for QCSEE UTW Engine Accelerometers.	6
2.	Typical Steady-State Fan Synchronous Vibration Response for QCSEE UTW Engine Accelerometers.	7
3.	UTW Fan Blade Scope Limits.	24
4.	Dynamic Stress Wind Effect.	31
5.	UTW Reduction Gear Design Details.	38
6.	Engine Heat Rejection.	49
7.	Comparison of Turbine Temperature Calculations.	93
8.	Comparison of Set and Measured Fan Pitch Angles.	106
9.	Fan Pitch Control System Problems.	107

1.0 SUMMARY

Approximately 50 hours of engine operation were completed on the initial buildup of the QCSEE UTW engine. In addition to aeroperformance mapping, a great deal of operational experience was acquired with the many new technology elements of the propulsion system. Mechanical observations and problems encountered during Buildup No. 1 testing are summarized as follows:

1.1 SYSTEM DYNAMICS

The overall vibratory response of the UTW propulsion system was found to be within acceptable limits for normal engine operation. Low pressure rotor synchronous response in the subidle region was higher than predicted, necessitating avoidance of steady-state operation at certain speeds.

1.2 COMPOSITE FAN BLADES

The natural frequencies and steady-state levels measured during engine test agreed closely with predicted values. Dynamic stress levels exceeded scope limits on several occasions. These instances were associated with the region of first-flex 2/rev crossover and were sensitive to crosswind. By avoiding steady-state operation in the critical speed range, the blades were satisfactory for ground testing. However, further development and design modification of the composite blades are required to make them fully operational.

1.3 REDUCTION GEAR

The UTW main reduction gear operated very satisfactorily throughout the test. Measured stresses and bearing temperatures remained within established limits at all times. Posttest inspection revealed that the gears were in excellent condition. Star gear bearings showed minor distress from debris damage and evidence of skidding on two of the inner races. All parts were judged suitable for further service.

1.4 LUBE AND ACCESSORY DRIVE SYSTEM

Initial testing was delayed by oil leakage from several areas of the composite frame sump. To permit testing to continue, a shop air-powered eductor was employed to reduce the sump pressure slightly below ambient. The eductor was connected to the air-oil separator on the accessory gearbox. Although not fully understood at the time, the eductor drew air upward through the AGB scavenge tubes, interfering with normal oil scavenging. In addition, the original design of gear baffles was less than optimum, with a result that the AGB was flooded with oil, causing excessive temperatures. An additional

scavenge pickup tube was added to the AGB with an external pump to return the scavenge oil to the tank. This setup was used for the remainder of Buildup No. 1 testing. Rig testing has now demonstrated that the gearbox will scavenge satisfactorily for future testing with proper baffles and without the eductor.

1.5 FAN FRAME

Leakage problems were encountered during buildup in the fan frame sump region. These problems were associated with penetrations into the composite sump wall by metal lube and instrumentation tubes. The leaks were stopped by coating the inside of the sump with Dow Corning DC 94-009 fluorosilicone rubber.

During engine test, an oil leak developed from an inaccessible area of the scavenge duct due to a tear in the coating. This leak allowed oil to get into the six o'clock core strut and thence into the fan flowpath. The leak was stopped by filling the core struts and splitter leading edge cavity with Furane 9210 adhesive.

No structural or stress problems were encountered with the composite fan frame.

1.6 INLET

Cracks in some of the attachment bosses in the hardwall insert panels immediately in front of the fan occurred during the test. This failure was attributed to a combination of poor fit-up of the panels, inadequate welds retaining the mounting bosses in the boilerplate adapter, and a hostile vibratory environment. Replacement panels were made of solid aluminum, replacing the original honeycomb panels, and the adapter was weld-repaired to allow continued testing.

1.7 CORE COWL COOLING

The boilerplate core cowl was cooled with shop air, and thermocouple data verified that temperatures were consistent with design values.

1.8 FAN EXHAUST NOZZLE

During initial reverse thrust testing, the fan exhaust nozzle mounting ring failed. This ring was a graphite/epoxy composite channel to which the nozzle flap hinges were mounted. The ring was designed to be bonded to the inner and outer skins of the composite fan cowl doors; however, in the boilerplate installation, the ring halves were bolted to the cowl doors.

The failure consisted of the ring quadrant holding the lower-right nozzle flap pulling loose from the cowl door and permitting the flap and associated

hardware to be ingested by the engine. Secondary damage resulted to all fan blades, the fan frame, and several acoustic panels.

The primary cause of the failure was an inadequately designed bolted joint having insufficient bearing and shear area under the bolt heads. The failure resulted in premature termination of Buildup No. 1 testing.

1.9 DIGITAL CONTROL SYSTEM

All engine testing was done in the manual-control mode, in which the operator commanded fan speed (fuel flow), fan pitch, and fan exhaust nozzle area. These variables were controlled accurately and stably. Safety overrides were also demonstrated, limiting T41C and core speed.

Several nuisance problems were encountered in setting the fan pitch. The most troublesome of these was occasional unplanned closure of the fan blades to the limit switch setting (+14°). The cause has not yet been definitely established but is believed to be a fault in the analog-to-digital multiplexer. The control modules will be modified to correct this problem prior to further testing.

2.0 INTRODUCTION

The General Electric Company currently is engaged in the Quiet, Clean, Short-Haul Experimental Engine Program (QCSEE) under Contract NAS3-18021 to the NASA Lewis Research Center. The under-the-wing (UTW) experimental engine was designed and built under the program to develop and demonstrate technology applicable to engines for future commercial shorthaul turbofan aircraft.

The initial buildup of the UTW engine and boilerplate nacelle was tested at General Electric, Peebles, Ohio Outdoor Test Site 4D during the period from September 2 through December 17, 1976. Initial testing included a mechanical and systems checkout with hardwall acoustic panels and a bellmouth inlet. Performance data were then taken over a range of speeds, exhaust nozzle areas, and fan blade angles. This phase of testing provided data in the range of takeoff and approach operating conditions to explore "uninstalled" performance with minimal loss of ram recovery. In addition, fan performance characteristics were mapped over a limited range of blade settings.

The inlet then was changed to the boilerplate high Mach number design to investigate installed performance with real ram recovery losses. Points were repeated at takeoff and approach operating conditions.

Initial reverse thrust testing was attempted by transitioning the blades to the reverse setting (through stall pitch) while motoring on the starter. The engine then was fired in the reverse mode and operated to higher speeds. During this phase of testing, the exhaust nozzle support ring failed, allowing one nozzle flap and associated hardware to be ingested by the engine. This failure resulted in a premature conclusion of the test before much of the desired reverse mode and acoustic data could be acquired.

This volume of the propulsion system test report includes a detailed discussion of mechanical performance of the engine with emphasis on the advanced technology components.

3.0 SYSTEM DYNAMICS

The overall vibration response characteristics of the QCSEE UTW engine were found to be within acceptable limits for normal engine operation. Twenty vibration sensors were used to measure the engine response.

The synchronous vibration levels for both the LP and HP rotor activities were very low. In general, the levels were less than 0.00254 cm (1 mil) double amplitude (DA), which is consistent with the predicted system behavior. This indicates that the LP and HP rotor systems were well-balanced.

The fan synchronous vibration levels also were low for most of the fan operating range. However, the near-idle fan activity was higher than expected. In particular, the horizontal pickup for the No. 2 bearing housing (front bearing for the LP shaft) had 0.0216 cm (8.5 mils) DA fan 1/rev at 1300 rpm. In addition, the reduction gear horizontal sensor had 0.0188 cm (7.4 mils) DA fan 1/rev at 1800 rpm. The fan synchronous vibration levels for the other sensors generally were less than 0.0102 cm (4 mils) DA for the normal operating range (see Table 1).

It should be emphasized that Table 1 is a compilation of the maximum levels experienced for all the testing. It includes peak values recorded during transient as well as steady-state levels. Presented in Table 2 is a list of some typical 1/rev fan synchronous vibration readings which indicate lower levels at certain steady-state conditions.

Table 1. Maximum Synchronous Vibration Response for QCSEE UTW Engine Accelerometers.

Vibration Sensor	Fan Maximum Response cm	Fan Maximum Response (mils-DA)	Fan Speed rpm	LP System Maximum Response cm	LP System Maximum Response (mils-DA)	LP System Speed rpm	HP System Maximum Response cm	HP System Maximum Response (mils-DA)	HP System Speed rpm
Fan Cowl	0.0056	(2.2)	1800	0.0010	(0.4)	7200	0.0003	(0.1)	12300
Slip Ring	0.0178	(7.0)	3100	0.0051	(2.0)	4600	0.0038	(1.5)	11600
Fan Frame-V	0.0071	(2.8)	2700	0.0005	(0.2)	6000	0.0018	(0.7)	11300
Fan Frame-H	0.0089	(3.5)	2700	0.0012	(0.5)	7200	0.0025	(1.0)	11600
No. 1 Brg.-V	0.0086	(3.4)	2900	0.0008	(0.3)	7300	0.0008	(0.3)	11400
No. 1 Brg.-H	0.0056	(2.2)	2200	0.0008	(0.3)	7300	0.0010	(0.4)	11600
No. 2 Brg.-V	0.0102	(4.0)	1550	0.0008	(0.3)	4600	0.0010	(0.4)	11000
No. 2 Brg.-H	0.0216	(8.5)	1300	0.0020	(0.8)	3400	0.0012	(0.5)	10700
No. 3 Brg.-V	0.0051	(2.0)	2900	0.0008	(0.3)	4600	0.0005	(0.2)	11500
No. 3 Brg.-H	0.0102	(4.0)	2900	0.0012	(0.5)	7500	0.0005	(0.2)	11500
Red. Gear-V	0.0112	(4.4)	1800	0.0015	(0.6)	7300	0.0008	(0.3)	11600
Red. Gear-H	0.0188	(7.4)	1800	0.0025	(1.0)	4700	0.0008	(1.0)	11600
Comp. Stator Aft Flange-Y	0.0061	(2.4)	3000	0.0020	(0.8)	7300	0.0025	(1.0)	12600
Comp. Stator Aft Flange-H	0.0081	(3.2)	3000	0.0012	(0.5)	7200	0.0012	(0.5)	12600
No. 5 Brg.-V	0.0056	(2.2)	2900	0.0015	(0.6)	7300	0.0030	(1.2)	12600
No. 5 Brg.-H	0.0089	(3.5)	1500	0.0010	(0.4)	7100	0.0036	(1.4)	10900
Exhaust Cone	0.0048	(1.9)	2900	0.0008	(0.3)	7100	0.0015	(0.6)	11600
Accessory Gearbox-A	0.0064	(2.5)	2300	0.0010	(0.4)	7300	0.0033	(1.3)	11100
Accessory Gearbox-H	0.0053	(2.1)	1900	0.0008	(0.3)	5400	0.0012	(0.5)	11600
Digital Control	0.0081	(3.2)	2500	0.0012	(0.5)	7100	0.0015	(0.6)	11600

Table 2. Typical Steady-State Fan Synchronous Vibration Response for QCSEE UTW Engine Accelerometers.

Vibration Pickup	Steady-State Fan Speed (rpm) 1473 cm	1473 (mils-DA)	1945 cm	1945 (mils-DA)	2090 cm	2090 (mils-DA)	2580 cm	2580 (mils-DA)	2845 cm	2845 (mils-DA)	3054 cm	3054 (mils-DA)	3103 cm	3103 (mils-DA)
Fan Cowl	0.0020	(0.8)	0.0051	(2.0)	0.0051	(2.0)	0.0015	(0.6)	0.0015	(0.6)	0.0051	(2.0)	0.0028	(1.1)
Slip Ring	0.0081	(3.2)	0.0033	(1.3)	0.0033	(1.3)	0.0076	(3.0)	0.0015	(0.6)	0.0081	(3.2)	0.0178	(7.0)
Fan Frame-V	0.0023	(0.9)	0.0008	(0.3)	0.0018	(0.7)	0.0051	(2.0)	---	---	---	---	---	---
Fan Frame-H	---	---	0.0020	(0.8)	0.0056	(2.2)	0.0056	(2.2)	0.0025	(1.0)	0.0023	(0.9)	0.0081	(3.2)
No. 1 Brg.-V	0.0036	(1.4)	0.0023	(0.9)	0.0010	(0.4)	0.0036	(1.4)	0.0041	(1.6)	0.0029	(1.1)	0.0020	(0.8)
No. 1 Brg.-H	0.0015	(0.6)	0.0003	(0.1)	0.0023	(0.9)	0.0025	(1.0)	0.0028	(1.1)	0.0041	(1.6)	0.0033	(1.3)
No. 2 Brg.-V	0.0036	(1.4)	0.0041	(1.6)	0.0056	(2.2)	0.0036	(1.4)	0.0015	(0.6)	0.0033	(1.3)	0.0025	(1.0)
No. 2 Brg.-H	0.0112	(4.4)	0.0023	(0.9)	0.0102	(4.0)	0.0033	(1.3)	0.0028	(1.1)	0.0069	(2.7)	0.0018	(0.7)
No. 3 Brg.-V	0.0015	(0.6)	0.0015	(0.6)	0.0010	(0.4)	0.0023	(0.9)	0.0015	(0.6)	0.0013	(0.5)	---	---
No. 3 Brg.-H	0.0015	(0.6)	0.0015	(0.6)	0.0028	(1.1)	0.0033	(1.3)	0.0028	(1.1)	0.0033	(1.3)	0.0018	(0.7)
Red. Gear-V	0.0036	(1.4)	0.0010	(0.4)	0.0015	(0.6)	0.0013	(0.5)	0.0036	(1.4)	0.0071	(2.8)	0.0033	(1.3)
Red. Gear-H	0.0018	(0.7)	0.0018	(0.7)	0.0051	(2.0)	0.0020	(0.8)	0.0036	(1.4)	0.0056	(2.2)	0.0058	(2.3)
Comp. Stator Aft Flange-V	0.0005	(0.2)	0.0013	(0.5)	0.0005	(0.2)	0.0025	(1.0)	0.0015	(0.6)	0.0020	(0.8)	0.0013	(0.5)
Comp. Stator Aft Flange-H	0.0005	(0.2)	0.0015	(0.6)	0.0013	(0.5)	0.0015	(0.6)	0.0020	(0.8)	0.0056	(2.2)	0.0020	(0.8)
No. 5 Brg.-V	0.0003	(0.1)	0.0003	(0.1)	0.0008	(0.3)	0.0008	(0.3)	0.0023	(0.9)	0.0015	(0.6)	0.0023	(0.9)
No. 5 Brg.-H	0.0028	(1.1)	0.0010	(0.4)	0.0041	(1.6)	0.0023	(0.9)	0.0015	(0.6)	0.0033	(1.3)	0.0018	(0.7)
Exhaust Cone	0.0025	(1.0)	0.0008	(0.3)	0.0028	(1.1)	0.0023	(0.9)	0.0015	(0.6)	0.0041	(1.6)	---	---
Accessory Gearbox-A	0.0003	(0.1)	0.0023	(0.9)	0.0028	(1.1)	0.0033	(1.3)	0.0036	(1.4)	0.0041	(1.6)	---	---
Accessory Gearbox-H	0.0015	(0.6)	0.0020	(0.8)	0.0018	(0.7)	0.0028	(1.1)	0.0023	(0.9)	---	---	0.0023	(0.9)
Digital Control	---	---	0.0038	(1.5)	0.0023	(0.9)	0.0025	(1.0)	0.0041	(1.6)	---	---	0.0003	(0.1)

4.0 COMPOSITE FAN BLADES

4.1 BLADE DESCRIPTION

The blades incorporated in the UTW fan rotor are a variable-pitch design that offers full reverse thrust capability. The design includes 18 composite fan blades fabricated from a hybrid combination of Kevlar 49, AS graphite, boron, and S-glass fibers in a PR288 epoxy resin matrix. The blades incorporate a metal leading edge to provide FOD (foreign object damage) and erosion protection. Solidity of the blade airfoil is 0.95 at the OD and 0.98 at the ID, permitting rotation of the blades into the reverse thrust mode of operation through both the flat-pitch and stall-pitch directions. A spherical casing radius and a spherical blade tip provide close blade tip clearances throughout the range of blade pitch angle settings. Each blade is attached by a dovetail to a rotor trunnion at the blade's root. The trunnions are retained in the disk by ball bearings. Retainer straps, attached to the trunnion, lock the blade in axial position and resist trunnion opening deflections under blade centrifugal loading.

Design requirements for the UTW composite fan blade were established to provide realistic long-life operation of a flight engine. Design details are provided in Reference 1. Results of bench and whirligig testing showing that the blades have satisfactory margins for the structural and aeromechanical requirements of the engine are provided in Reference 2.

The finished composite fan blade is shown in Figure 1. It consists of a molded composite blade, a molded composite platform, and a metal outsert on the dovetail. The blade is made up of a solid composite airfoil and a straight bell-shaped composite dovetail. The blade has a reduced leading edge thickness to allow a final coating of wire mesh/nickel plate for leading edge protection within the final aerodynamic contour. The dovetail is undercut at the leading and trailing edges to permit better transitioning of the cambered airfoil section into the straight dovetail to match the rotor trunnion configuration.

The blade is made up of 0.25-mm (0.010-in.) plies of Kevlar 49, AS graphite, boron, and S-glass fibers impregnated with PR288 epoxy resin. The S-glass plies are placed near the surface in the lower region of the blade to provide high tensile strength and high strain-to-failure characteristics for flexural loading. Boron and graphite torsional stiffening plies in the airfoil region of the blade are oriented at ±45° to provide the shear modulus required for a high first-torsional frequency. The boron plies are placed toward the outer surface and graphite in the inner regions. Plies of Kevlar 49 are interspersed throughout the blade with the majority of them being oriented with their fibers in the longitudinal direction of the blade. Several Kevlar 49 plies in the tip region of the blade are oriented at 90° to the longitudinal axis to provide chordwise strength and stiffness to the blade. All airfoil plies extend continuously down into the dovetail and are

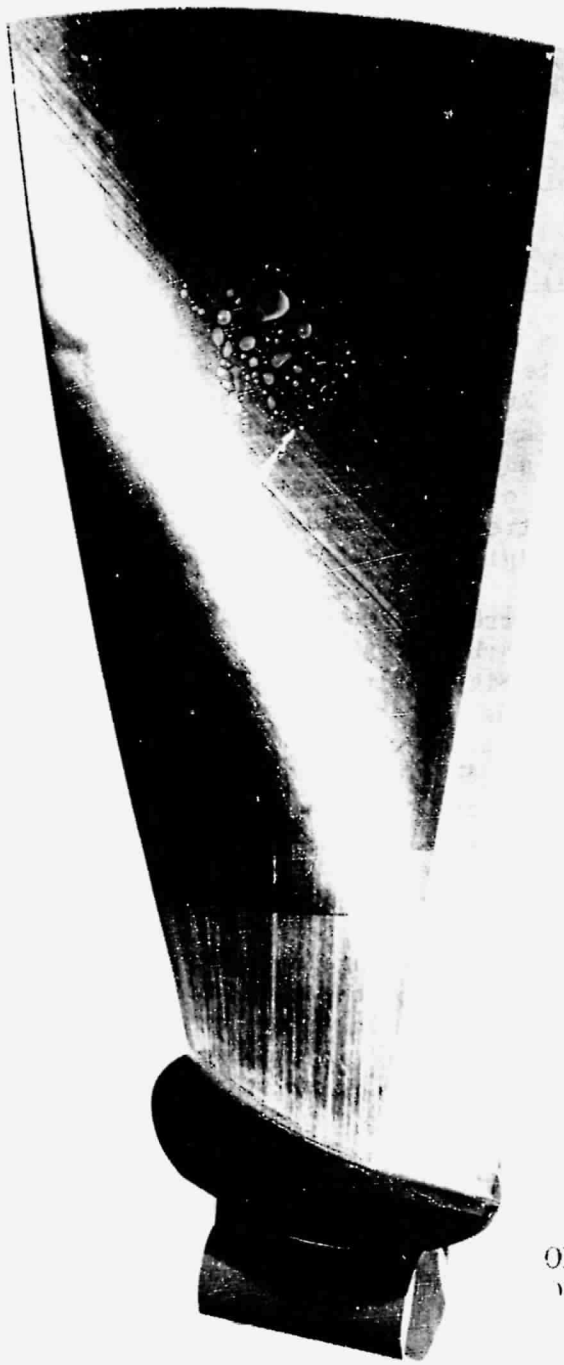

ORIGINAL PAGE IS
OF POOR QUALITY

Figure 1. QCSEE UTW Composite Blade with Platform (C76011062).

REPRODUCIBILITY OF THE
ORIGINAL PAGE IS POOR

interspersed with insert plies which act to fill out the enlarged dovetail cross section.

The composite platform is a tapered beam, cantilevered from the blade root, and consists of a honeycomb core stabilized by upper and lower graphite/epoxy face sheets. The platform is molded and bonded in place on the blade forming a one-piece structure. Structural plies extend around the blade root leading and trailing edge undercuts, entrapping the platform beneath the airfoil overhangs. The platform construction is shown in Figure 2, and the overall blade dimensions and configuration are shown in Figure 3.

4.2 PRETEST PREDICTIONS

The blade stress and vibratory characteristics were determined from a three-dimension finite-element analysis, blade bench testing, and single-blade spin testing. Figure 4 is a map of calculated radial steady-state stresses for the concave and convex blade faces, and Figures 5, 6, and 7 show calculated relative radial stresses over the blade for the first three vibratory modes. The maps of relative radial stresses under vibratory conditions show the changes in stress locations for the different vibratory modes. Blade bench and whirligig test data agreed closely with these predictions.

Blade vibratory strengths were determined from specimen and QCSEE blade tests and are shown on the fatigue S-N curve (Figure 8), and the fatigue stress-range diagram (Figure 9). The fatigue S-N curve shows the maximum blade stress for various numbers of flexural cycles that will cause the blade to initiate delamination and cause loss of blade frequency. The upper curve gives the minimum strength of the composite material based on flat specimen, axial-axial fatigue testing. The allowable blade fatigue strength was based on the material minimum-strength curve and blade high-cycle-fatigue test data. It includes allowance for three standard deviations of strength property variation. The lower curve defines the stress limits for engine testing and was determined using various factors which are discussed under "scope limits". The fatigue stress-range diagram shows the allowable radial alternating stress as a function of the blade mean stress. The allowable stress levels for this curve were selected as the point on the S-N curve for allowable blade stress where no loss in frequency would occur after 1,000,000 flexural cycles with allowance for 3 standard deviations of material property variation. Measured strains in the blade radial (spanwise) direction along with a material modulus of elasticity of 6.9×10^6 N/cm^2 (10×10^6 psi), were used to calculate all stresses and strengths. This approach provided a consistent basis for setting scope limits, gage monitoring, and comparing stresses during the various phases of blade testing. Blade "instability" or "limit cycle variation" was a primary consideration in the blade design. Detailed discussion of this is covered in Reference 1.

Critical speeds of the coupled blade/trunnion/disk system were calculated and plotted in the form of a Campbell diagram. The predicted criticals are discussed and compared to engine test data in a subsequent paragraph.

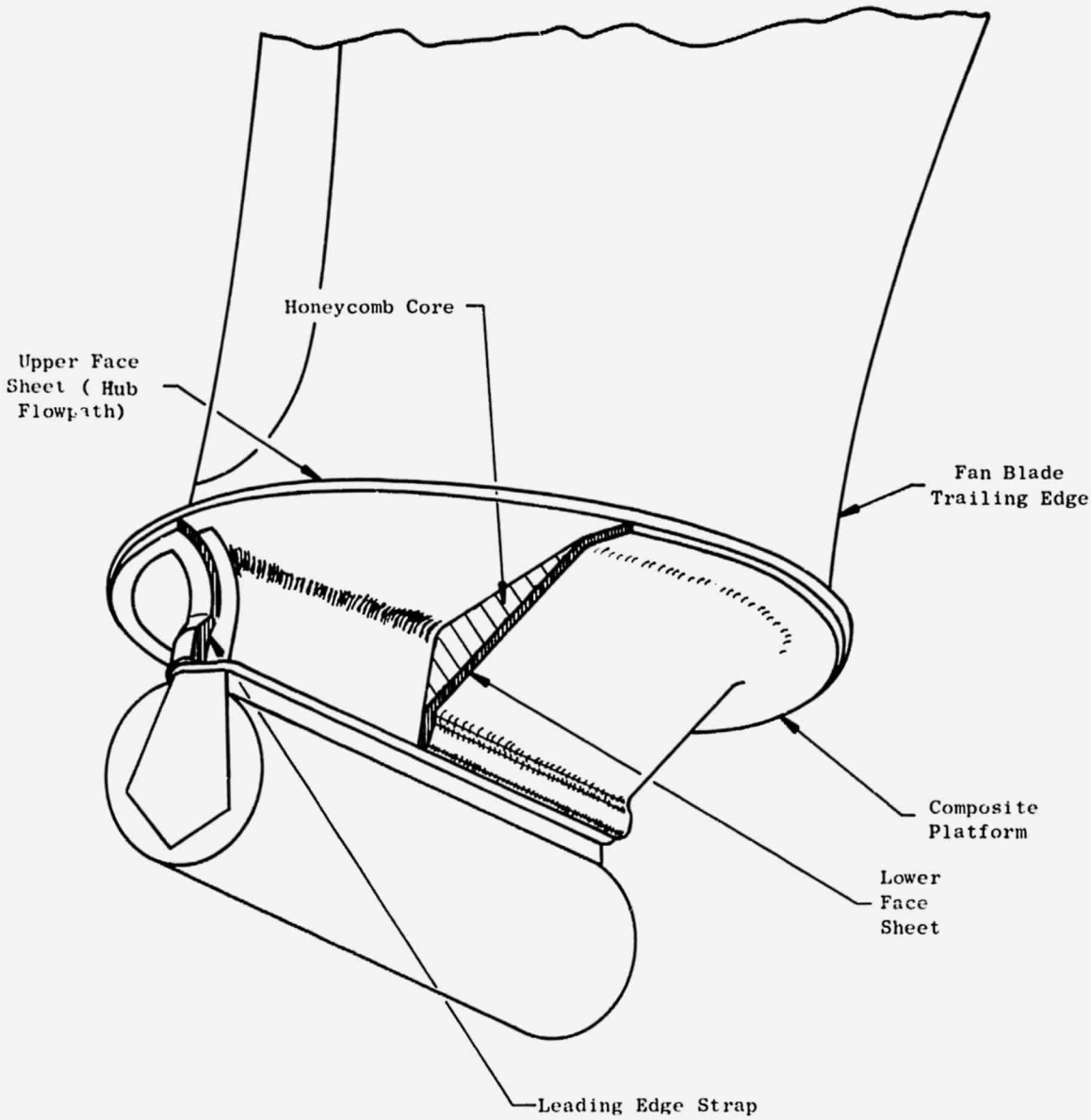

Figure 2. Platform Construction.

ORIGINAL PAGE IS
OF POOR QUALITY

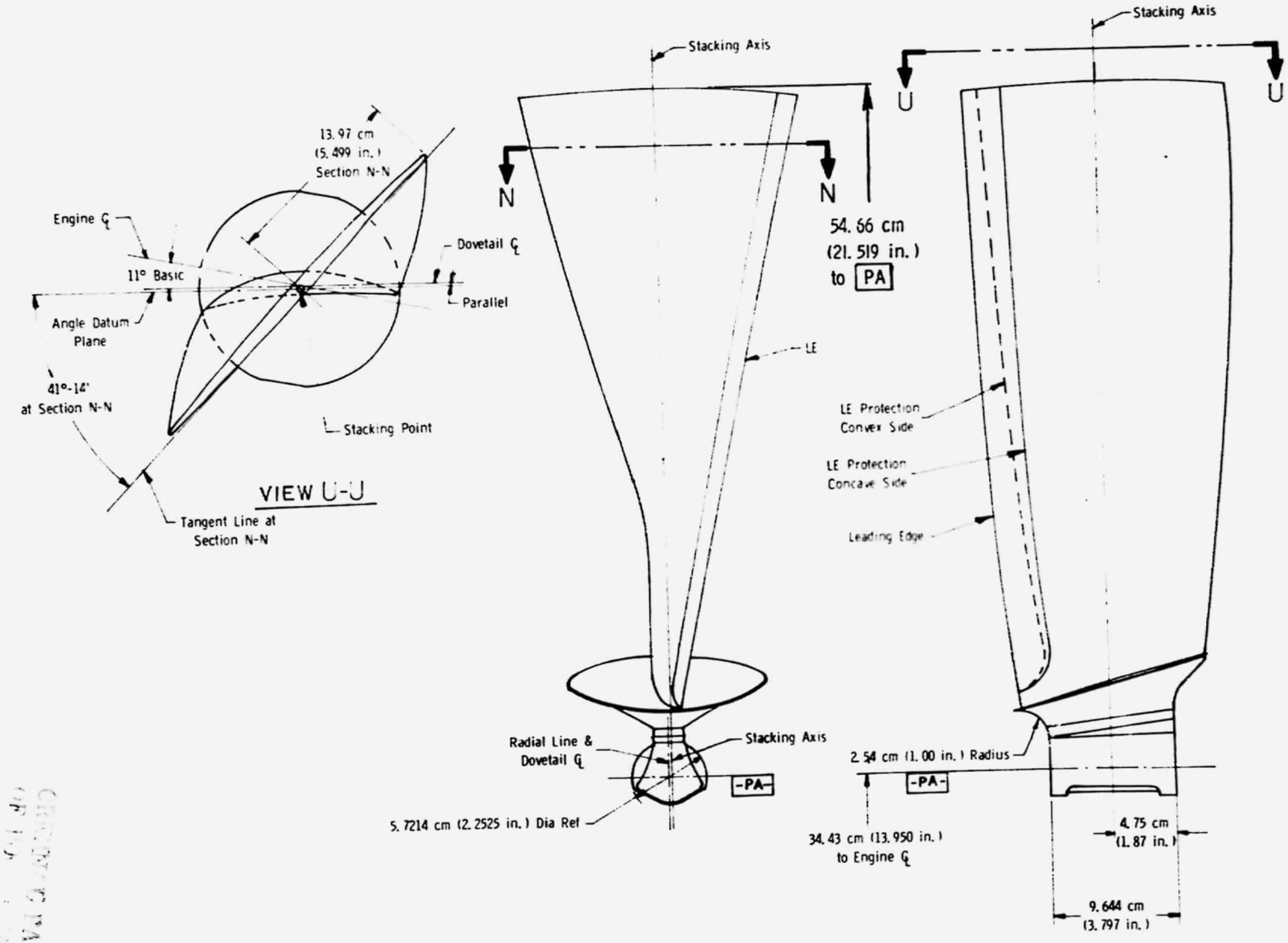

Figure 3. Composite Blade Configuration.

ORIGINAL PAGE IS
OF POOR QUALITY

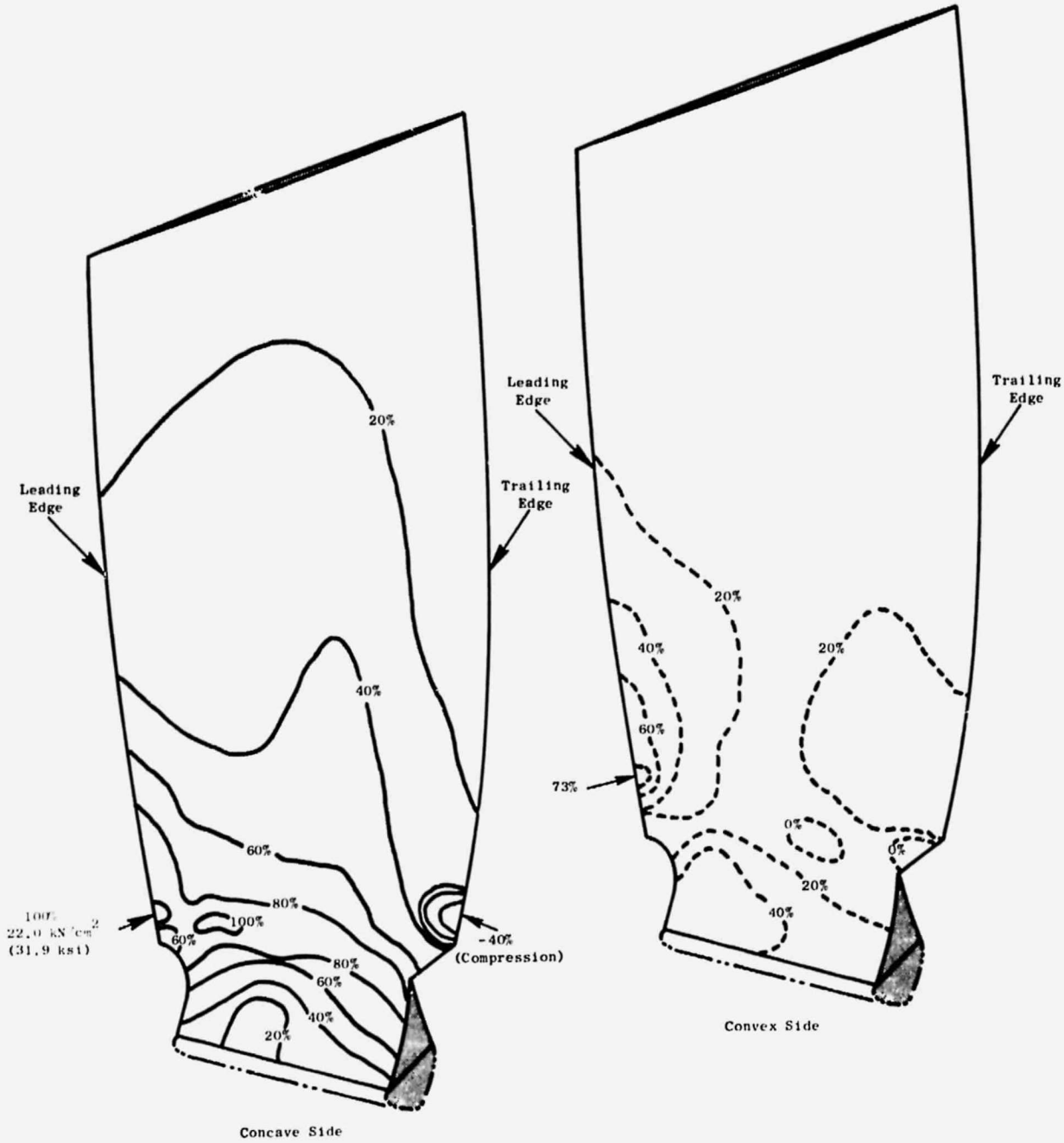

Figure 4. Calculated Blade Radial Stress.

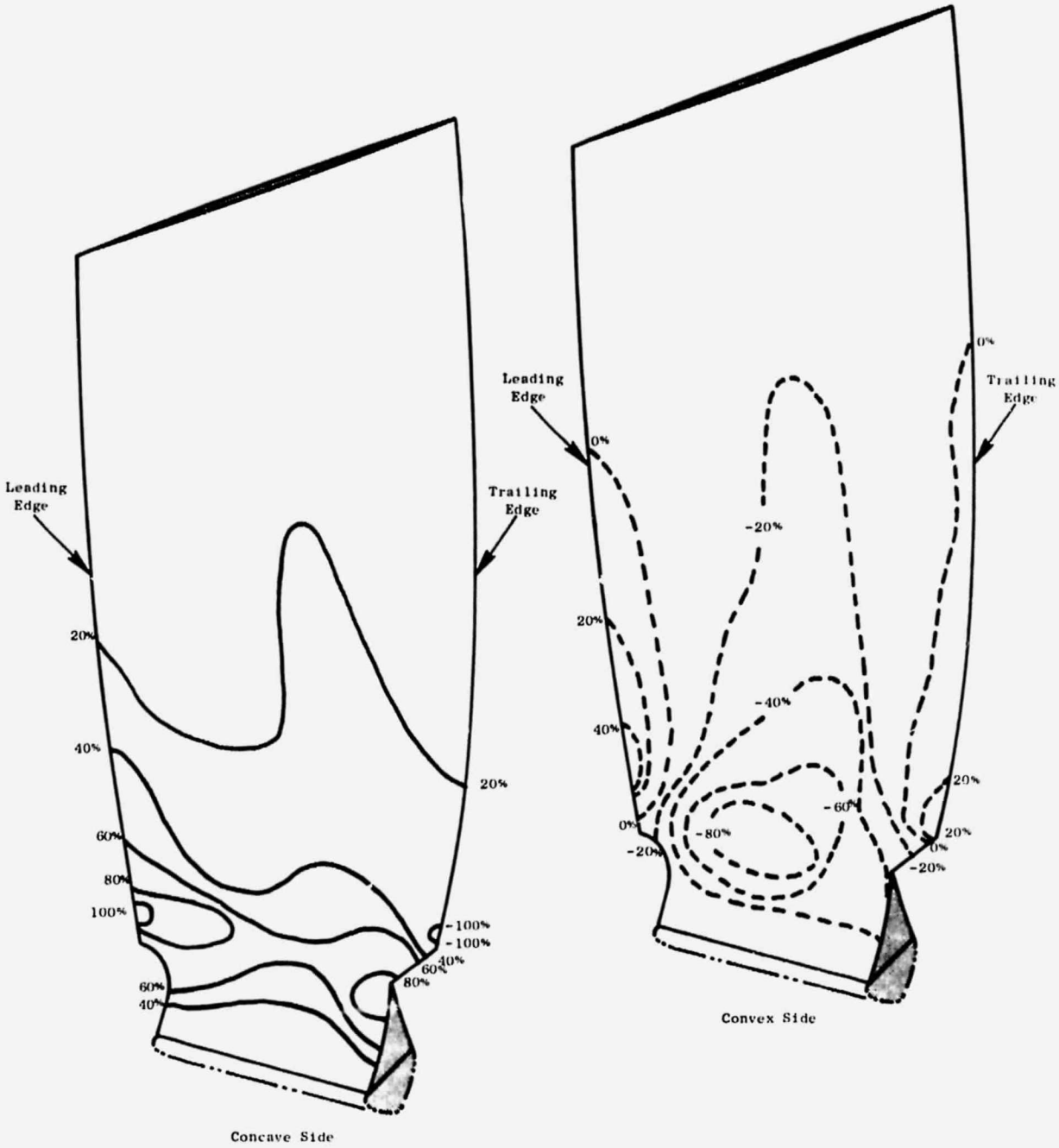

Figure 5. Calculated Blade Relative Radial Stresses for First Flexural Modes.

ORIGINAL PAGE IS
OF POOR QUALITY

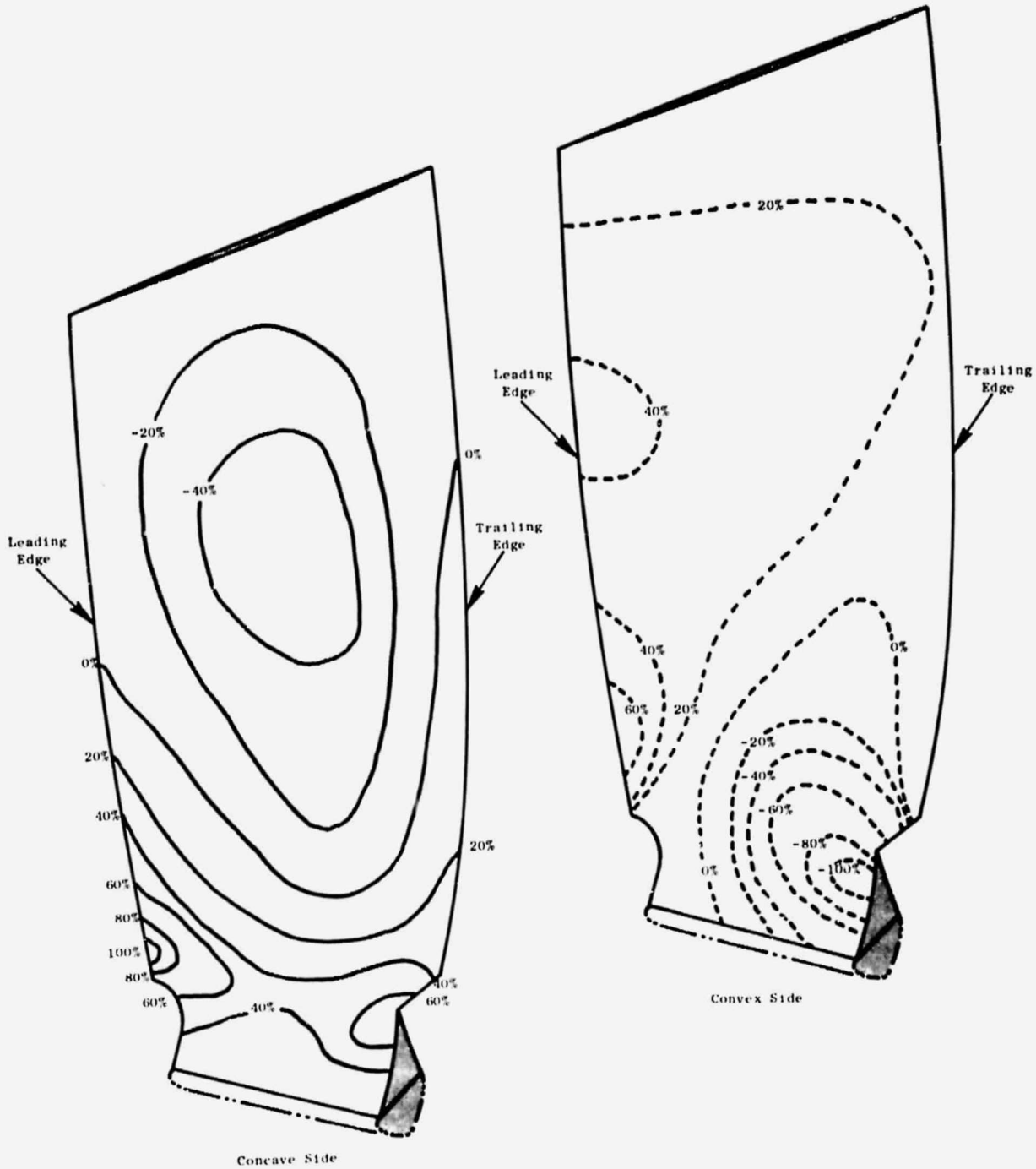

Figure 6. Calculated Blade Relative Radial Stresses for Second Flexural Modes.

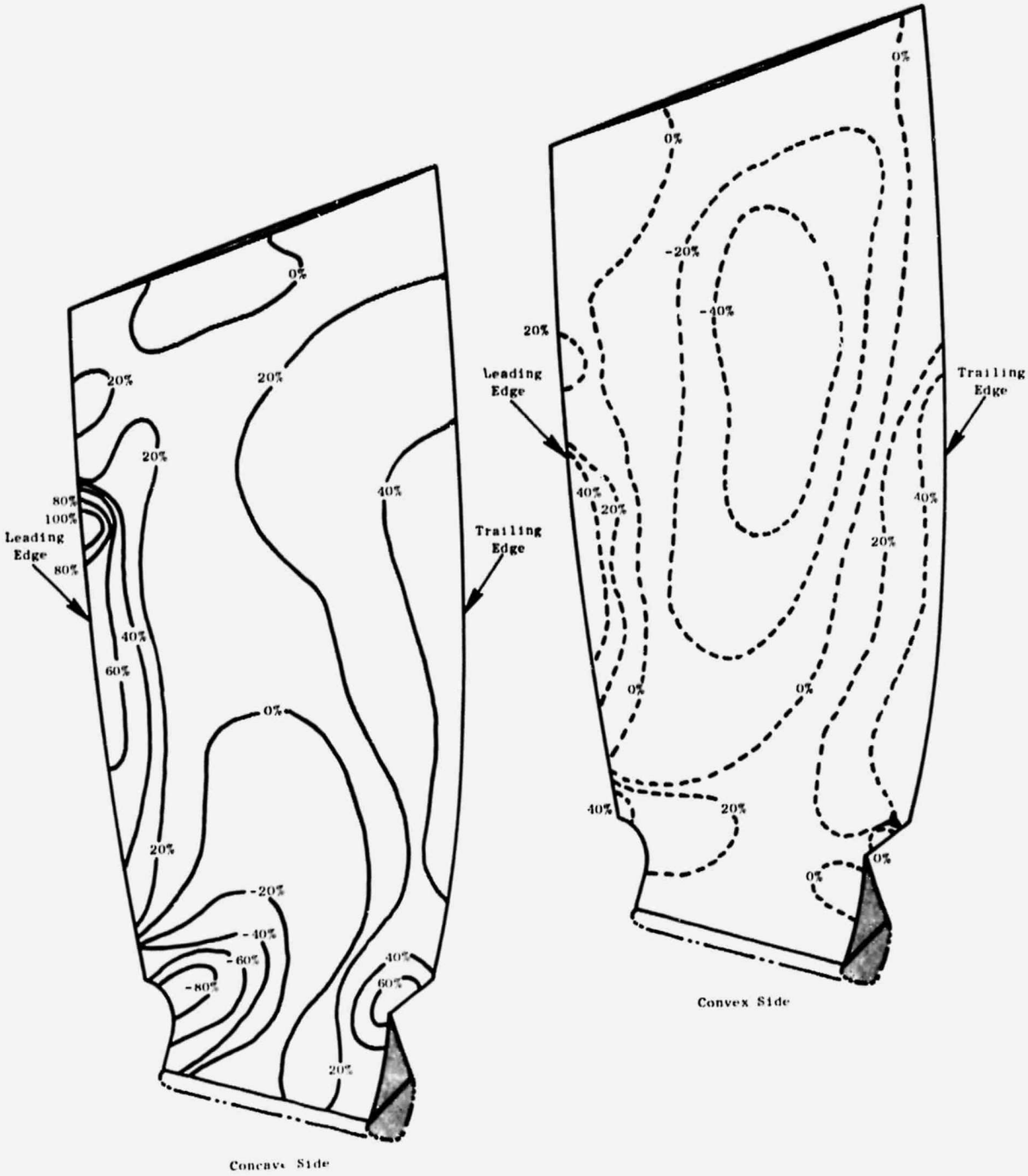

Figure 7. Calculated Blade Relative Radial Stresses for First Torsional Modes.

ORIGINAL PAGE IS
OF POOR QUALITY

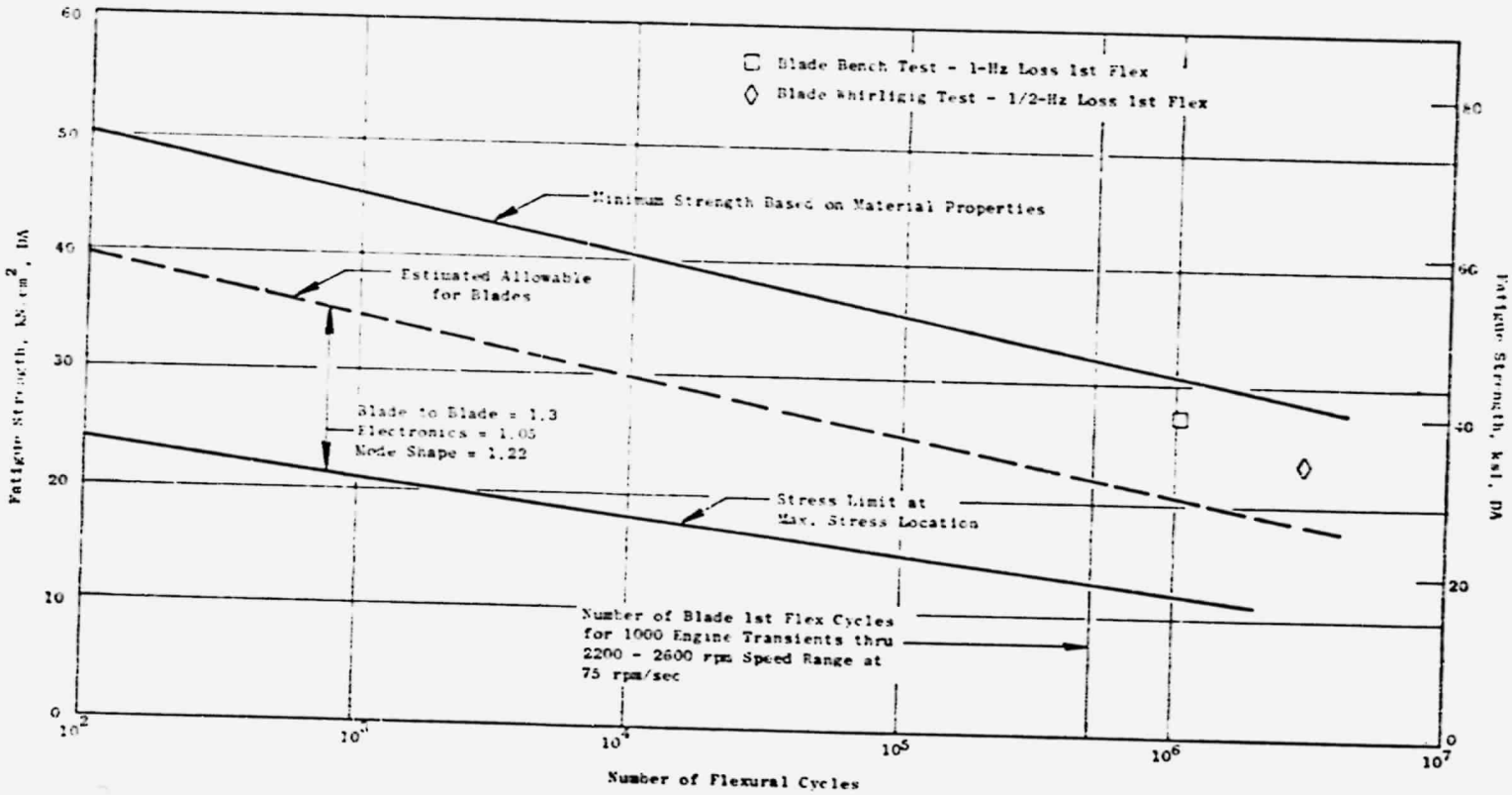

Figure 8. Fatigue S-N Curve for QCSEE Blade.

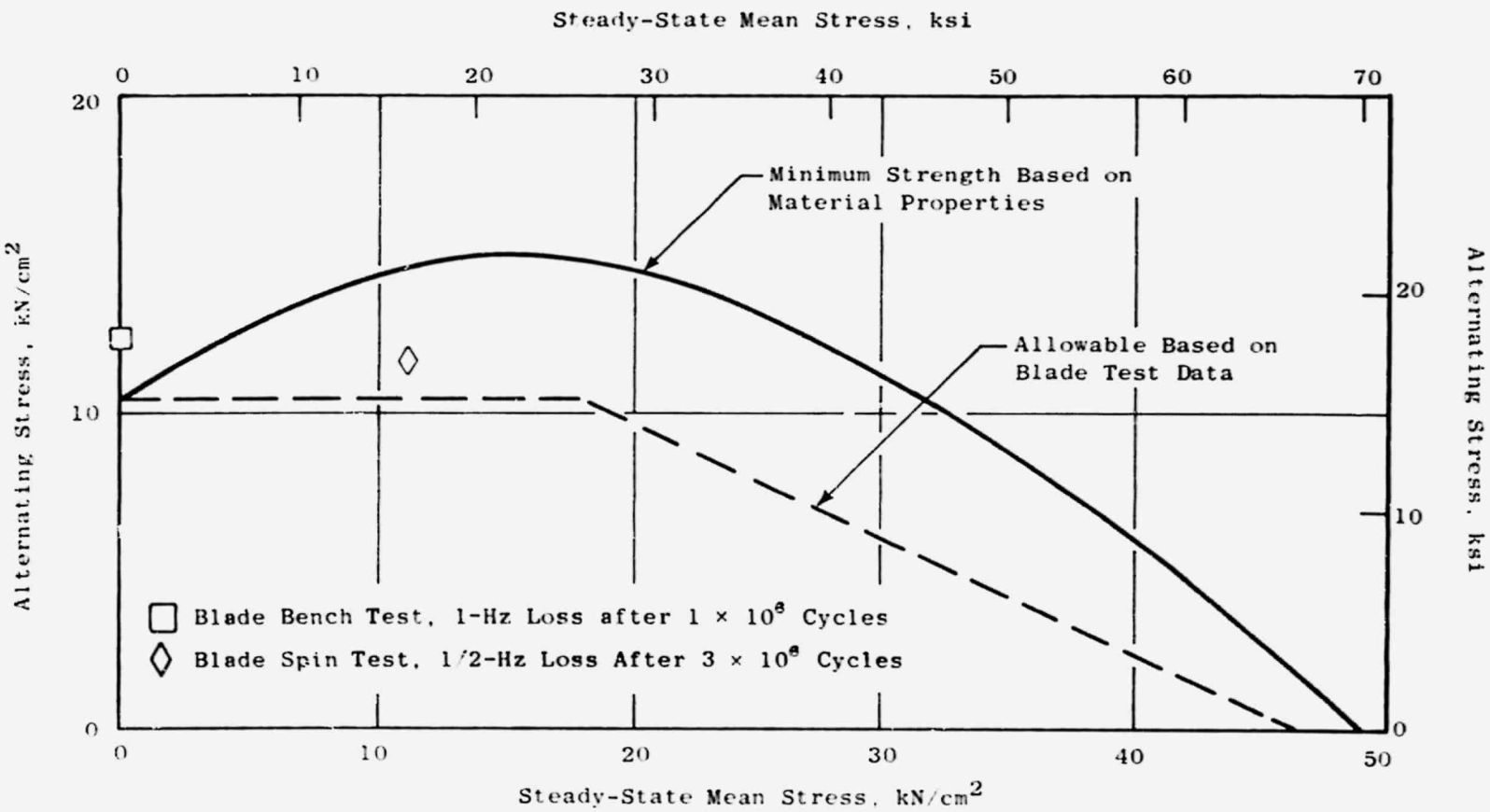

Figure 9. Allowable Stress-Range Diagram - Blade Radial Stress.

4.3 BLADE INSTRUMENTATION AND SCOPE LIMITS

Six of the fan blades were instrumented with a total of four static strain gages and 14 dynamic strain gages with locations on the blade as shown in Figures 10, 11, and 12. The static gages were placed to measure the steady-state and bending stresses in the lower airfoil and root region of the blade to permit monitoring blade stresses during the test and to verify the predicted steady-state stress distribution. Each of these static gages had an adjacent skin thermocouple to allow accurate temperature compensation. The steady-state stress pattern was determined by the TAMP finite-element analysis and by laboratory test.

The 14 dynamic gages were located at five different locations on the blades to provide a balance between having commonality of gages, having gages at different strain levels for gage-life considerations, having gages responsive to the different vibratory modes, and providing verification of the vibratory stress distributions on the blades during engine test. As with the steady-state stresses, the vibratory stress patterns for the blade vibratory modes were determined by finite-element analysis and by laboratory tests. The blade strain gage locations were selected so that at least one of the locations would be responsive to blade vibration in each of the five lower blade modes.

"Scope limits" or vibratory stress limits for these gages were calculated for each of the lower-blade modes. These limits normally represent the maximum vibratory stress at which the blade may be allowed to continuously vibrate without initiating a fatigue failure at some location on the blade. This point where the fatigue crack would be initiated is referred to as the "critical location" and is different for each vibratory mode. In the QCSEE composite blades, the fatigue failure mode would be an internal delamination which would result in a drop in blade material frequency rather than the usual fatigue crack.

The critical location and the fatigue strength normally depend upon both the steady-state and vibratory stresses; since the blade steady-state stress pattern increases roughly with the speed squared, the scope limits normally would be calculated as a function of fan speed. However, over the range of steady-state stresses anticipated for the QCSEE blade, the composite material fatigue strength is insensitive to the level of steady-state stress, i.e., is constant. The scope limits, therefore, can be considered independent of fan speed over the operating range.

Another complication encountered in calculating scope limits for an adjustable-pitch fan is that the steady-state stress pattern is also a function of the blade pitch angle. This is because the aerodynamic blade loading and the twisting moment generated by the radial centrifugal field are pitch-angle-dependent. The effect of these changes on the blade steady-state stress pattern is not insignificant for a fan to be tested in a pitch angle range of approximately 180°. Technically, correct blade scope limits normally would require the calculating of a carpet-of-values as a function of both speed and pitch angle. Again, it was not necessary to take this approach

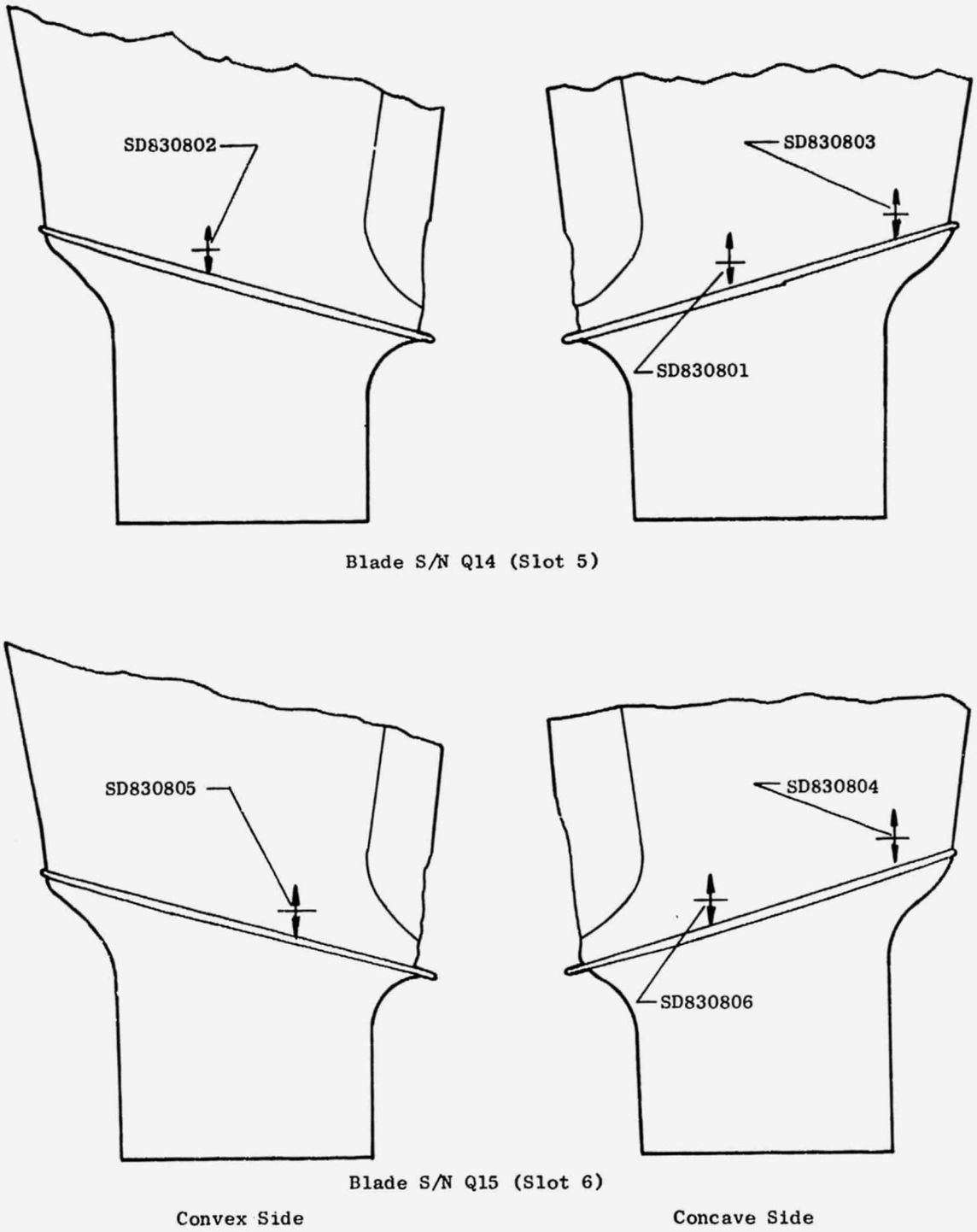

Figure 10. Locations of Fan Blade Instrumentation.

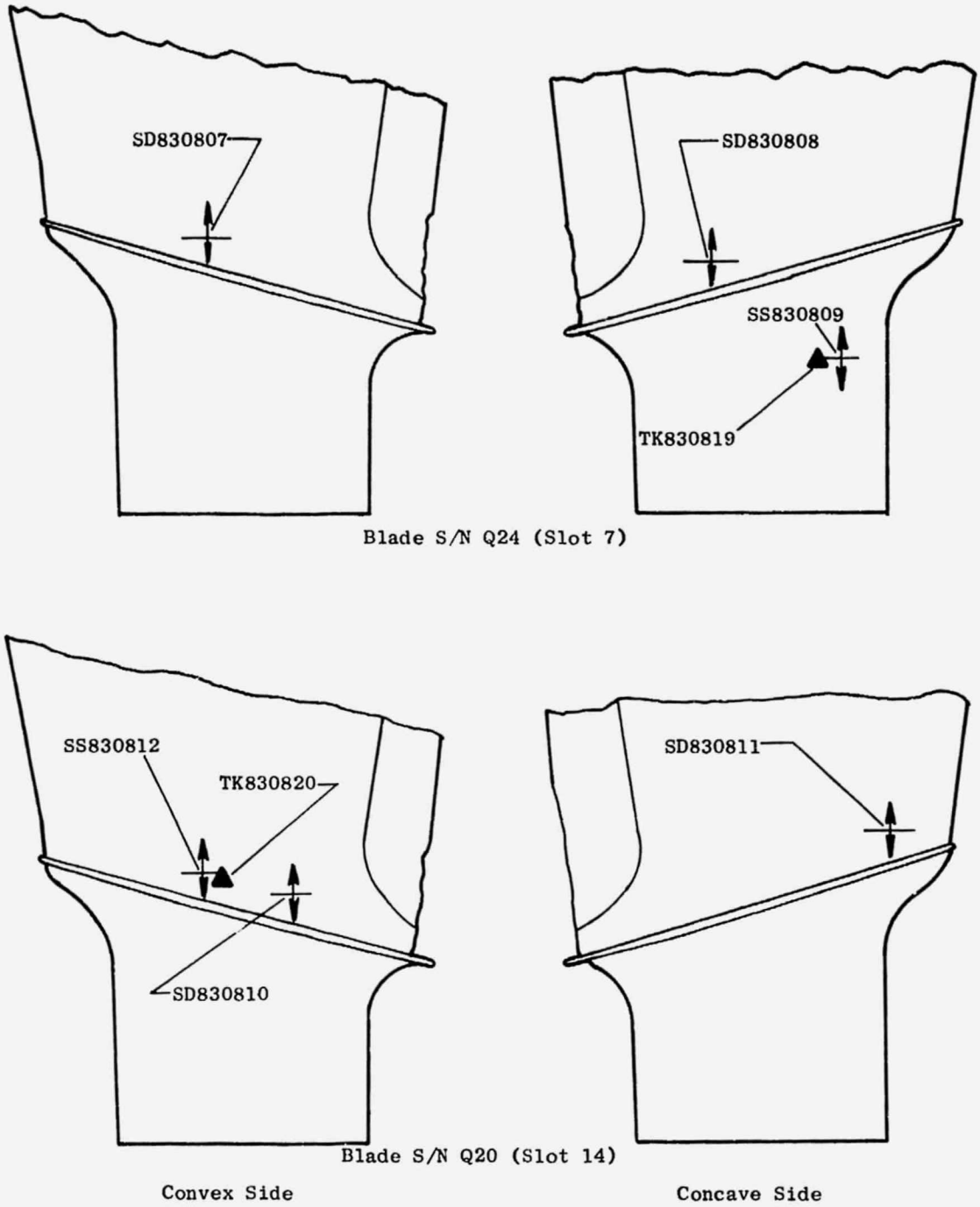

Figure 11. Locations of Fan Blade Instrumentation.

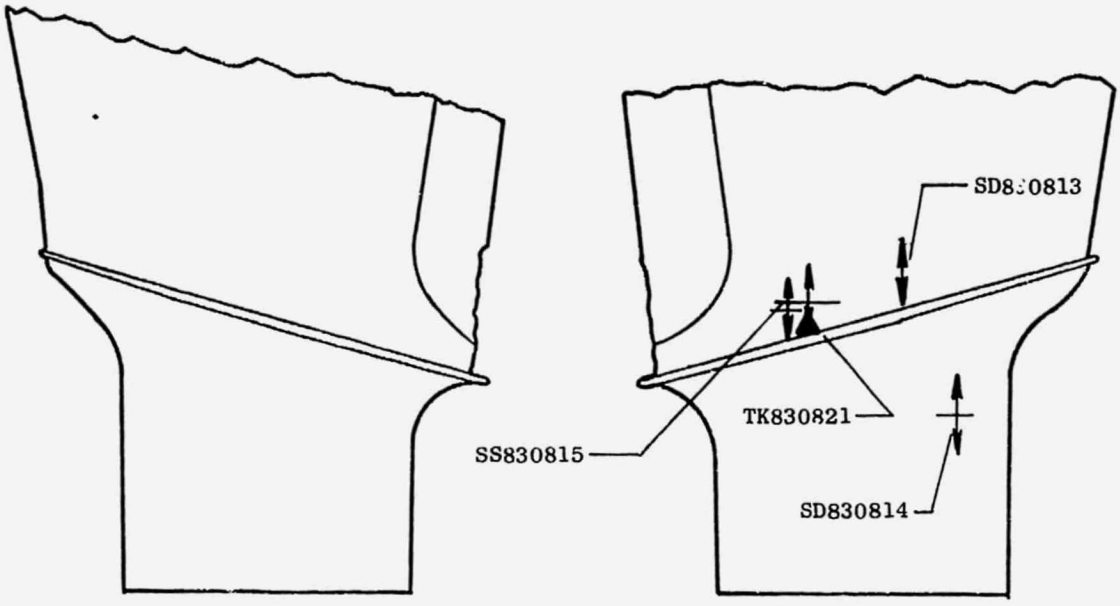

Blade S/N Q27 (Slot 15)

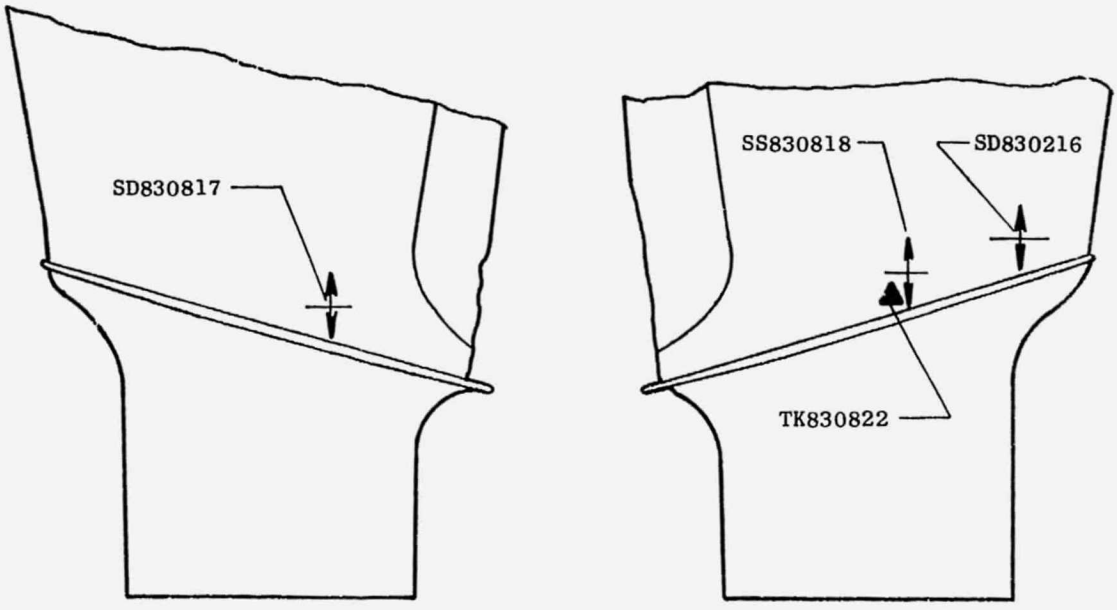

Blade S/N Q23 (Slot 16)

Convex Side

Concave Side

Figure 12. Locations of Fan Blade Instrumentation.

since the composite-blade fatigue limit is independent of the steady-state stress patterns. The fatigue limit diagram used was the average fatigue limit curve minus three standard deviations which represents the minimum expected material properties.

With the critical point located, the allowable vibratory stress at this location available, and the vibratory stress pattern known, the scope limit for a particular airfoil strain gage may be calculated using the following equation:

$$\text{Scope Limit} = \frac{2\ (\sigma\ \text{Gage}/\sigma\ \text{Critical Point})\ \sigma e}{K_1 K_2 K_3}$$

where

σ_e = The single-amplitude endurance limit at the critical point on the blade in this vibratory mode as determined by the Fatigue Limit Diagram for the blade material.

$\frac{\sigma\ \text{gage}}{\sigma\ \text{critical point}}$ = The ratio of the vibratory stress at the location of the strain gage to the vibratory stress at the critical point on the blade for the vibration mode being considered.

K1 = A blade-to-blade vibratory response variation allowance factor (1.3 based on past experience).

K2 = A factor for allowance for tolerance in the strain gage electronics circuit (1.05).

K3 = An allowance for the sensitivity of the monitoring gage to slight changes in mode shape, such as might be expected due to manufacturing tolerance, 0.32 cm (1/8 in.) gage mislocation, etc. (1.22).

It is easier in practice to read a vibratory stress signal on an oscilloscope from the peak-to-peak of the wave rather than its amplitude. Scope limits, therefore, normally are calculated in this manner. This peak-to-peak or double-amplitude method of presenting scope limits is the reason behind the "two" in the numerator of the scope limit equation. The scope limits for the QCSEE fan blades are listed in Table 3.

4.4 TEST RESULTS

During engine testing, blade monitoring efforts were directed toward assuring blade mechanical design integrity and obtaining data applicable to future safe operation. Dynamic blade stresses were monitored and recorded during all testing phases and steady-state stresses were monitored and

Table 3. UTW Fan Blade Scope Limits.

kN/cm^2 (ksi) - Double Amplitude with $E = 6.9 \times 10^6$ N/cm^2 (10×10^6 psi)

Group	Gage Number	Mode (Zero Speed Frequency, Hz)				
		1F (62)	2F (186)	1T (292)	4th (396)	5th (613)
A	SD830801	4.0 (5.8)	5.0 (7.2)	3.2 (4.7)	3.9 (5.6)	2.8 (4.0
	806	4.0 (5.8)	5.0 (7.2)	3.2 (4.7)	3.9 (5.6)	2.8 (4.0)
	808	4.0 (5.8)	5.0 (7.2)	3.2 (4.7)	3.9 (5.6)	2.8 (4.0)
	813	4.0 (5.8)	5.0 (7.2)	3.2 (4.7)	3.9 (5.6)	2.8 (4.0)
B	SD830802	4.7 (6.8)	5.6 (8.1)	--- ---	2.8 (4.0)	2.6 (3.8)
	807	4.7 (6.8)	5.6 (8.1)	--- ---	2.8 (4.0)	2.6 (3.8)
C	SD830803	3.5 (5.1)	2.1 (3.0)	3.7 (5.4)	4.3 (6.3)	3.2 (4.7)
	804	3.5 (5.1)	2.1 (3.0)	3.7 (5.4)	4.3 (6.3)	3.2 (4.7)
	811	3.5 (5.1)	2.1 (3.0)	3.7 (5.4)	4.3 (6.3)	3.2 (4.7)
	816	3.5 (5.1)	2.1 (3.0)	3.7 (5.4)	4.3 (6.3)	3.2 (4.7)
D	SD830805	5.6 (8.2)	3.3 (4.8)	--- ---	5.9 (8.6)	6.5 (9.4)
	810	5.6 (8.2)	3.3 (4.8)	--- ---	5.9 (8.6)	6.5 (9.4)
	817	5.6 (8.2)	3.3 (4.8)	--- ---	5.9 (8.6)	6.5 (9.4)
E	SD830814	3.6 (5.3)	3.3 (4.8)	1.4 (2.0)	2.0 (2.9)	2.0 (2.9)

recorded during all testing phases and steady-state stresses were monitored and recorded during initial mechanical checkout and reverse thrust testing. Blade frequencies were measured both during and between tests to determine if any changes had occurred.

Engine testing phases consisted of mechanical checkout of the engine in forward mode with a bellmouth inlet installed, forward mode testing with the bellmouth inlet replaced by a hardwall accelerating inlet, and reverse mode operation with the hardwall accelerating inlet. Mechanical checkout included performance mapping on five operating lines at 85%, 90%, and 95% fan speed with blade angles of primarily +5° (blade closed), 0° (nominal), and -5° (blade opened). During mechanical checkout, the engine was tested for 27.5 hours of which 10 hours was above 2400 rpm. During the forward mode, data were obtained for various takeoff and approach power settings. Blade angles were similar to those for mechanical checkout and approximately 16 hours of engine operation were accumulated. Reverse mode testing was conducted with the hardwall accelerating inlet configuration and consisted primarily of testing at -105° and -100° (blade open) blade angles at various thrust levels. Blade responses due to traversing from forward-to-reverse mode and from reverse-to-forward mode at operating speeds were not determined because of the termination of testing after the fan exhaust nozzle flap failure. Approximately four hours of running were accomplished in the reverse mode.

Blade steady-state stresses during all testing were very close to or below predicted stress levels and did not present a problem at any time.

Dynamic vibratory stresses were observed to be higher than scope limits on several occasions which caused a backoff situation on engine speed. These high levels generally occurred near the 2/rev crossover (2400 rpm) or during engine tests with tail and/or crosswind conditions.

Steady-state stresses from centrifugal and bending were determined from the four steady-state gages during the initial portion of mechanical checkout and during the reverse mode testing. The steady-state stresses and output from thermocouples located adjacent to the steady-state gages were continuously monitored while being recorded on an 8-channel Sanborn recorder during engine testing. Corrected thermocouple readings were recorded in the ADH printouts throughout all testing. After ascertaining that the steady-state stresses were close to predicted levels and not presenting any problem during the initial portion of mechanical checkout, these data were deleted from the Sanborn to permit using the Sanborn recorder to obtain other engine parameters. The blade steady-state data again were recorded and monitored during reverse mode testing.

The steady-state stresses during forward mode testing are plotted as a function of fan speed in Figure 13 and during reverse mode in Figure 14. These data were taken from the Sanborn charts at points where speed changes were moderately rapid and temperature changes were very small. Therefore, it was unnecessary to correct for apparent strain temperature effects.

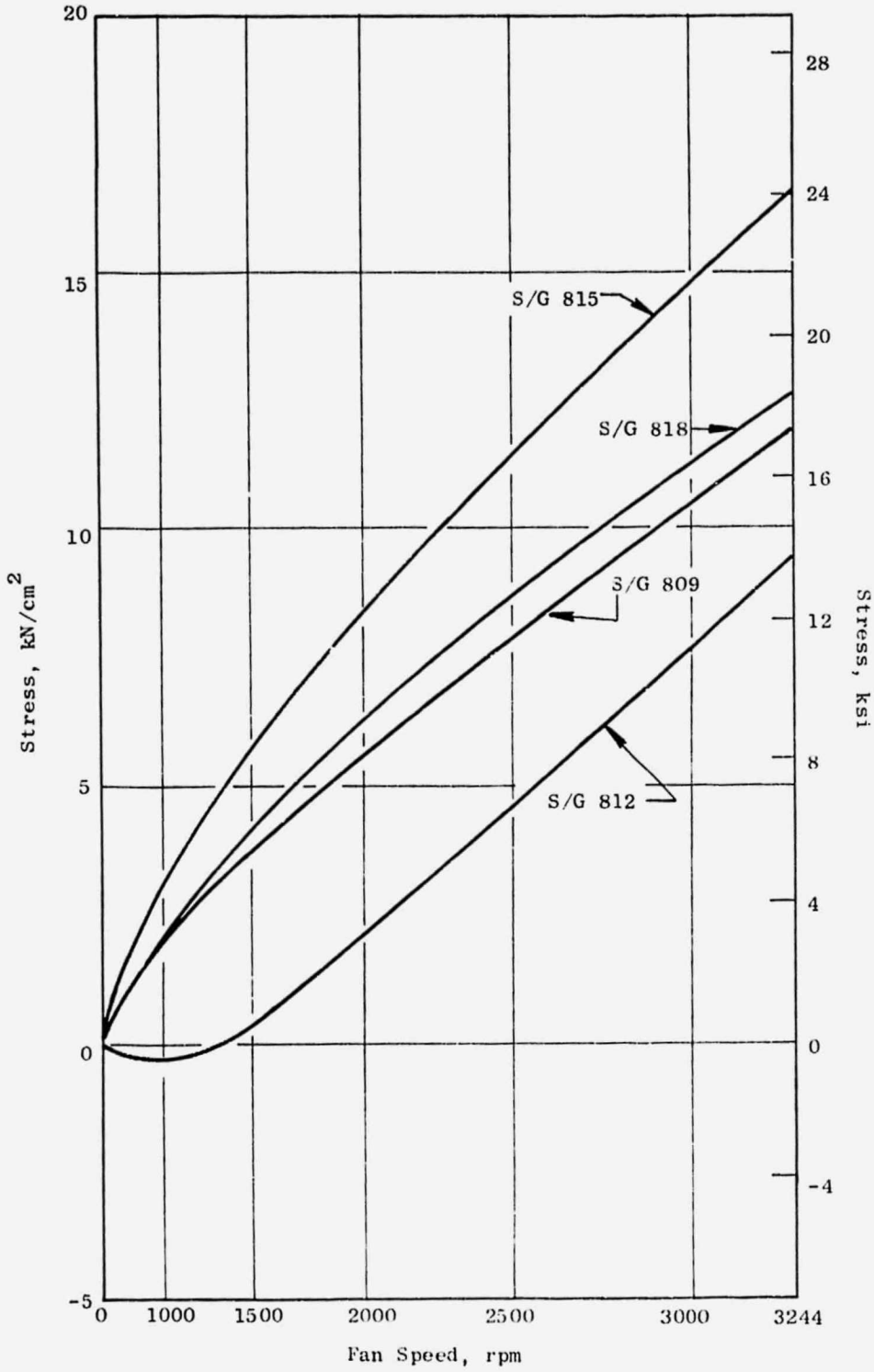

Figure 13. Steady-State Stresses, Forward Mode.

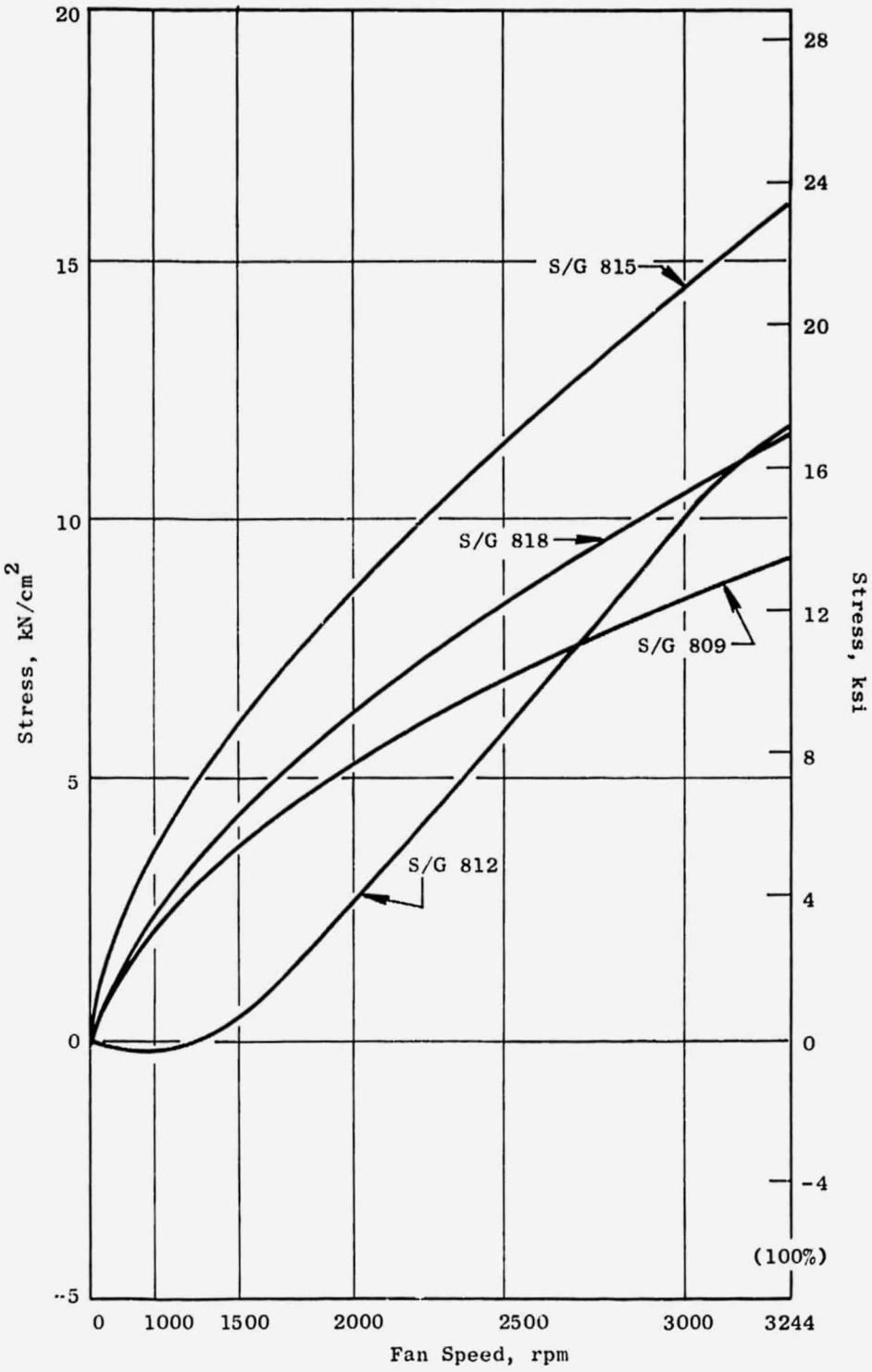

Figure 14. Steady-State Stresses, Reverse Mode.

The forward mode testing data show that the maximum measured stress was at the airfoil midchord, concave side, slightly above the platform (S/G 815) and was 15 kN/cm^2 (22 ksi) at 3100 rpm. Gages on opposite sides of the blade at the same chord and spanwise location, and slightly aft of the maximum-reading gage (S/G 818 on concave side and S/G 812 on the convex side), had stresses of 12 kN/cm^2 (17 ksi) and 8 kN/cm^2 (12 ksi), respectively, at 3100 rpm. Root stress on the concave side, S/G 809, was approximately 11 kN/cm^2 (16 ksi) at this same speed.

Review of the Sanborn-recorded data showed that the steady-state stress levels at a given fan speed were quite insensitive to changes in pitch angle and fan nozzle area within a given mode of operation.

In reverse mode operation, the measured stresses on the airfoil concave side were very close to those for the forward mode. S/G 815 was 15 kN/cm^2 (22 ksi) and S/G 818 was 11 kN/cm^2 (16 ksi) at 3100 rpm. The airfoil convex side stress (S/G 812) increased to 11 kN/cm^2 (16 ksi). These differences reflect the change in bending due to reduced aerodynamic loading and changed twisting moment in the reverse mode. The concave-side root stress (S/G 809) reduced to 9 kN/cm^2 (13 ksi) at 3100 rpm.

Based on the finite element analysis, the calculated stresses for forward mode operation for the locations of S/G 815, 818, 812, and 809 were 18,16,4, and 12 kN/cm^2 (26,23,6, and 17 ksi), respectively. Comparison of the observed stresses to the calculated stresses shows the concave-side stress to be lower and the convex-side stress higher than calculated, and that bending is less severe than calculated. This is as expected, since the finite-element analysis conservatively assumed fixity at the blade root, whereas the actual blade has the ability to rotate at the dovetail and to reduce the blade bending. The results of these data indicated that the blade design is acceptable for steady-state stresses.

The pre-engine-test Campbell diagram for the UTW blade assembled in the trunnion and disk was determined from single-blade whirligig spin testing. This is presented with the frequencies observed during engine test in Figure 15. The plotted frequencies reflect the coupled frequency of the blade trunnion assembly and agree closely with predictions. The flexural frequency at the 2/rev crossover was predicted to occur at about 70% of the maximum steady-state speed. This is above flight idle speed and below normal operating speed for takeoff, climb, and maximum-cruise flight conditions. It therefore was considered a transient point and not subject to continuous steady-state conditions. Blade excitation stresses at 2/rev crossover were monitored carefully during engine testing. Blade pitch control and moderate acceleration through this point were employed to prevent these stress levels from becoming excessive.

The margin for first flexural frequency over 1/rev at 115% speed is approximately 50%, and the margin for first flexural frequency below 2/rev at 100% speed is approximately 13%.

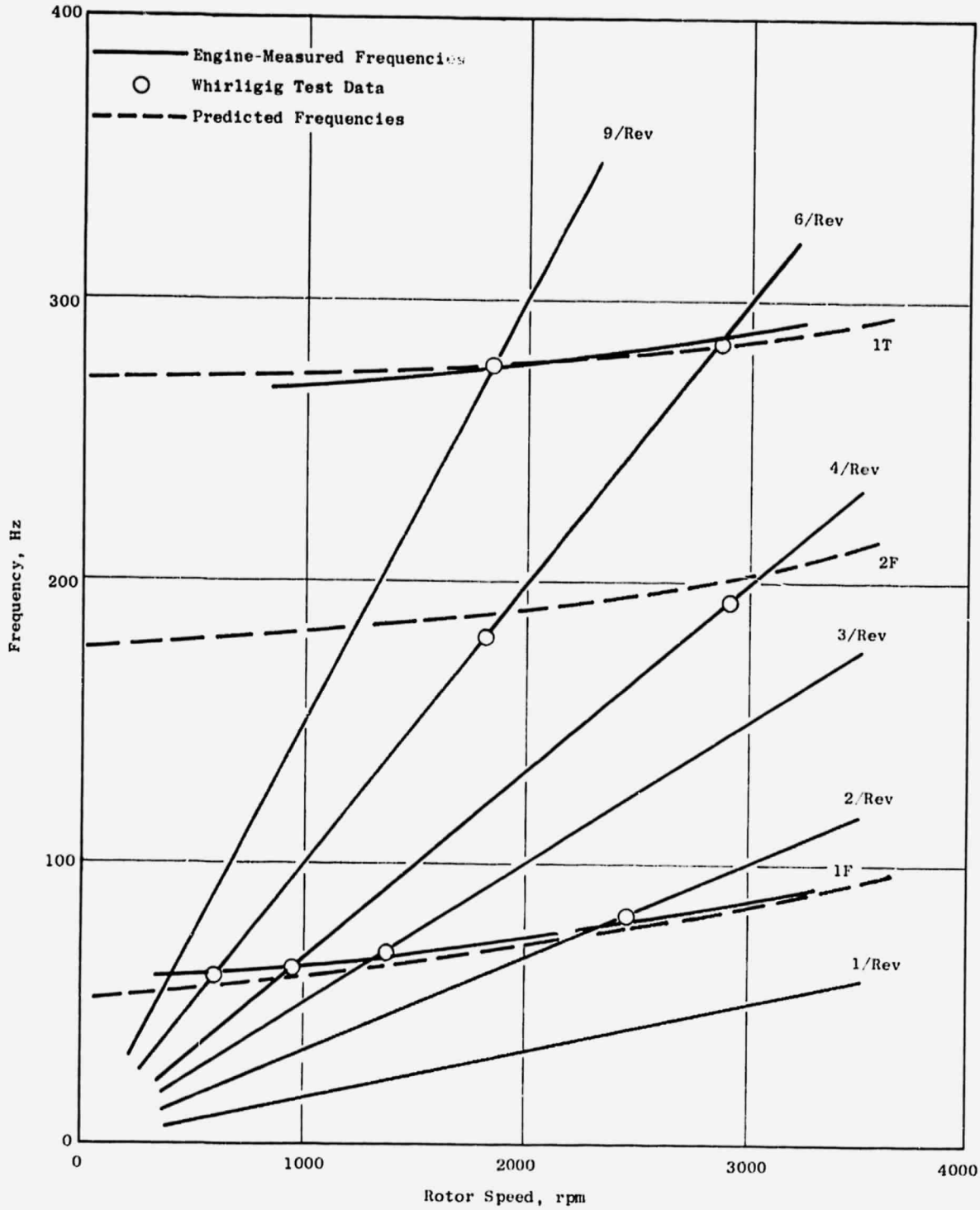

Figure 15. Campbell Diagram.

The second flexural mode crosses several per-rev lines in the operating speed range. Each of these crossings represents a potential for forced resonances; however, it takes considerably more energy to drive the higher vibration frequencies such as second flex and no problems were anticipated.

The first torsional frequency 6/rev crossover is at approximately 83% speed with the 100% speed frequency margin being approximately 6% over 5/rev. Since the excitation forces were expected to be small at the higher order crossovers, no torsional vibratory problems were anticipated during normal engine operating conditions.

Forward Thrust Response, Bellmouth Inlet - Dynamic stresses induced by vibratory effects were determined from the 14 dynamic gages throughout all phases of testing. The stresses were continuously recorded on a 28-channel tape recorder and monitored on individual scopes. One selected gage was continuously displayed and monitored with a frequency spectrum analyzer. For the mechanical-checkout portion of the testing, the engine had a bellmouth inlet and operated in the forward thrust mode with blade angles between -5° (open) and +9° (closed) and to a fan speed of 3100 rpm. Stresses exceeded scope limits on a number of occasions and required a backoff of the engine speed. The first high stress occurrance was on initial acceleration to approximately 40% fan speed (1297 rpm) which coincides with the blade first-flex 3/rev crossover. Stress levels of about 120% of scope limits were reached. There were no reoccurrances of this condition since the fan idle speed was set at a significantly higher speed (1600 rpm at a blade pitch angle of 0°) and the engine was accelerated through this point on subsequent startups.

The second occurrance of high stress was on the first accel to a fan speed of 2375 rpm which coincides with the blade first-flex 2/rev crossover. Fan blade stresses at this condition reached approximately 200% of scope limits. Subsequent testing generally showed less severe 2/rev stress conditions (usually below scope limits) principally due to adapting an operating procedure of accelerating and decelerating through the 2/rev crossover. Stresses observed during mechanical checkout did exceed scope limits on approximately 20 occasions. These usually were associated with relatively high winds and occurred, not only at the 2/rev crossover, but also at other operating conditions. Generally, no significant change in stress was observed due to variations in fan nozzle area (A18) from 18,700 cm^2 (2900 $in.^2$) (open) to 13,500 cm^2 (2100 $in.^2$) (closed) or with fan blade angle variations from +5° (closed) to -5° (open).

During mechanical checkout, the occasions on which blade stresses exceeded scope limits were all due to forced 2/rev response of the first-flex response forced by 2/rev. Of the 20 overstressed conditions, one reached 295% of limits, one was 220% of limits, seven were between 160% and 200% of limits, six between 120% and 160% of limits, and the remaining five were between 100% and 120% of limits. Table 4 summarizes a number of these instances and shows the general relationship of wind conditions. There was a maximum of 400 cycles per overstress occurrance. The potential for blade

Table 4. Dynamic Stress Wind Effect.

ksi - Double Amplitude with E = 6.9 × 10^6 N/cm^2 (10 × 10^6 psi)

Fan Speed, rpm	Wind Speed, M/S (mph)	Wind Direction, θ, degrees	DA Stress, kN/cm^2 (ksi) at Strain Gage				Limiting Gage	% of Scope Limit
			A	B	C	D		
1800	2.7 (6)	240	1.4 (2.0)	1.4 (2.0)	2.1 (3.0)	1.7 (2.5)	C	59
	4.5 (10)	240	1.7 (2.5)	2.3 (3.4)	2.3 (3.3)	1.7 (2.5)	C	65
	6.7 (15)	240	2.4 (3.5)	3.0 (4.4)	2.8 (4.0)	3.7 (5.4)	C	78
	8.9 (20)	280	3.4 (5.0)	4.0 (5.8)	5.2 (7.5)	4.8 (7.0)	C	147
2000	1.8 (4)	300	2.1 (3.0)	3.0 (4.4)	2.1 (3.0)	3.4 (5.0)	B	65
	3.6 (8)	320	6.6 (9.5)	10.3 (15.0)	10.3 (15.0)	8.3 (12.0)	C	295
2375	1.1 (2.5)	330	2.4 (3.5)	3.1 (4.5)	2.1 (3.0)	2.4 (3.5)	B	66
	4.5 (12)	270	6.9 (10.0)	9.0 (13.0)	5.5 (8.0)	8.3 (12.0)	B	191
2650	2.2 (5)	220	2.1 (3.0)	2.4 (3.5)	2.3 (3.4)	2.9 (4.2)	C	67
	4.5 (10)	250	3.4 (5.0)	4.3 (6.2)	2.8 (4.0)	3.7 (5.4)	D	91
	6.7 (15)	300	4.1 (6.0)	5.2 (7.6)	3.2 (4.6)	4.4 (6.4)	B	112
	8.9 (20)	250	5.9 (8.5)	7.6 (11.0)	6.9 (10.0)	6.9 (10.0)	C	196
2800	0.4 (1)	260	1.5 (2.2)	1.8 (2.6)	1.7 (2.5)	2.3 (3.4)	C	49
	2.2 (5)	160	1.4 (2.0)	1.7 (2.5)	2.1 (3.0)	2.8 (4.0)	C	59
	4.5 (10)	200	3.1 (4.5)	3.9 (5.6)	2.8 (4.0)	3.3 (4.8)	B	82
3058	0.9 (2)	100	3.4 (5.0)	3.4 (5.0)	2.1 (3.0)	3.1 (4.5)	A	86

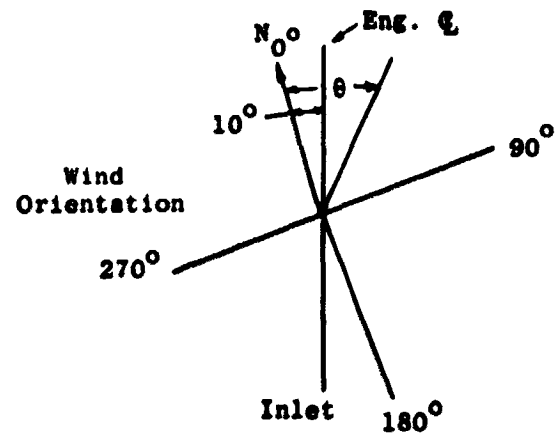

damage from these stresses was very low based on the number of cycles at the observed stress levels and the conservatism built into the scope limits. From the high amplitude, low cycle fatigue (S/N) curve, reference Figure 8, it is evident that all stresses were below the most conservative curve which included material variabilities, electronics, and mode shape sensitivity (established by GE metal blade standards), and a 1/2-cycle-per-second loss in first-flex frequency.

The first flexural mode was the most active mode with responses to other modes essentially being nonexistent. Figure 16 shows a typical vibratory response for acceleration through the 2/rev crossover and through the operating region. The magnitude of vibratory stress at the various frequencies is shown by the length of vertical lines on the diagram. It is seen that essentially all stresses are in first flexural mode forced by the 2/rev stimulus.

Frequencies versus speed were periodically monitored during all phases of the testing for the instrumented blades, and zero-speed (bench) frequencies were measured after each major phase of testing on all the blades. The Campbell diagram determined from the blade frequencies (observed during engine and whirligig tests, reference Figure 15) agreed closely with the predicted frequencies. There was no detectable change in static frequency through completion of the accelerating inlet testing on any blade, and there was no change in frequency at speed through reverse thrust testing on any of the instrumented blades. Subsequent instrumented nondestructive examination of the blades showed that no delamination had occurred in any of the blades. If some slight internal damage (delamination) had occurred from overstress conditions, it would take approximately 1,000,000 cycles (3.5 hours) at 21 kN/cm^2 (30 ksi) DA to propagate the delamination to the point of losing 1.5% on first flex frequency. Even at this point, the blade still would be structurally sound. During single-blade whirligig spin testing, a drop in frequency of 5% was considered to be failure even though the blade still was structurally sound from a centrifugal load standpoint. Although there is conservatism in the blade fatigue and scope limits, it was considered appropriate that the same limits be observed throughout the program and that high stress conditions be avoided.

Forward Thrust Response, Accelerating Inlet - Upon completion of the mechanical checkout, the bellmouth inlet was removed and replaced by the hardwall accelerating inlet. Forward mode testing was continued with operations consisting of determining engine performance data for various takeoff and approach power settings. Blade angles between -7° (open) and +10° (closed) and fan speeds to 3100 rpm were investigated. Additional instances were encountered where fan blade dynamic stresses reached scope limits at or near the 2/rev first-flex crossover in the presence of a crosswind. In each case, the fan speeds were selected to avoid operating close to the 2/rev crossover. Throughout testing with the accelerating inlet, engine operation was limited to 100% of scope limits. On several occasions, operations were delayed until high winds subsided. The blade response to crosswind, when testing with the accelerating inlet, was similar to that with the bellmouth inlet.

ORIGINAL PAGE IS
OF POOR QUALITY

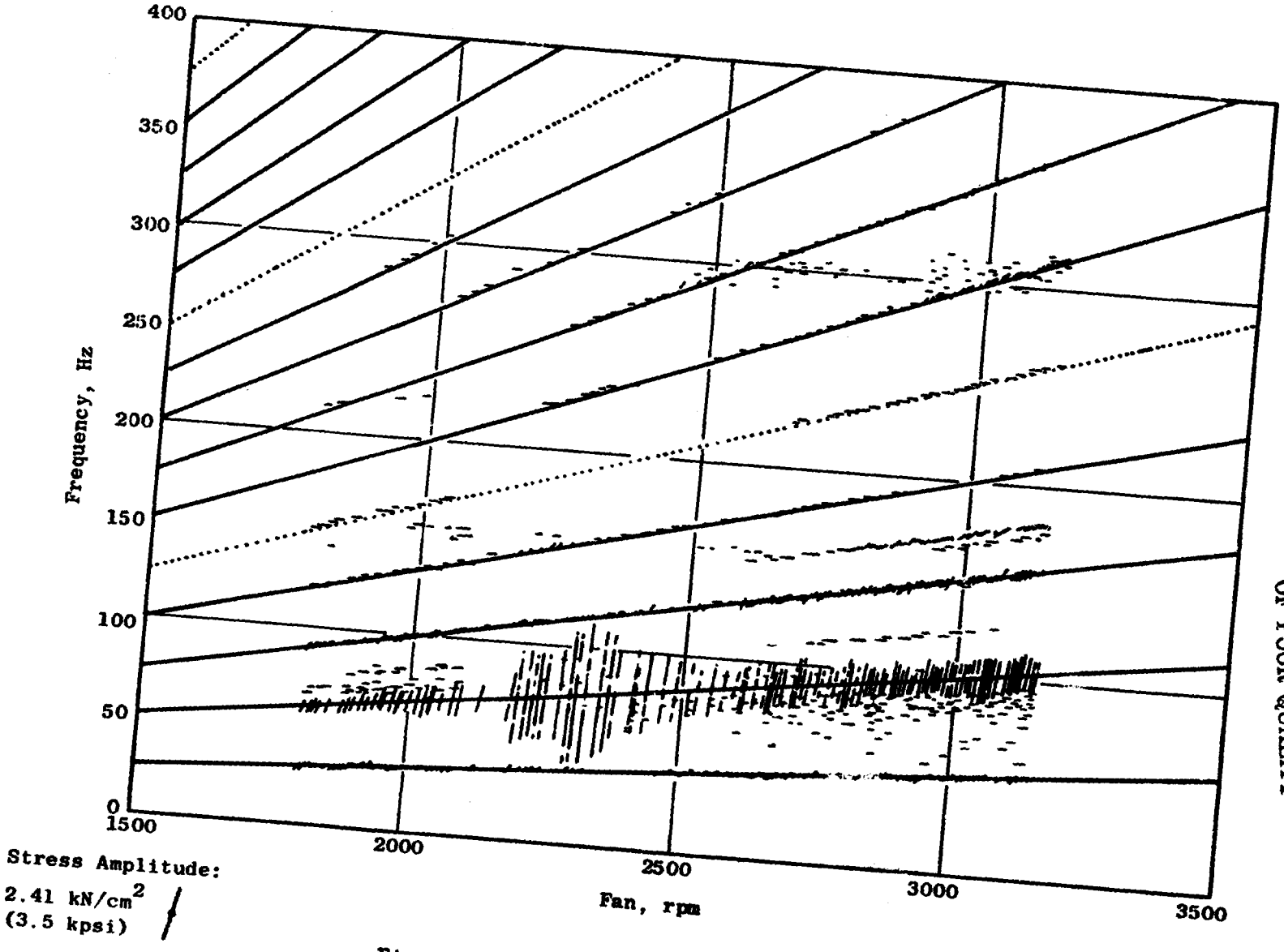

Figure 16. Dynamic Blade Stress Response.

REPRODUCIBILITY OF THE
ORIGINAL PAGE IS POOR

The blade response during this portion of the testing was similar to that during mechanical checkout, with the first flexural mode being the most active and other higher mode responses essentially being nonexistent. As during mechanical checkout, blade frequencies were monitored and showed no indications of any changes or signs of blade damage.

Reverse Thrust Response, Accelerating Inlet - Upon completion of forward thrust performance, testing, the engine was prepared for reverse thrust operation with the hardwall accelerating inlet. Reverse thrust operation consisted of a checkout cycle in forward mode, several actuations of the blades from forward to reverse position and return while air motoring, and then operation in reverse mode at blade angles of -100° and -105° (open) with fan speed to 3100 rpm. During the early portion of the test (in forward mode), winds of 4.5-7.2 m/s (10-16 mph) at 90° to the inlet were a problem causing high but within-limit blade stresses. As blades were opened, stresses became limiting at -22° and were characterized by very active scope patterns. In reverse mode operation, stress responses appeared similar to those in forward mode. Moderately rapid accelerations through the 2/rev first-flex crossover assisted in keeping blade stresses from exceeding scope limits. After testing in reverse mode for various blade angles and thrust level conditions, the engine was accelerated slowly to 3100 rpm when the fan exhaust nozzle flap failure occurred. Flap debris, consisting of bolts, nuts, seals, and flap skin material, impacted upon the fan blades damaging the outer airfoil trailing edges of all the blades. Immediately following impact, all fan blade dynamic stresses exceeded scope limits for about four cycles and exceeded 300% of scope limits.

Subsequent examination of the blades showed that all damage was restricted to the outer blade panels and that the high dynamic stresses had not caused any delamination in the blade roots.

4.5 CONCLUSIONS

The operation of the QCSEE UTW engine with composite blades represents a major advancement in that the composite blade design was not a scaled metal blade but a totally new blade with aerodynamic configuration and material selected specifically for the application. These conditions resulted in the blades having essentially unknown aeromechanical characteristics. Considering this, the agreement between measured and predicted responses are considered quite good. Also, no blade-related problems were identified which would prevent engine test operations. More specifically, the results of the composite blade engine testing provide the following conclusions:

- Blade frequencies are close to predicted and appear satisfactory for continued demonstrator engine operations.

- Blade steady-state stresses were low as predicted and satisfied requirements.

- Blade dynamic stresses exceeded limits and were sensitive to crosswind conditions. Inspection showed that no damage occurred from overstress. Analysis of results showed that the blades were satisfactory for test engine operations but required avoidance of certain steady-state fan speeds during crosswind conditions. Blade stresses due to wind effects were essentially the same for both the bellmouth and accelerating inlets.

- There were no indications of torsional instability during any of the engine testing, giving added confidence that blade stresses during reverse mode testing will be acceptable.

5.0 MAIN REDUCTION GEAR

The UTW engine has a star-type epicyclic reduction gearset located in the forward engine sump to reduce the low-pressure turbine speed to fan rotor speed. The gearset is shown schematically in Figure 17. The gearset consists of a flexibly mounted sun gear, which drives six star gears, which in turn drive a ring gear. The ring gear is flexibly mounted to the fan shaft. Principle design characteristics of the gears are listed in Table 5.

During testing of the UTW engine, the main reduction gear operated without significant problems. Gear efficiency data were inconclusive because of the accessory gearbox-flooding problem that caused high-heat rejection levels throughout the test.

5.1 TEST RESULTS

The data obtained from the ring gear strain gages were processed through the Fast Fourier Analysis, yielding the Campbell diagram in Figure 18. Note that no significant resonances are apparent and that the maximum vibratory stress of about 7000-psi double amplitude occurred primarily at the 6/rev star gear passing frequency.

When compared with allowable vibratory stress as shown in Figure 19, the stress was very close to predictions.

Unfortunately, the proximity gage installed to measure "wobble", which was a concern during component testing, was not operable.

During operation, the pretest maximum bearing temperature limit of 265° F was not exceeded.

Posttest inspection of the parts indicated the following:

5.2 POSTTEST INSPECTION

5.2.1 Gears - All gears were "Magnafluxed" and found to be in good condition. Wear patterns before and after test were not significantly different, indicating that the gears were "worn in" during development and that the engine test did not appreciably increase wear.

The ring gear evidenced pitting corrosion on the exposed surfaces. Inspection indicated that the most likely cause for the corrosion was fingerprints. To avoid a reoccurrence, this gear was cleaned and a black oxide finish was applied. During the next buildup, fingerprint remover will be used on all main reduction gears prior to assembly. They then will be oiled and handled in the manner prescribed for bearings.

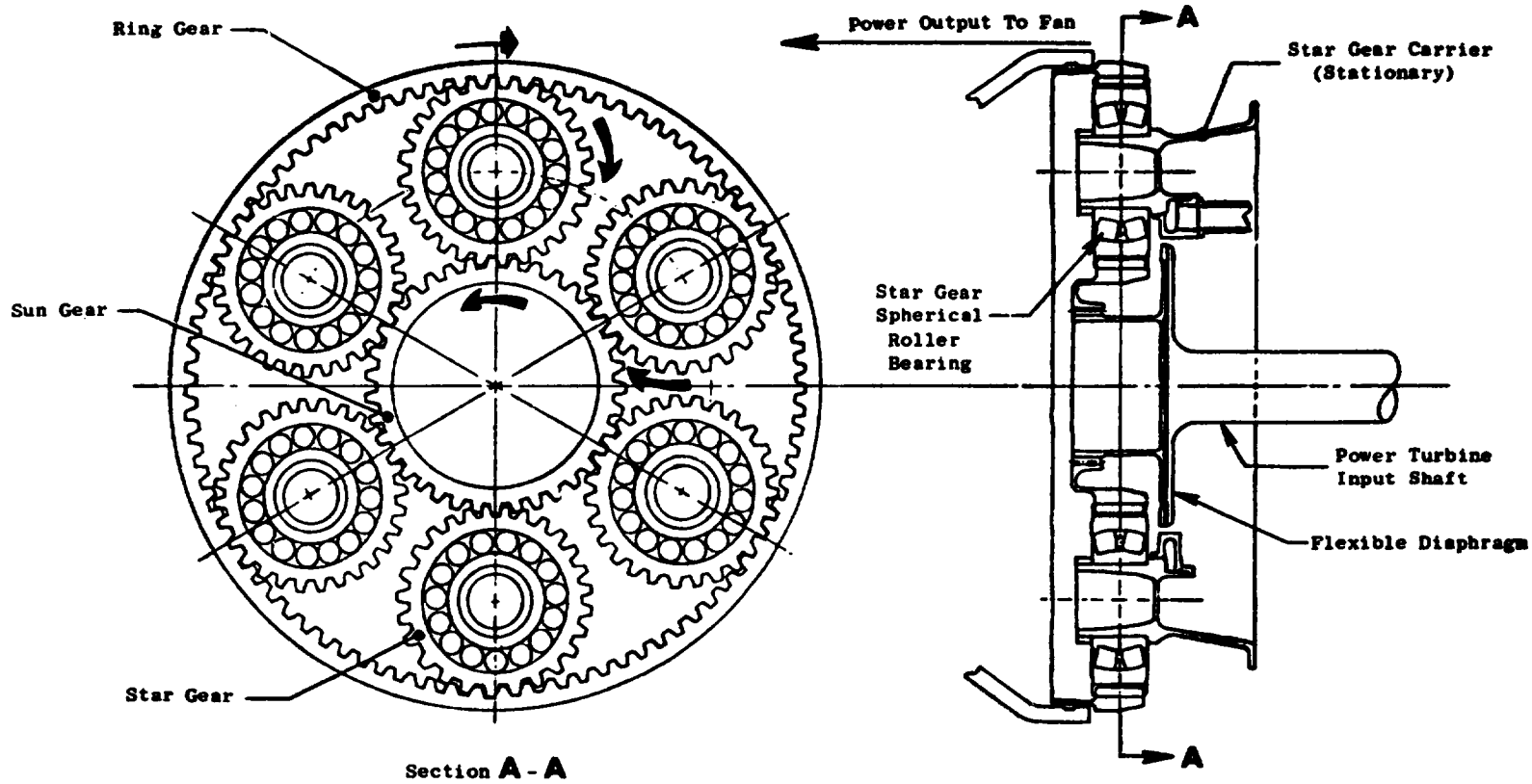

Figure 17. Main Reduction Gear Configuration.

ORIGINAL PAGE IS
OF POOR QUALITY

Table 5. UTW Reduction Gear Design Details.

[Takeoff, 306 K (90° F) Day]
(100% Power, 100% Speed)

Gear Ratio	2.465
Turbine Power	9889 kw (13,256 hp)
Turbine Speed	7747 rpm
Gear Pitch Line Velocity	97.1 m/sec (19,117 ft/min)
Star Gear Speed	10,577 rpm
Bearing Load	33,925 N (7627 lb)
Number of Stars	6
Number of Gear Teeth	
Sun Gear	71
Star Gear	52
Ring Gear	175
Hunting	Yes
Nonfactoring	Yes

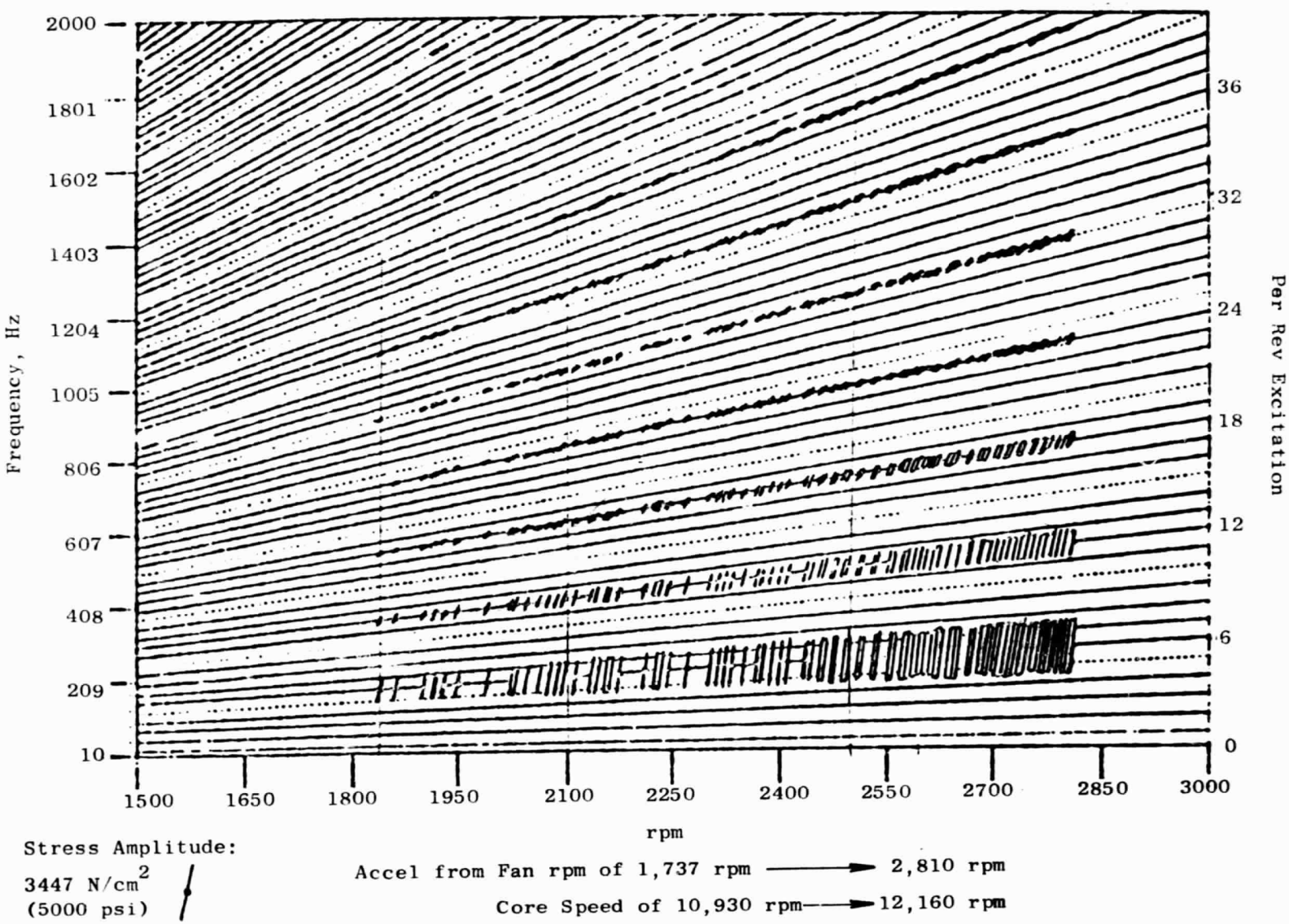

Figure 18. Dynamic Ring Gear Stress Response.

ORIGINAL PAGE IS
OF POOR QUALITY

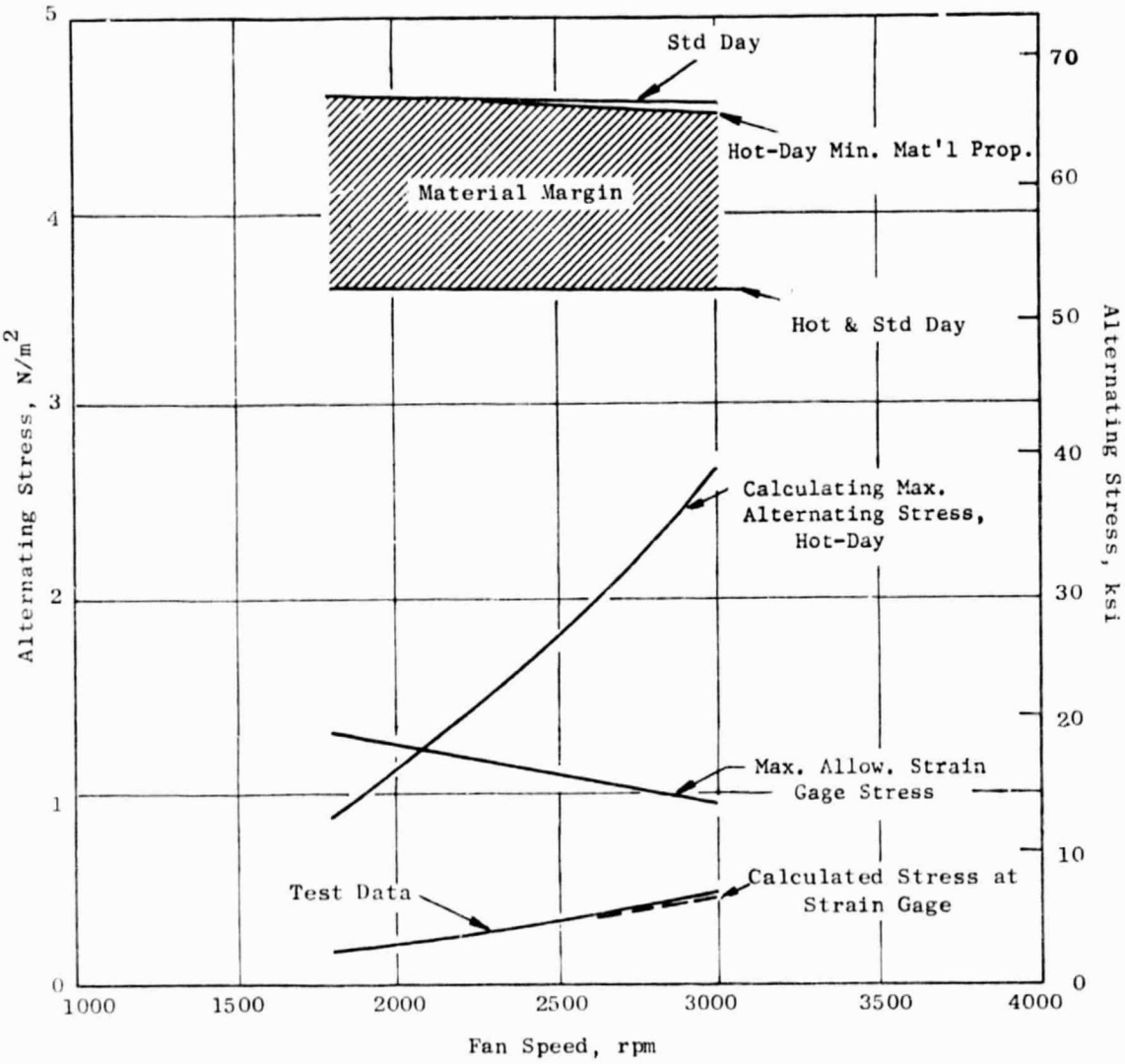

Figure 19. Ring Gear Allowable Stress.

5.2.2 Bearings - One roll was removed from each bearing and both the inner and outer races were inspected. The inner race of two bearings, T14 and T15, showed skidding distress in the loaded zone. The inner race of the remaining four bearings showed no evidence of skidding. It is hypothesized that this defect was caused by the unloading of these bearings during the vibration caused during the nozzle failure incident. In order to reduce cost, the same bearings will be used in the next buildup. The defect will be rotated out of the load zone. Figure 20 shows a typical skid mark. The outer race indicated mild pitting toward the center of the raceway at the edge of the roller track. This is attributed to debris damage. Figure 21 shows the minor extent of the damage.

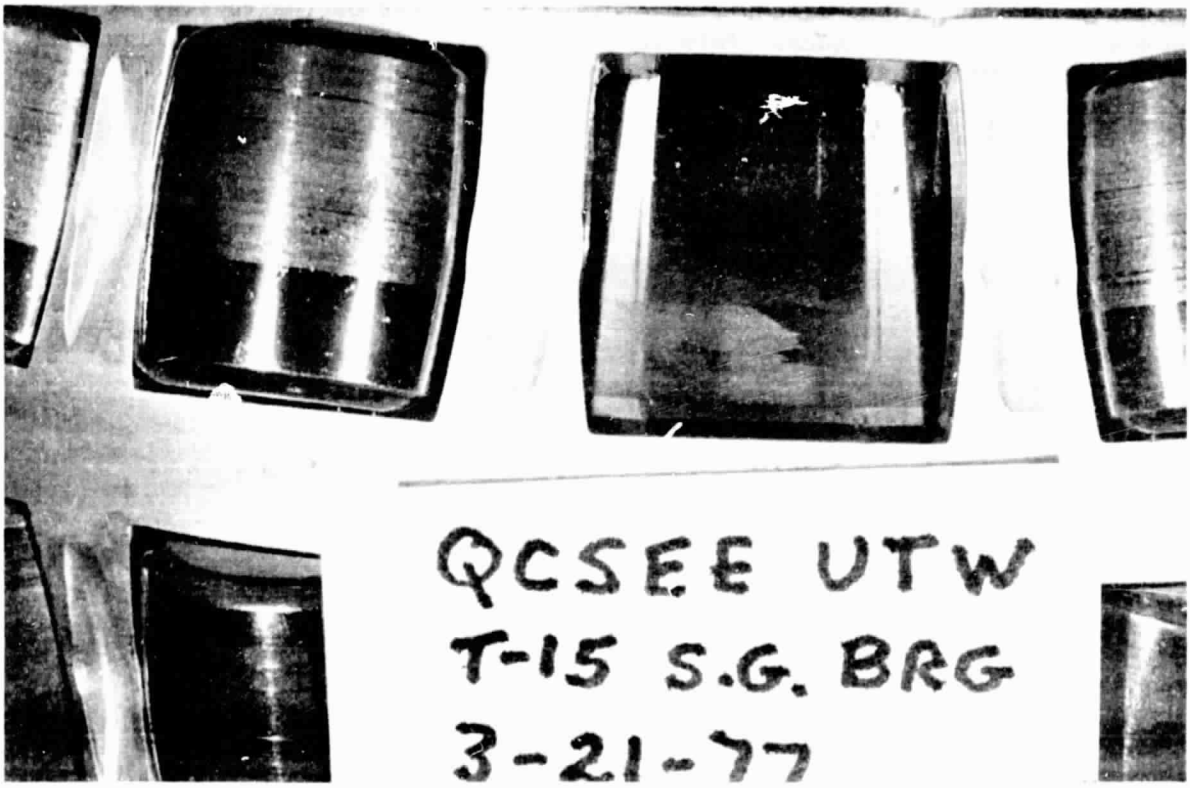

Figure 20. QCSEE UTW Bearing Inner Race Skidding Distress.

ORIGINAL PAGE IS
OF POOR QUALITY

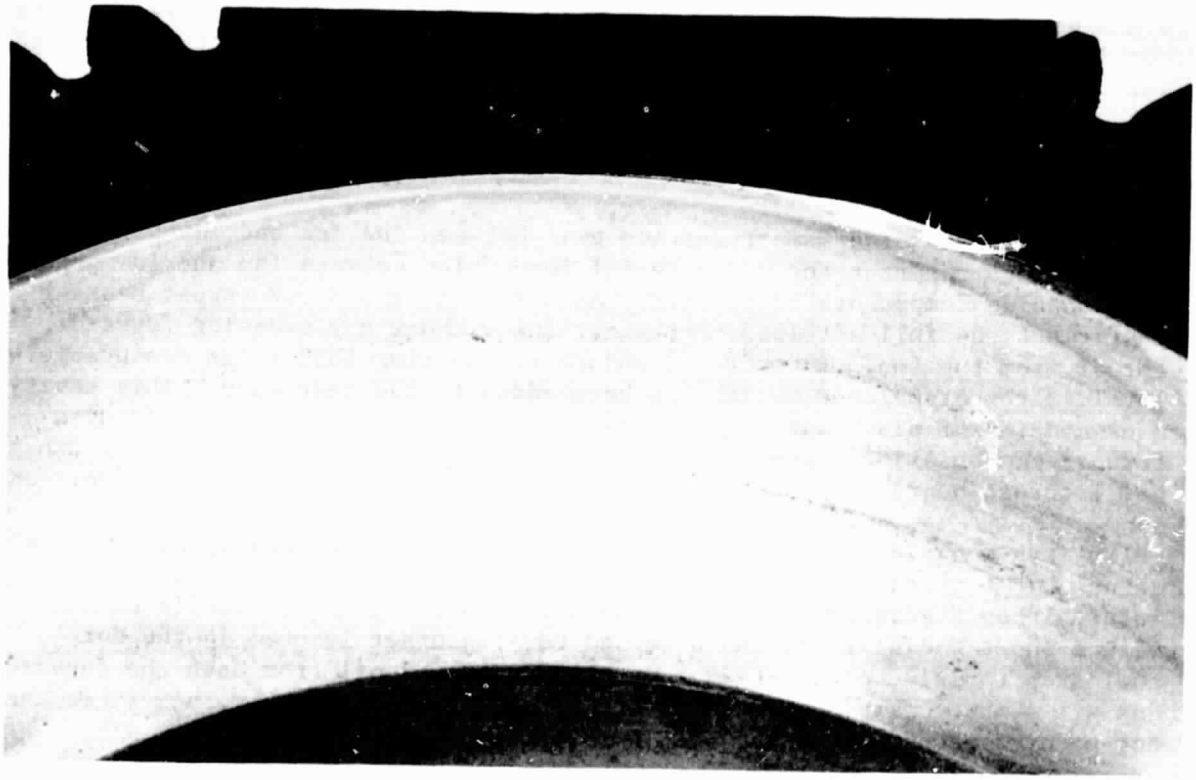

Figure 21. QCSEE UTW Outer Race Debris Damage.

ORIGINAL PAGE IS
OF POOR QUALITY

6.0 LUBRICATION AND ACCESSORY DRIVE SYSTEM

6.1 SYSTEM DESCRIPTION

The UTW engine utilizes six main shaft bearings to support the rotating turbomachinery. The short construction of the concentric UTW rotors permits a two-bearing support system for each rotor. The No. 1B and 1R bearings support the fan rotor. The high-pressure core rotor is supported by the No. 3 and No. 4 bearings. The No. 2 and No. 5 bearings support the low pressure turbine and power transmission shaft. Both the fan and low pressure turbine shaft are soft-coupled to the engine main reduction gear to minimize induced loads on the gears. The thrust bearings have been located in the engine forward sump to provide more precise control of fan and compressor blade clearances.

Application of a main reduction gear between the fan and low pressure turbine requires that the normal axial load "tie" between fan and low pressure turbine components be severed. As a result, the No. 2 thrust bearing must react the full aft load of the turbine without any negating forward thrust from the fan. In order to reduce the bearing load to an acceptable level, a thrust balance cavity has been added to the rear sump. This cavity uses compressor discharge air to pressurize a balance piston, providing a forward-compensating force on the turbine rotor. A high-load-capacity CF6 No. 1 thrust bearing is used in the design to react the fan axial loads.

A top-mounted accessory gearbox is driven from the core by an F101 internal bevel gearset and a long radial drive shaft. An additional F101 internal bevel gearset located in the bottom half of the engine is combined with a short radial shaft and a second bevel gearset located in the core cowl area to drive a vane-type pump that scavenges oil from both the forward and aft sumps. This pump, along with a remotely mounted pump, scavenges the top-mounted accessory gearbox.

The lubrication system is designed on the basis of current dry-sump technology utilizing a circulating oil system. Internal engine and gearbox passages are used wherever possible for oil delivery and return. Venting and pressurization functions also make use of internal engine passages when possible.

6.2 INSTRUMENTATION

Each sump of the QCSEE UTW engine was instrumented as follows to ensure safe operation of the engine:

1) The outer race temperature of each main shaft bearing was measured in two places.

2) The sump pressures and the carbon seal ΔP were measured for each main shaft seal.

3) Temperature in the aft sump cavity was measured.

4) The pressure and temperature were measured in the balance piston pressurization and exhaust cavities.

5) The inner race temperature of each star gear bearing was measured.

6) The lube pressure in the manifold supplying oil to the reduction gearing was measured.

7) The lube supply and scavenge pump discharge pressures were measured.

8) ΔP across the supply filter was measured.

The lube system package was instrumented to measure the following parameters:

1) Oil reservoir lube level
2) Oil reservoir internal pressure
3) Scavenge filter ΔP
4) Scavenge discharge temperature
5) Lube supply temperature
6) Heat exchanger ΔT on oil side
7) Heat exchanger waterflow and ΔT on water side

6.3 TEST EXPERIENCE

The sump and accessory system, with the exceptions of oil leakage from the composite frame sump and an oil flooding problem associated with the top-mounted accessory gearbox, performed well throughout the test phase of the first build of the QCSEE UTW engine. After adding a remote scavenge pump to remove trapped oil from the accessory gearbox, the remainder of the testing was completed with no major problems.

6.3.1 Main Shaft Bearings

Test limits of 450 K (350° F) were not exceeded by any of the main shaft bearings during the majority of the testing. Figures 22 through 24 show representative temperature data for these bearings as a function of engine speed. The No. 2 ball thrust bearing experienced temperatures of 588 K (600° F) on three occasions for very short periods of time before the oil flooding problem was identified in the accessory gearbox. This high temperature was a result of overheated oil discharged from the accessory gear-

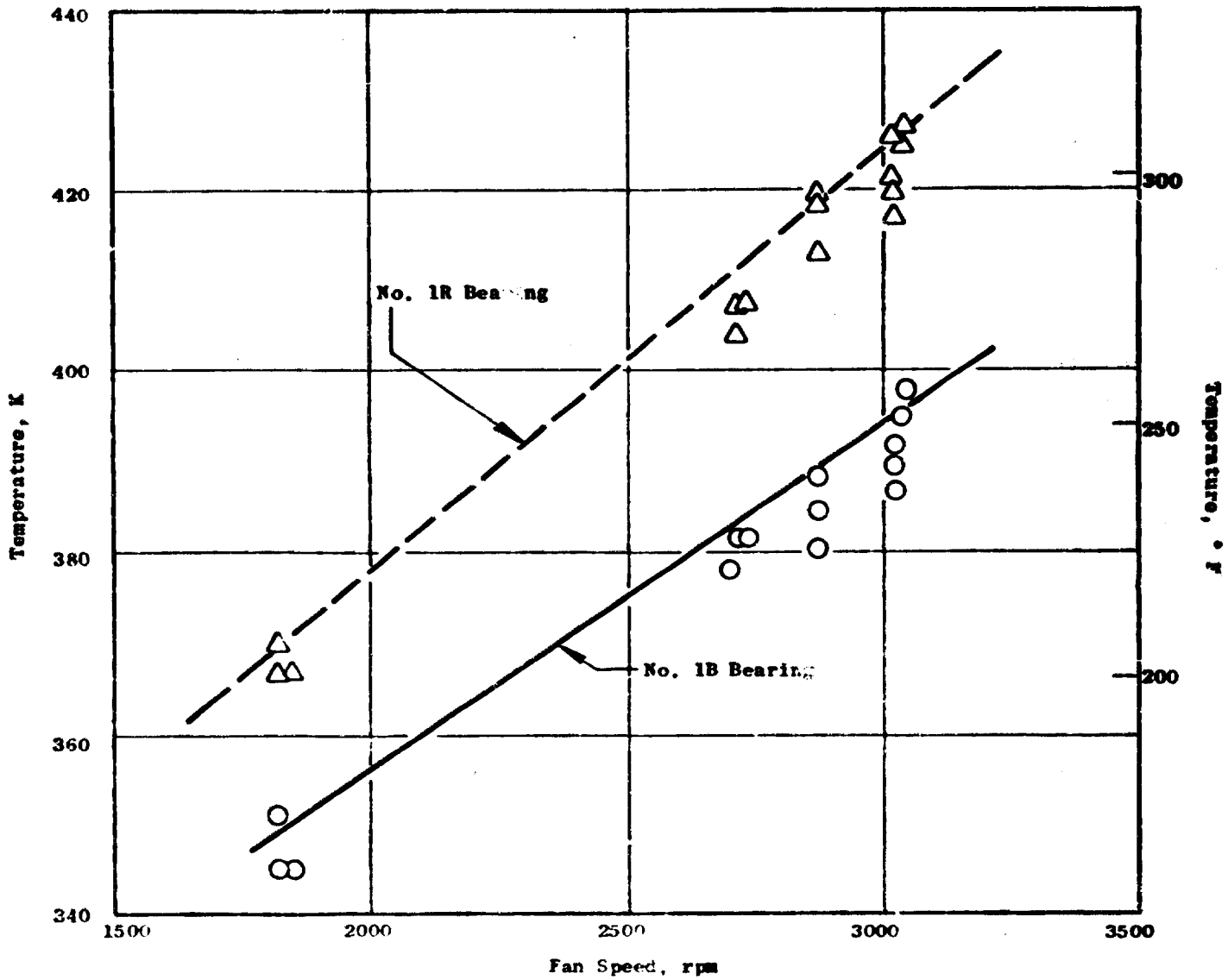

Figure 22. Outer Race Temperature Versus Fan Speed.

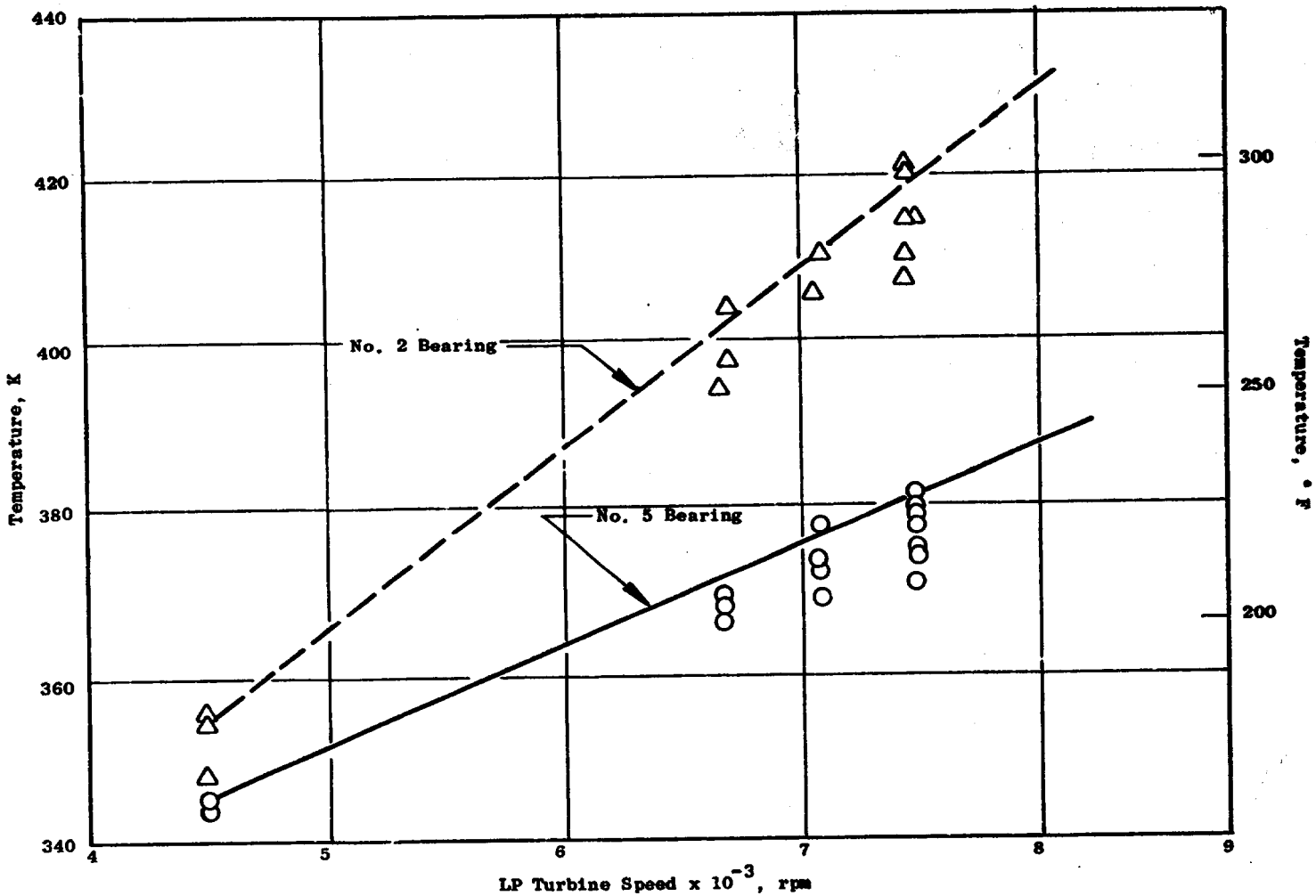

Figure 23. Outer Race Temperature Versus LP Turbine Speed.

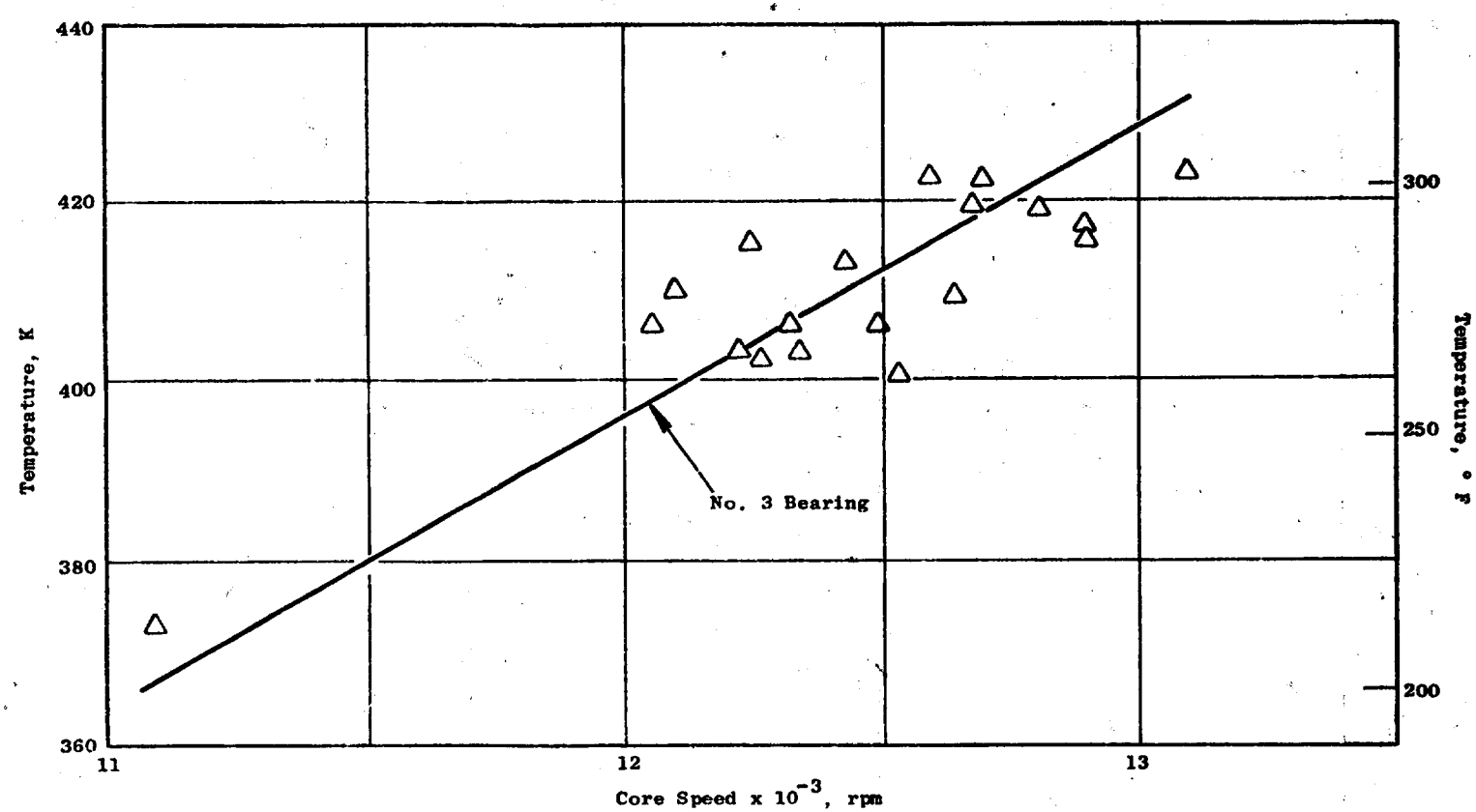

Figure 24. Outer Race Temperature Versus Core Speed.

box. The material of this bearing is M50 which retains its hot-hardness at these temperatures; a borescope inspection did not reveal any apparent damage.

6.3.2 Lube Supply and Scavenge System

Lube discharge pressure as a function of core speed is shown in Figure 25. The actual filter ΔP of 2.76 N/cm^2 (4 psid) was less than the predicted 11.72 N/cm^2 (17 psid), accounting for the difference between the predicted and the measured data. The lube supply pressure to the main reduction gear was as predicted and is shown versus core speed in Figure 25. The bypass valve for all engine testing was adjusted to one-half-turn open to achieve the predicted pressures and flows.

Lube supply temperatures were controlled by varying the water flow to the heat exchanger. For some portions of the high power/speed testing, the maximum flow of 9463.5 cm^3/sec (150 gpm) was required to keep the temperature of the star gear bearings below 402.4 K (265° F).

The scavenge pump servicing the forward sump, aft sump, and scavenge gearbox functioned well, and the combined scavenge temperature during all testing was below 402.4 K (265° F). The scavenge discharge pressure versus core speed is shown in Figure 26 and was close to predictions.

6.3.3 Engine Heat Rejection

Table 6 shows the measured-versus-predicted heat rejection for the QCSEE UTW engine. These data were obtained during the mechanical checkout of the engine. Figure 27 also shows the engine heat rejection as a function of fan speed.

Table 6. Engine Heat Rejection.

	Predicted	Measured
HPT % rpm	87.7%	80.6%
LPT % rpm	94.5%	94.5%
Lube Flow	2157.7 cm^3/sec (34.2 gpm)	2189.2 cm^3/sec (34.7 gpm)
Scavenge Temperature	<380.2 K (<225° F)	<393 K (<248° F)
Lube Temperature	<344.1 K (<160° F)	<331.9 K (<138° F)
Total Engine Heat Rejection	2186 J/min (7453 Btu min)	4673 J/min (15933 Btu min)

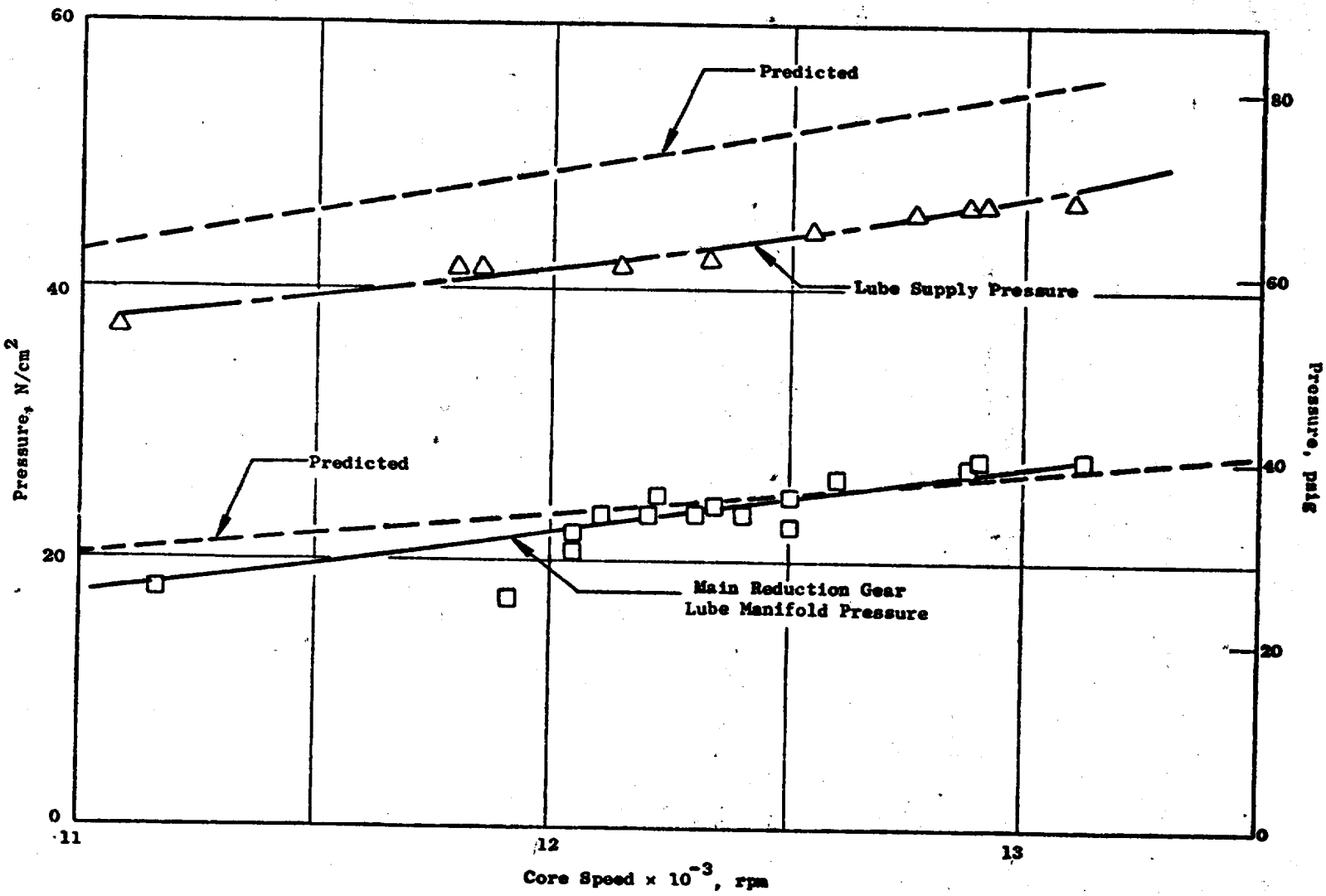

Figure 25. Lube Supply Pressure Versus Core Speed.

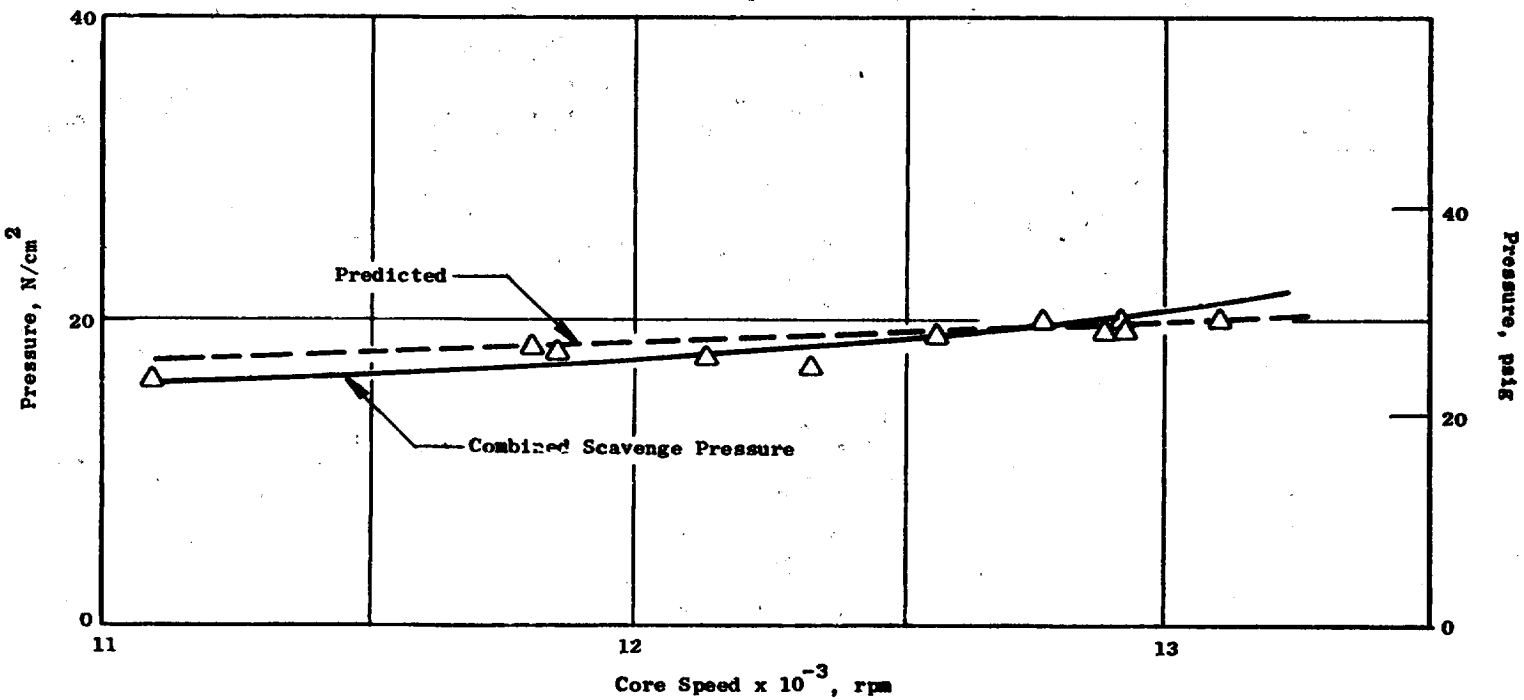

Figure 26. Lube Scavenge Pressure Versus Core Speed.

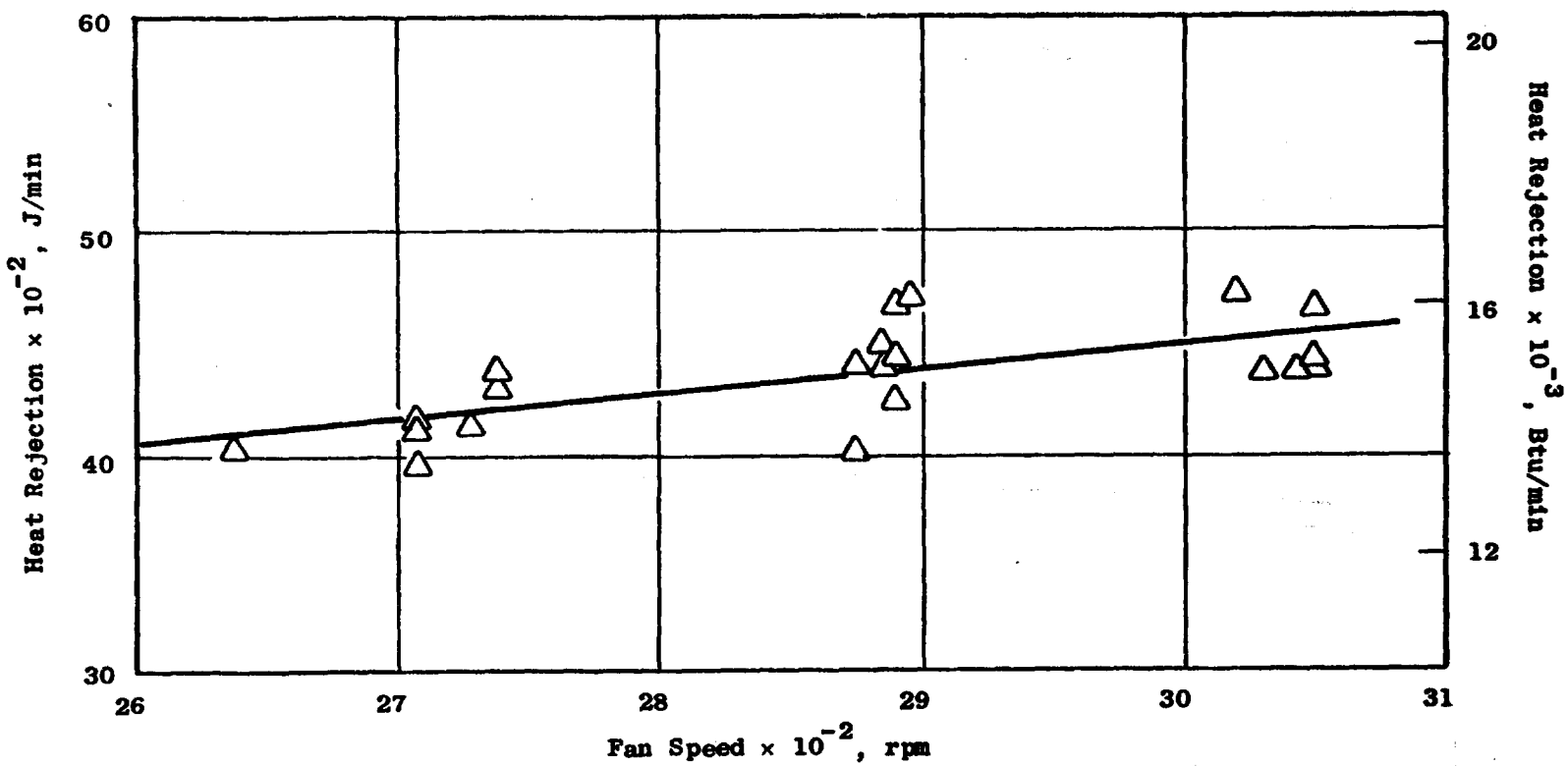

Figure 27. Engine Heat Rejection Versus Fan Speed.

The increased engine heat rejection was caused by lower-than-expected efficiency in the main reduction gears and the added heat load of approximately 587 J/min (2000 Btu/min) for the partially oil-flooded accessory gearbox.

To maintain the main reduction gear, star bearing outer race temperatures below the 402.4 K (265° F) limit, the water flow through the heat exchanger was at the maximum facility capability of 9463.5 cm^3/sec (150 gpm). It originally was calculated that 6309.0 cm^3/sec (100 gpm) with a water inlet temperature of 299.7 K (80° F) would adequately remove the engine heat load. The actual heat exchanger performance also was lower than expected as can be seen from Figure 28. The deficiency of the heat exchanger is believed to be caused by any or all of the following:

1) Viscous maldistribution of oil flow across the heat exchanger tubes. Cold tube walls resulting from high water-side heat transfer and cold 283.6 K (51° F) water temperature cause a thick boundary layer buildup of oil on tubes and increase the influence of dead zones (low oil flow) in the heat exchanger. This results in an insulated tube wall and ineffective oil-side heat transfer area.

2) Air trapped in the upper portion of the space between the oil baffles preventing the tube bundle from being completely submerged in oil.

3) Air and oil flows are separated into a "slug" flow, rather than a homogeneous mixture, which decreases the overall effectiveness.

It was planned to install a second heat exchanger in series with the existing one, but the engine testing was terminated before this could be done.

6.3.4 Lube System Problems

Early in the QCSEE UTW testing, several lube system problems were uncovered. These manifested themselves in the following manner:

1) Oil loss through the fan frame sump walls and associated cavities into the fan airstream. This was especially prevalent at high speeds (>2700 rpm).

2) Rapid decrease in lube tank level.

3) Rapid increase in No. 2 and radial drive shaft bearing temperatures when reducing to idle speed after a decrease in oil level.

An LM2500 eductor was installed on the accessory gearbox overboard vent to reduce the sump pressures approximately 0.69 N/cm^2 (1 psi) below ambient. Extensive sealing of fan frame struts was required to eliminate oil leakage

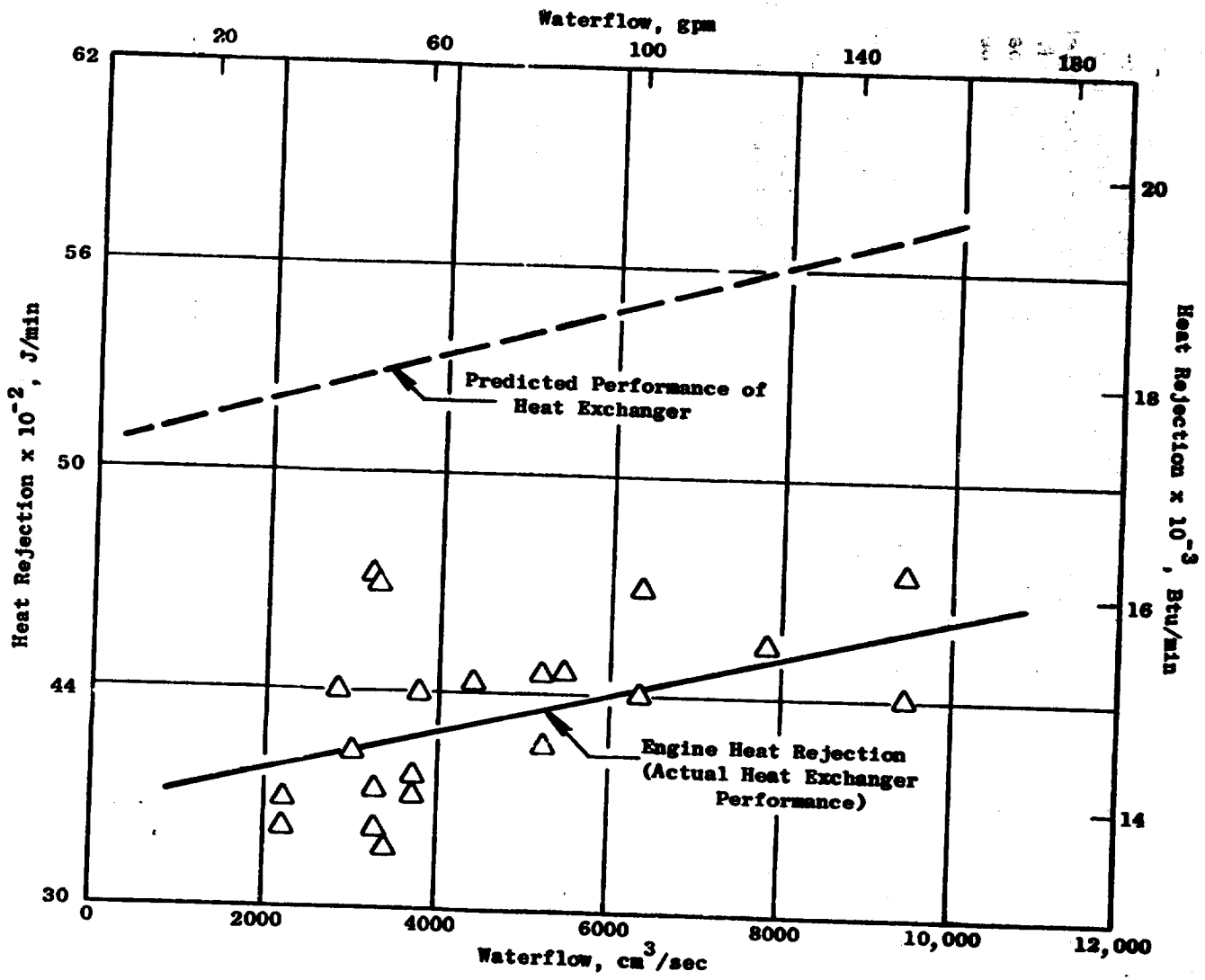

Figure 28. Heat Rejection Data.

into the airstream. After the fan frame was sealed, the problem of decreasing lube level associated with an increase in No. 2 bearing temperature still persisted. The possible causes were identified as:

1) Oil flooding the forward sump causing the No. 2 bearing temperature to increase.

2) Oil flooding the top accessory gearbox with the No. 2 bearing temperature rise caused by hot oil draining past it when reducing speed to idle.

3) Oil flooding of accessory gearbox caused by extensive oil flow in the lube tank vent line to the gearbox.

Additional engine instrumentation was added to isolate the problem area. This instrumentation, in a subsequent engine test, showed that the gearbox surface temperature increased as the oil level decreased, revealing the problem to be oil flooding of the accessory gearbox above 11,600 rpm core speed.

The two oil tanks were replaced by a single larger tank to increase oil capacity and to more accurately determine the oil level. Also, a 630.9 cm^3/sec (10 gpm) Viking scavenge pump was installed for the accessory gearbox. A scavenge port was drilled into the side of the accessory gearbox and piped to the remote scavenge pump. A tube had to be added which relocated the oil pickup point inside the housing to the other side of the gearbox before the mechanical checkout could be completed. The scavenge pump discharge was piped directly to the lube tank. The maximum temperature of the accessory gearbox scavenge oil reached 460.8 K (370° F) at the maximum core speed attained (13,150 rpm).

6.3.5 Posttest Inspection

The accessory gearbox was disassembled and inspected at the completion of testing. The inspection revealed that the excessive heat generated by oil churning during flooded operation had discolored the gears and bearings. Several seals had failed from overtemperature, the casing had warped out of flatness limits, and several of the gears had lost some of the required case hardness. These parts will be replaced, and modifications to the baffles will be made prior to the next buildup. Also, the eductor will be eliminated to permit proper scavenging.

7.0 FAN FRAME

The QCSEE integrated fan frame is a graphite/epoxy structure that incorporates the fan casing, fan bypass vanes, and core frame. It provides the primary support for the engine and is 2.00 m (78.8 in.) in diameter, 0.9525 m (37.5 in.) in length and weighs 315.2 kg (695 lb) (at engine assembly) not including the engine mounts.

The frame initially was instrumented with a total of 11 strain gages. Eight of these were located in the engine mount area as shown in Figure 29. The other three gages were located on the fan bypass vanes as shown in Figure 30. An electrical check just prior to engine operation showed that gages 1 and 11 were open, leaving nine gages to be monitored during the test.

None of the gages in the mount area showed any significant response during engine operation. This was expected since normal operating loads are quite low compared to the five-blade-out loads for which the structure was designed. The highest stress observed during engine test was only 2% of the ultimate strength of the material. Stresses that low cannot be detected on the engine monitor scopes.

The only frame gages showing any activity during engine operation were the two working gages on the bypass vanes. All observed stresses on these vanes were low, less than 4% of the ultimate strength of the material at the worst case of 95% fan speed, an A18 of 1.87 m^2 (2900 $in.^2$), and a blade angle of -5°. These stresses were caused by a 2/rev forced input. The stresses became less as A18 was decreased and/or the blade angle moved from negative angles toward positive angles.

It was possible, by increasing the scope sensitivity, to detect the vane natural frequencies (first flex only) as they were excited by a fan 18/rev. These frequencies were lower than expected based on bench testing of a single vane. It is probable that the actual end fixity of the vanes is somewhat less than it was for the bench test specimen which had its ends cast in Devcon (a filled epoxy). The bench test results are shown in Figure 31 along with the natural frequency data obtained during engine running. The "open-2" expected values shown in Figure 31 were analytically extrapolated from the "closed-2" bench test data. Stresses increased momentarily as the fan speed passed through these frequencies but never exceeded 4% of the ultimate strength capability.

The only problem encountered with the fan frame during engine testing involved oil leakage from the sump. During initial checkout of the engine, oil was seen coming from the splitter area and between the fan rotor aft spinner and the fan OGV assembly. Initial checks indicated that the leak originated in the scavenge strut in the forward sump which allowed oil to get into the six o'clock core strut and, hence, into the aft fan rotor cavity through the access hole for the No. 1 seal drain tube. This leak

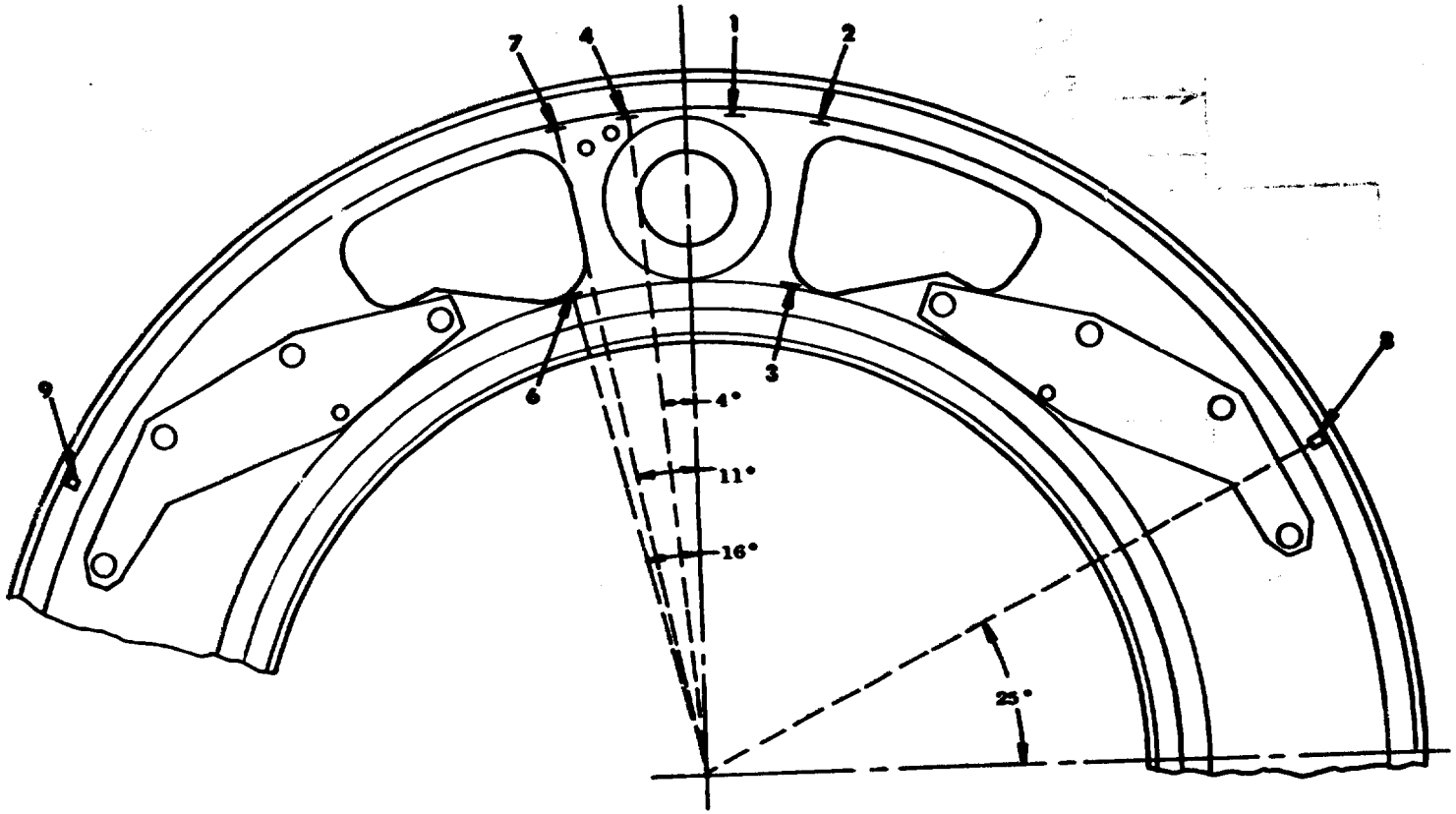

Back of Aft Wheel Splitter Ring - Mount Area

Gages are Symmetrical About Vertical Centerline

Note: Gages 8 and 9 are located on the fan flow splitter surface 10.16 cm (4 in.) forward of the vane trailing edge.

Figure 29. Strain Gage Locations for UTW Fan Frame, Mount Area.

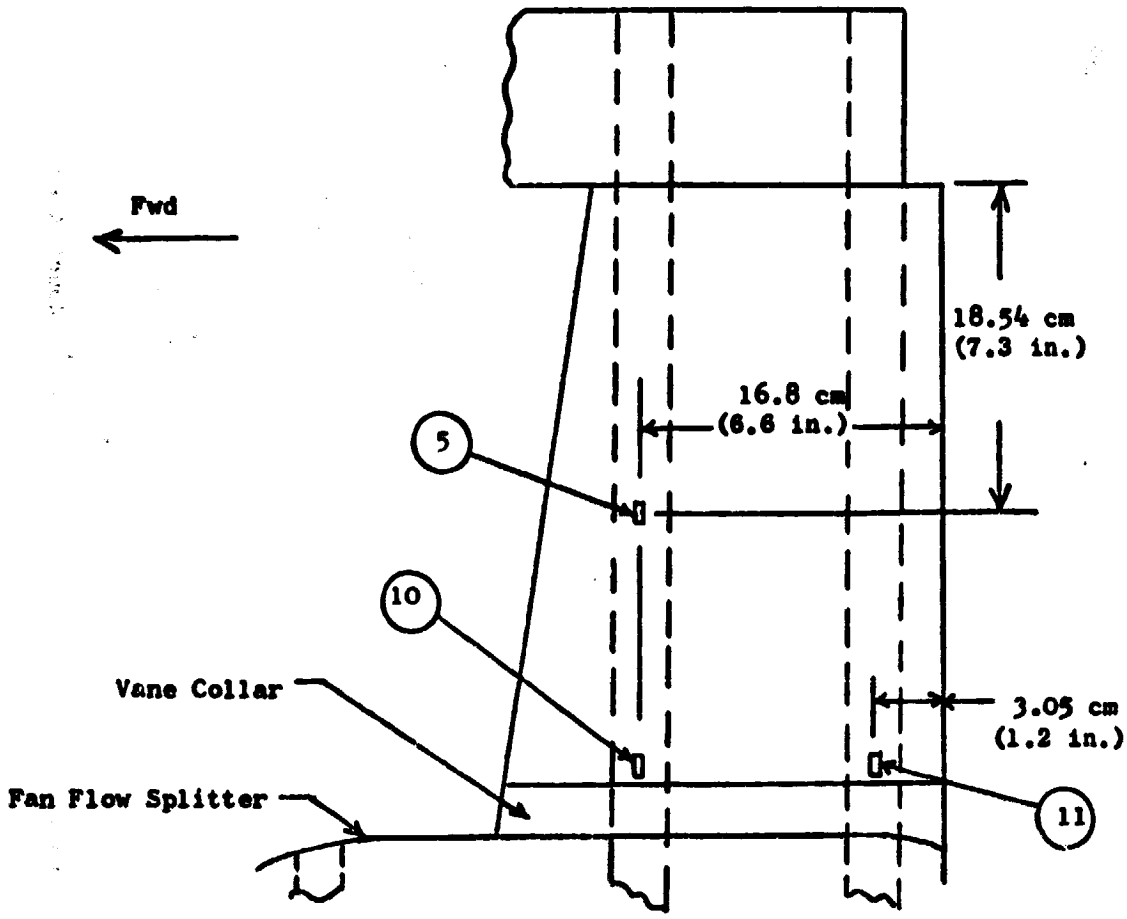

NOTES:

1. All gages are on the concave side of the vane.
2. Gage 5 is on vane 2 (clockwise, aft looking forward)
3. Gages 10 and 11 are on vane 26

Figure 30. Strain Gage Locations for UTW Fan Frame, Bypass Vanes.

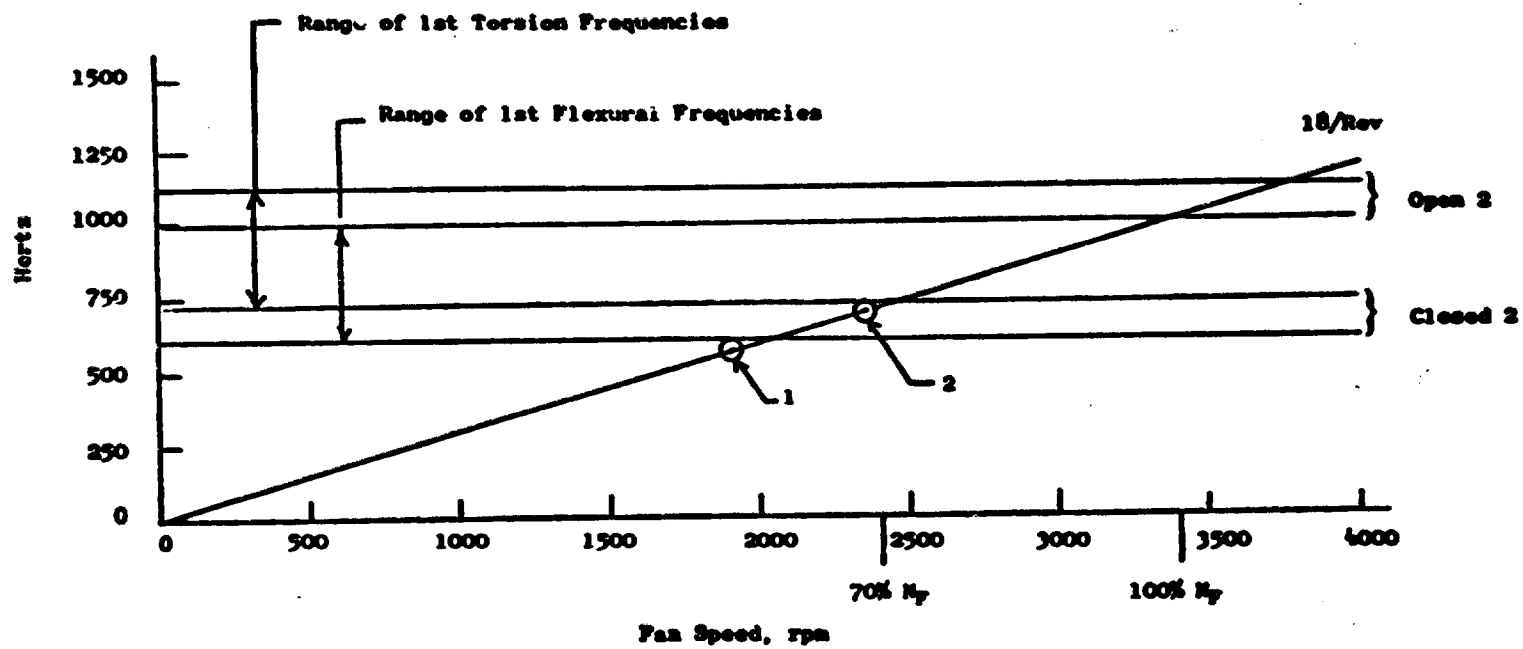

Natural Frequencies for the Closed-2 Vane Were Obtained from Bench Tests.

Natural Frequencies for the Open-2 Vanes Were Extrapolated from Closed-2 Data Analytically.

Results of Engine Tests:

1. Closed-1 Vane First Flex at N_F = 1900 RPM and 570 Hz.
2. Open-2 Vane First Flex at N_F = 2350 RPM and 704 Hz.

Figure 31. Natural Frequencies of QCSEE Bypass Vanes.

also allowed an accumulation of oil in the frame splitter leading edge. Since the source of the leak inside the sump was inaccessible without major engine disassembly, it was decided to block the leakage into the aft fan rotor cavity by filling the area around the seal drain tube where it enters this cavity, using Furane 9210 adhesive, and attempting to control the oil leaking into the splitter leading edge with an eductor. The eductor was installed by cutting the No. 1 seal drain tube where it passes through the splitter leading edge and attaching the eductor to the external end of this tube. A hole had to be made in the splitter to accomplish this; the splitter then was patched with glass cloth and sealed with adhesive. After this repair, the sump was checked by pouring oil into the sump. The aft rotor cavity stayed free of oil. Oil did go into the splitter leading edge and drained out the modified seal drain line through the eductor.

Mechanical checkout was continued after the above repair was completed. Attempts to run above 2750 rpm had to be aborted due to increased oil loss which appeared to be coming from the fan frame splitter in the four o'clock core strut area in the fan discharge. A visible oil plume was seen above this speed and the engine had to be shut down. The frame was checked completely by introducing helium into the sump and detecting where it exited the frame. Based on this check, the following repairs were made:

1. All core strut leading edges and the entire 360° splitter leading edge were filled with Furane 9210 adhesive.

2. The forward core strut cavities, between the forward internal frame wheel and the midwheel of all struts except the six o'clock strut, were partially filled with GE Silicone 560 RTV and then filled with Furane 9210 adhesive.

3. The aft core strut cavities between the midwheel and the aft wheel of the sturst at 2 o'clock, 4 o'clock, 8 o'clock, and 10 o'clock were filled with GE Silicone 560 RTV.

4. Approximately 50 cm^3 (3 $in.^3$) of RTV was added to the 12 o'clock aft core strut cavity. This strut was not filled in order to prevent overtemperature of the radial drive shaft during engine operation.

5. The No. 1 seal drain tube was respliced so that it again performed its primary function. The eductor was removed and the splitter repatched.

Another helium check indicated that the above repairs were successful in sealing the oil leaks. No more frame oil leaks occurred during the remainder of the engine run.

During the later runs of the engine, there was some oil leakage where the auxiliary gearbox mates with the frame housing containing the radial drive and oil drain tube. Subsequent disassembly showed that the "O"-ring seal in this area had been destroyed due to accessory gearbox overtemperature. The "O"-ring will be replaced.

A failure of the fan nozzle hinge ring occurred during reverse running, allowing one of the fan nozzle movable doors to be ingested into the fan bypass duct. Debris from this failure went forward through the fan causing extensive damage to the fan blades. The fan frame was impacted at numerous points with debris from both the primary failure and the secondary blade failures. Damage was relatively minor. Two struts were struck on the trailing edge and one strut on the leading edge. Damage was limited to the leading and trailing edge fairings and does not extend into the primary structure. The fan casing acoustic treatment had numerous holes punched in it but nothing went through the casing. In addition, the fan tip treatment was damaged locally. All damage appears to be easily repairable by filling and patching.

In summary, no structural problems or unexpected stresses were encountered during engine testing. The vane natural frequencies were somewhat lower than predicted and caused no problems. Several oil leaks were found in the frame during engine operation but these were repaired on the test stand. Damage sustained during the fan nozzle failure was minor and easily reparable.

8.0 NACELLE COMPONENTS

8.1 INLET

Testing of the UTW engine was done with two boilerplate inlet configurations. The NASA Quiet Engine "C" bellmouth inlet was used for aerodynamic engine mapping and baseline acoustic evaluation. A hybrid inlet which featured an elevated throat Mach number and multiple-acoustic-suppression design capability was employed for the aeromechanical and acoustical evaluations. Both inlets were decoupled mechanically from the engine by use of the Soft Mount Assembly (ref. Drawing 56J119656) to prevent overload of the composite fan frame due to excessive engine motion/vibration. The Soft Mount Assembly providing the decoupled joint is shown in Figure 32. It incorporates an air seal provided by an open-cell foam (Scottfelt), an acoustic seal provided by a lead foil in a vinyl cover, and provisions for mounting acoustic suppression panels.

Posttest inspection (after 43 hours of engine running time) of the Soft Mount Assembly revealed cracks in 9 of the 48 welded bosses that support the hardwall and acoustic panels which are immediately in front of the fan rotor blades. One of the eight hardwall panels that had been in operation for six hours since it had last been inspected also sustained extensive damage. It was concluded that the panel damage was due to an unpredicted hostile operating environment in the close proximity of the fan rotor blades and that the supporting structure damage was due to that same environment with one additional contributing factor. All of the cracked bosses were in the same row of 24 which are nearer the fan rotor and had been only partially welded. The remaining row of 24 bosses had been welded correctly (all around) and none showed any distress. The cracks had all originated at the stress concentration created at the terminal edge of the incomplete weld.

The hardwall and acoustic panels have been replaced with solid aluminum panels. The cracks were stop-drilled, ground out, and welded to prevent any future propagation. The remaining bosses that support the panels were welded properly to prevent additional cracks on future tests.

8.2 CORE COWL COOLING

The core cowl employed a cooling system utilizing pressurized shop air in conjunction with radiation shields and bleed air from the fan duct. This system was designed to adequately cool the cowl area and ensure a safe operating environment for the epoxy resins that were used in the construction of the acoustic and hardwall panels.

The bleed air from the fan duct is only used in the cavity forward of the engine firewall, and was incorporated into the boilerplate nacelle in order to obtain cooling information for the composite core cowl. The pres-

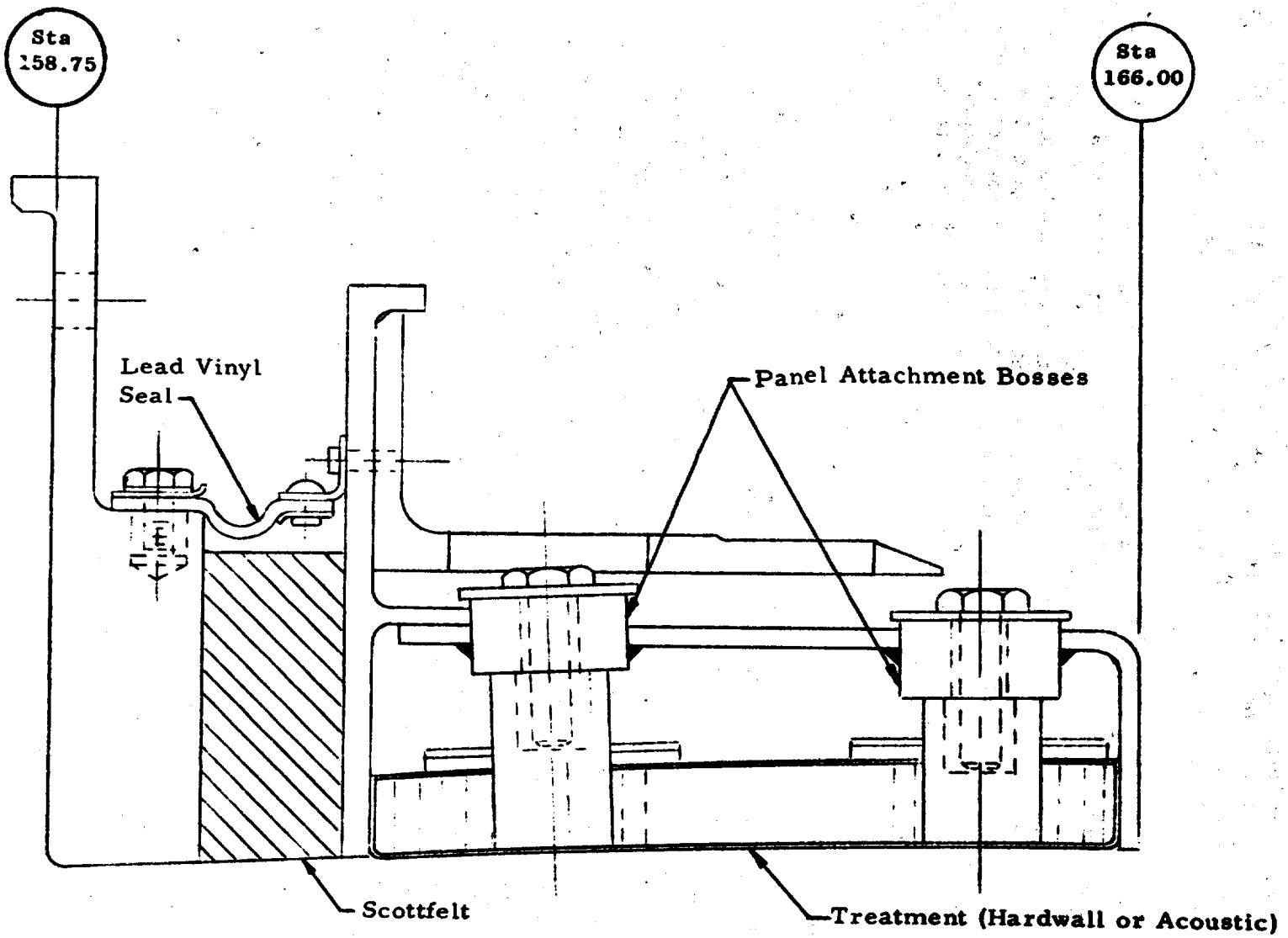

Figure 32. Inlet Decoupling Joint.

surized shop air cooling system is divided into forward and aft circuits with individual airflow controls (Figure 33). Cooling was accomplished by distributing the air around the plenum chamber and using the gap between the structural shell and the radiation shield to meter the cooling flow.

The cooling flow requirements were established by allowing a maximum structural shell skin temperature of 394 K (250° F) in the region of the removable panels. Thermocouples, mounted to the inside surface of the structural shell and spaced around the circumference, verified that the actual skin temperatures were within this limitation. Air thermocouples located aft of the firewall, however, measured temperatures above the predicted limit of 843 K (500° F). Since these temperatures are supplementary information only, that provide backup data for the core cowl cooling, it is inconsequential that they exceeded the limit. Overall, the cooling scheme appears to be satisfactory.

8.3 FAN EXHAUST NOZZLE

The only composite nacelle components that were installed for the UTW boilerplate nacelle testing were the variable fan exhaust nozzle and its mounting ring. The fan exhaust nozzle is a fully modulating, variable flap-type capable of providing various areas for forward thrust and also of flaring outward to provide increased area for inlet flow to the variable-pitch fan in the reverse thrust mode of operation. The nozzle consists of four hinged flaps, each 44.96 cm (17.7 in.) axially from hinge centerline to trailing edge. The upper flaps are 83.7° wide and the lower flaps are 84.5° wide. The flaps were attached to the mounting ring by means of hinges, each flap having a pair of hinges 30.5 cm (12 in.) apart at the flap centerline along the flap forward edge closeout. The flaps were connected to the actuation system in the outer cowl doors by links and link clevises which were located outboard of each hinge. Figure 34 shows the nozzle schematically. Located along the axial edges of each flap were seal assemblies which were designed to give full sealing up to a nozzle area of 1.678 m^2 (2600 $in.^2$). From this point to the full-reverse flap position, the seals disengaged. The flaps were of a full-depth aluminum honeycomb construction with Kevlar facings on the outer surface and graphite/epoxy facings on the inner (fan stream) surface.

The mounting ring to which the flap hinges were attached was of graphite/ epoxy construction and was an adaptation of the ring as it was originally designed for use with the composite, outer cowl door to be built for the second engine build. To adapt this ring to fit on the boilerplate outer cowl doors, the forward portion of the ring had to be slabbed off so that it would be flush with the aft edge of these doors. The ring then was bolted to the cowl doors. The differences between the ring as originally designed for use in the composite cowl doors and the modified ring as used with the boiler plate cowl doors are shown in Figure 35.

The only instrumentation associated with the variable fan nozzle was on one of the actuator rods which indicated actuator position and, thus, nozzle areas.

FOLDOUT FRAME 1

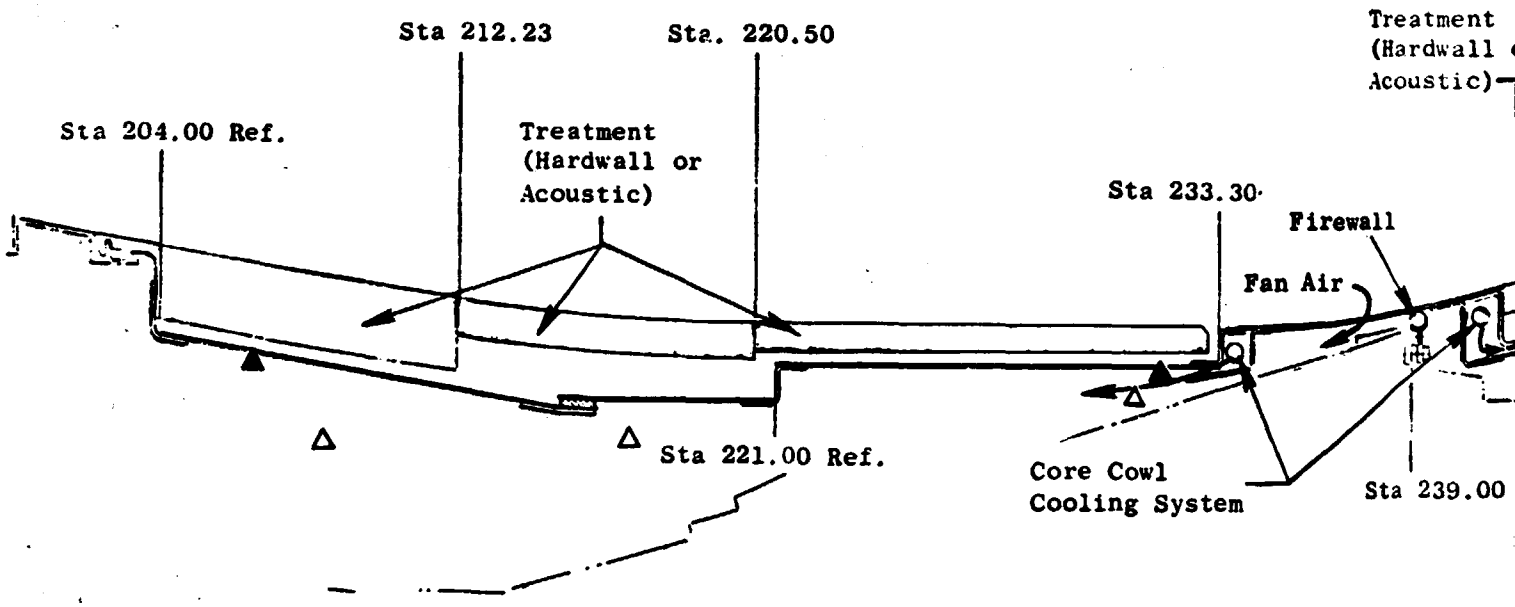

Figure 33. Core Cowl Assembly and

ORIGINAL PAGE IS
OF POOR QUALITY

FOLDOUT FRAME 2

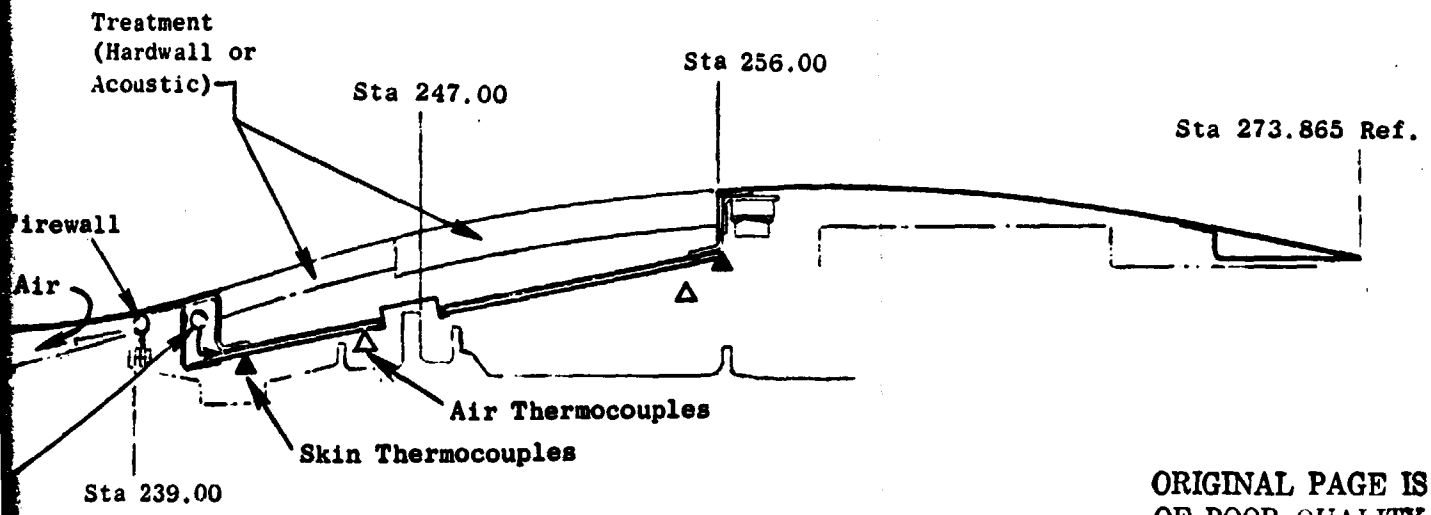

ORIGINAL PAGE IS
OF POOR QUALITY

1 Assembly and Cooling Air System.

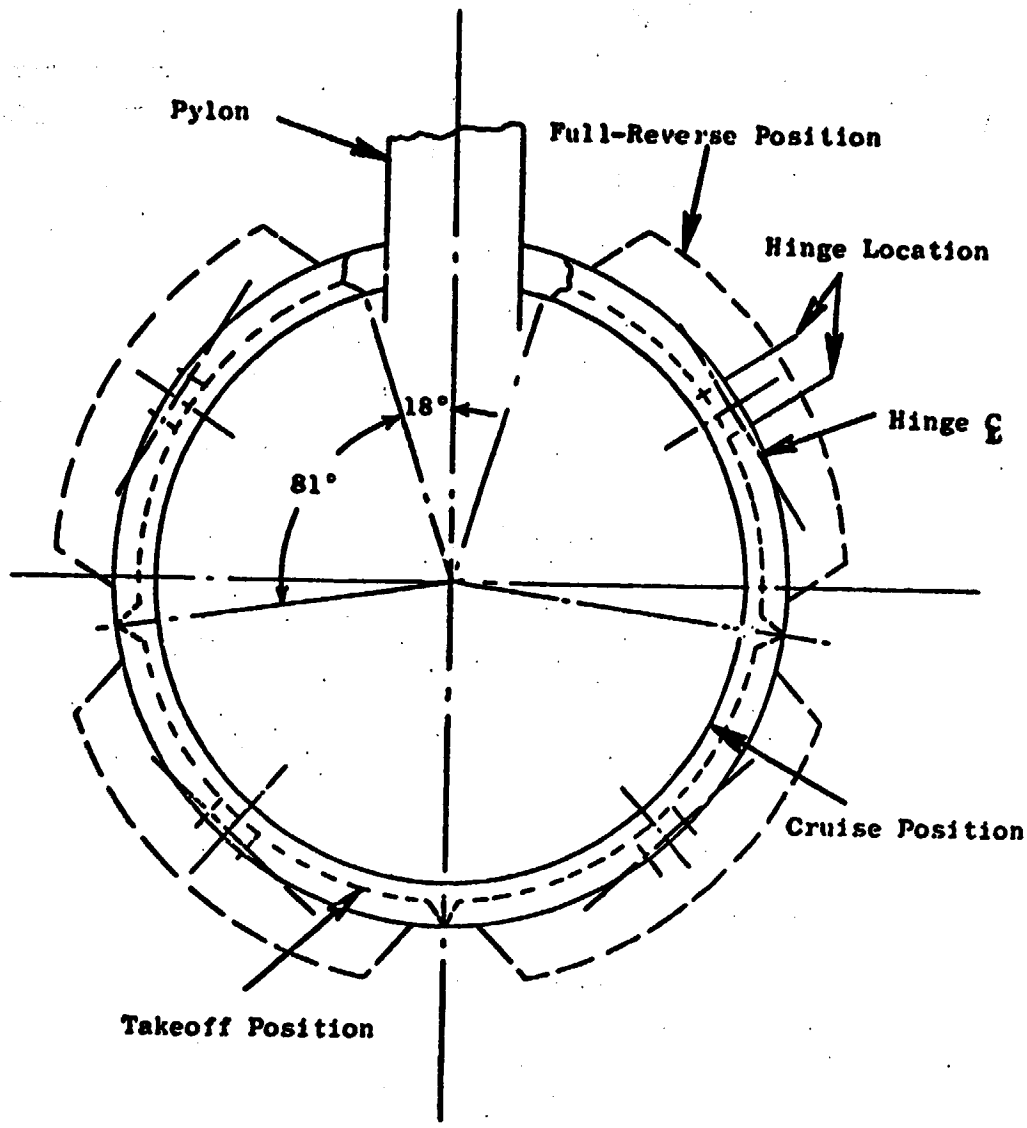

Figure 34. Flare Nozzle Flap Schematic.

ORIGINAL PAGE IS
OF POOR QUALITY

PRECEDING PAGE BLANK NOT FILMED

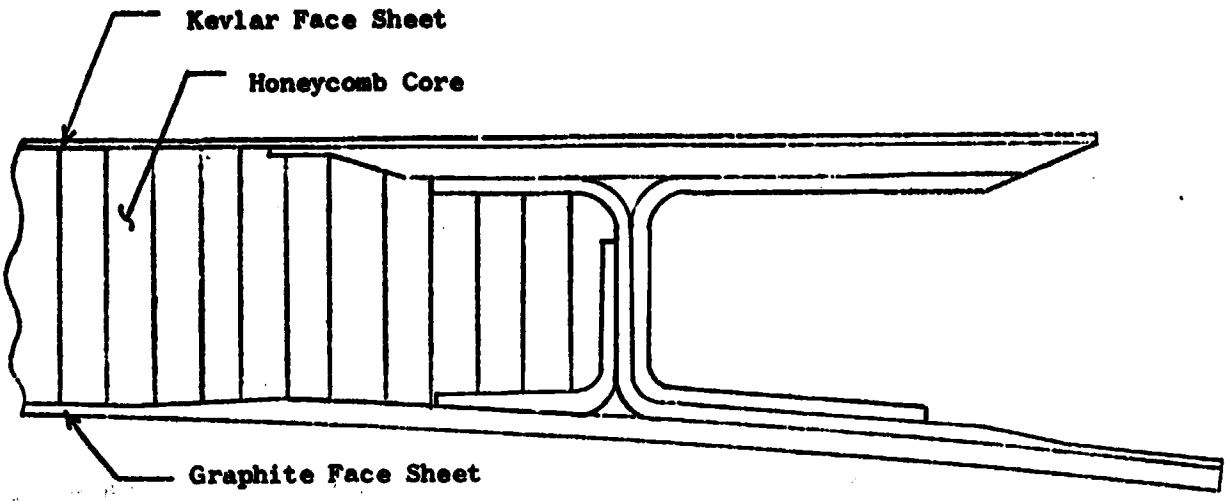

Fan Nozzle Mounting Ring Installed
In
Composite Outer Cowl Door
(All Bonded Construction)

AFT

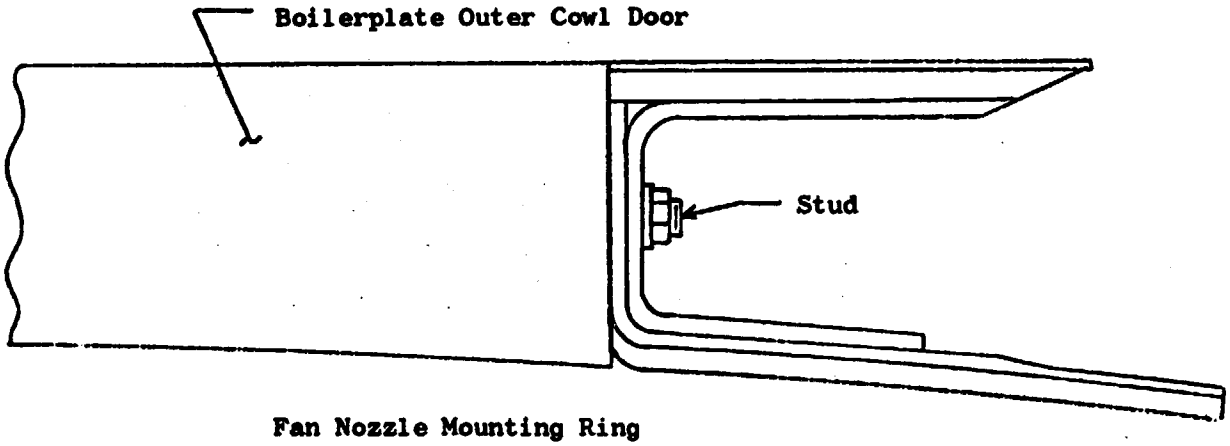

Fan Nozzle Mounting Ring
As
Adapted and Installed
On
Boilerplate Cowl Door

Figure 35. Fan Nozzle Mounting Ring Installations.

No problems were encountered with the fan nozzle in any of the forward thrust testing. During a hold in the reverse mode testing with the blades at -100° and holding fan rpm at 3000, the lower right-hand fan nozzle flap and the mounting-ring lower quadrant to which it was attached were torn loose from the fasteners holding the ring to the boilerplate outer cowl door; the ring portion separated from the upper quadrant at the upper edge of the cutout for the midactuator to the upper flap link. The ring circumferential seal, along with several of the graphite laminations, was torn loose from the upper quadrant and was still attached to the ring lower quadrant in one piece; this portion of the ring was still being attached to the lower right-hand flap by means of the flap hinges. The portion of the ring lower quadrant between the midactuator/upper flap-link cutout and the first axial ring fastener below the horizontal was separated from the rest of the lower quadrant. Both of the lower right-hand flap-link rod ends were severed in the thread area, the rod ends remaining attached to the flap. The severed flap and the portion of the mounting ring still tied to it were ingested into the fan flowpath and lodged against the acoustic splitter support struts. The lower axial seal was missing, as was approximately the last 10 cm (4 in.) of the upper axial seal. These apparently went forward through the fan. As the flap was being ingested, it struck the core nozzle breaking out a portion of the flap trailing edge approximately 63.5 cm (25 in.) wide and 15.2 cm (6 in.) long. The remainder of the trailing edge delaminated. Primary cause of the failure was the pulling of the fasteners, attaching the nozzle mounting ring to the boilerplate outer cowl doors, through the mounting ring material. All damage to the flap itself appears to be of a secondary nature caused by the primary failure.

9.0 DIGITAL CONTROL SYSTEM

The QCSEE UTW engine control system included both automatic and manual operating modes. Most of the engine testing to date has been under manual control wherein:

1. Fuel flow (W_F) was modulated to hold a demanded fan speed, regulated core idle speed, or a calculated maximum turbine inlet temperature.

2. Fan exhaust nozzle area (A18) was modulated to hold a demanded position.

3. Fan blade angle (βF) was modulated to hold a demanded position.

4. Core stator position (VSV) was scheduled as a function of corrected core speed.

The manual mode was provided to allow independent manipulation of the controlled variables so that engine characteristics could be completely explored. Limited testing was done in the reverse operating mode. In this condition, the control mode is the same as the manual mode except for the transient from forward to reverse.

The system also contained provisions for monitoring and displaying 48 engine and control variables, for detecting certain malfunctions, and for taking corrective action in the event of certain critical malfunctions such as loss of LP turbine load, high vibrations, loss of fan speed signal, and certain digital computation faults. The engine control system hydromechanically provided protection against core rotor overspeeds and compressor discharge overpressure.

9.1 GENERAL SYSTEM DESCRIPTION

A schematic diagram of the QCSEE UTW Control System is shown in Figure 36. The digital electronic control was the heart of the system and controlled the manipulated variables in response to commands representing those which would be received from an aircraft propulsion system computer. A photograph of the engine-mounted digital control is shown in Figure 37. The system included a modified F101 hydromechanical control. This control included an electrohydraulic torque motor servovalve through which the digital control maintained primary control of fuel flow. The fuel-operated servomechanisms in the hydromechanical control served primarily as backup fuel controlling elements and limits although they were the primary controlling elements for the core compressor stator actuators.

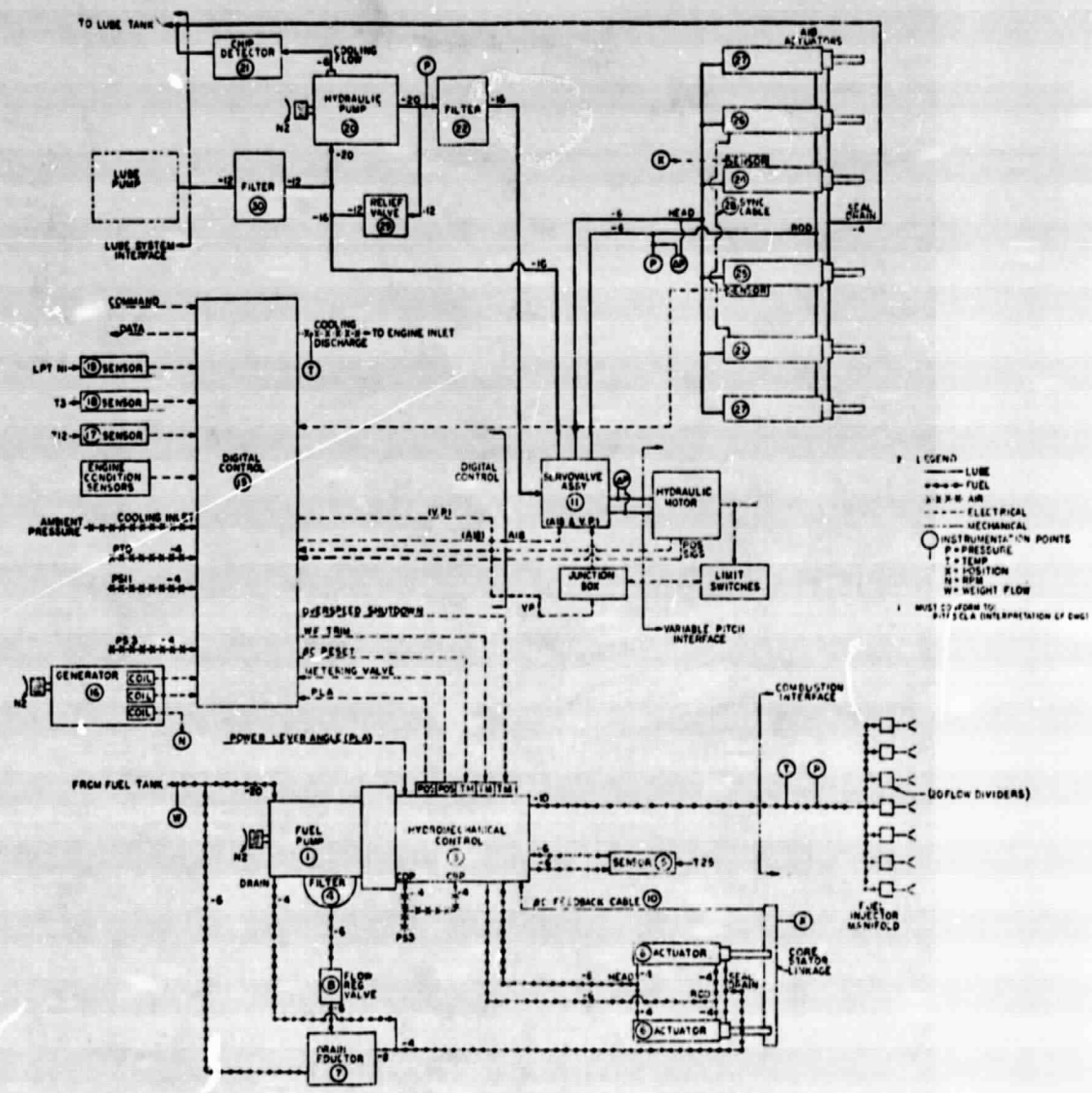

Figure 36. System Interconnection Schematic.

ORIGINAL PAGE IS
OF POOR QUALITY

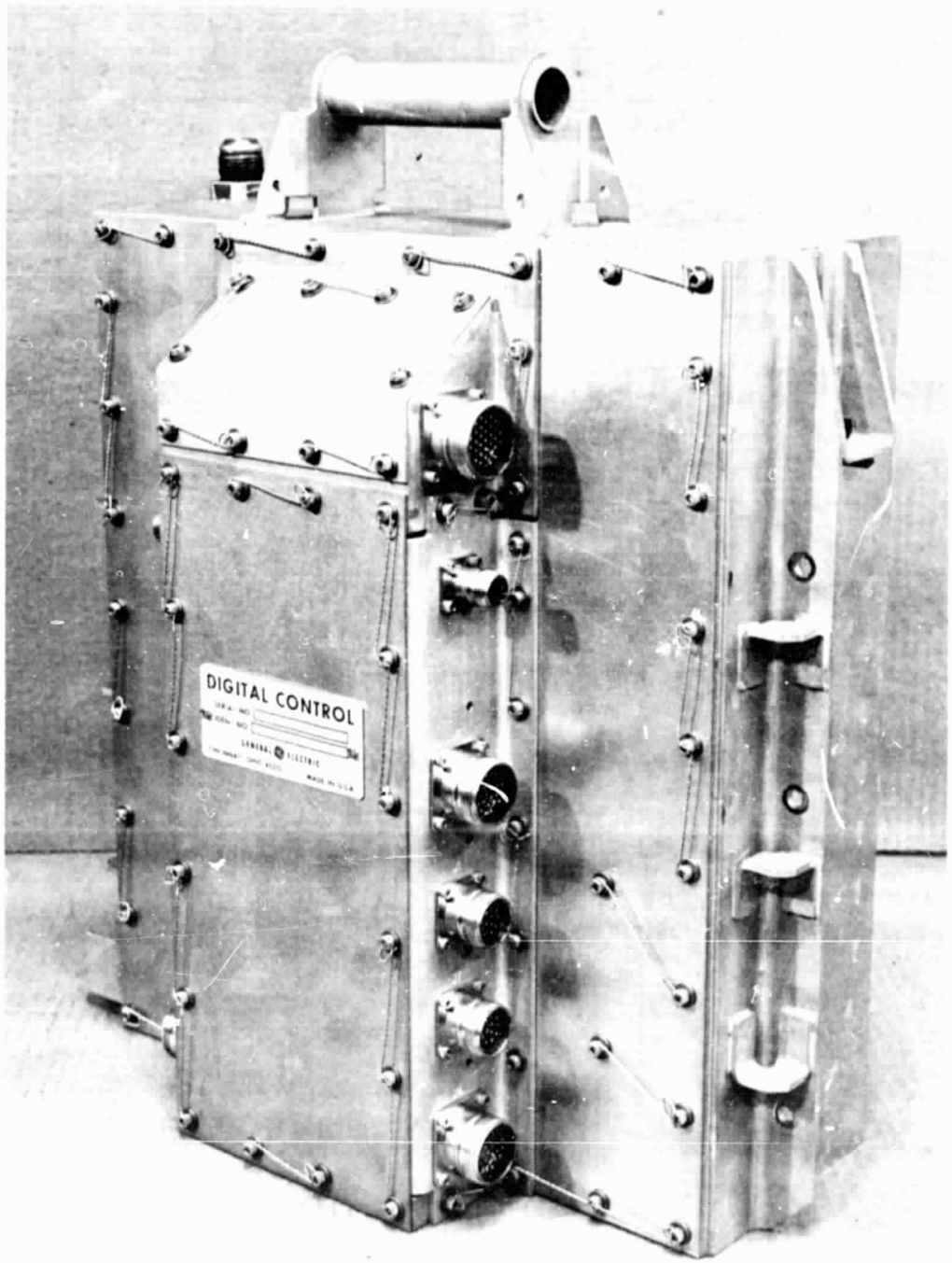

Figure 37. Digital Control Photograph.

ORIGINAL PAGE IS
OF POOR QUALITY

The hydromechanical control was mounted on an F101 fuel pump, a centrifugally boosted, positive displacement vane pump. Pump discharge flow was delivered to the control through the mounting interface, and the control returned excess fuel to the vane element inlet through a bypass valve.

Fan pitch angle and fan exhaust nozzle area were both controlled solely by the digital electronic control which furnished electrical signals to electrohydraulic servovalves in the servovalve assembly. These servovalves directed hydraulic fluid to the hydraulic motor which positioned the fan pitch mechanism and to the six hydraulic rams which positioned the variable fan exhaust nozzle.

The hydraulic system which supplied the pitch and nozzle servovalve assembly consisted of an engine-driven, variable-displacement, constant pressure piston pump, a filter, and the servovalves. Essentially, the system was a closed circuit with only a small fluid interchange with the engine lubrication system for cooling and, transiently, to account for differential actuation areas.

In order to achieve the operational flexibility required by the QCSEE program, the commands to the digital electronic control were introduced through the control room elements shown on Figure 38. The interconnect unit, operator panel, and engineering panel were actually peripheral elements of the digital control. They provided means for the engine operators to introduce commands, to adjust various control constants, and to monitor control and engine data.

In addition to these digital commands from the control room, the system also received a mechanical input in the form of a power lever angle (PLA) transmitted to the hydromechanical control. This served as an input to the backup governor and operated a positive fuel shutoff valve in the control.

A number of control and engine variables was sensed by the control system. The control and engine variables are shown schematically in Figure 39 and discussed briefly below:

Core Speed - Sensed electrically by measuring the output frequency of the generator which supplied digital control computer power and was sensed mechanically by a rotational input from the accessory gearbox to the hydromechanical control.

Low Pressure Turbine Speed - This speed, proportional to fan speed, was sensed by a stationary magnetic pickup located near a multitoothed disk which rotated with the LP turbine shaft.

Core Inlet Temperature - Sensed by means of a gas-filled coil in the core compressor inlet which operated a hydromechanical (fuel) sensing servomechanism.

Core Stator Position - Sensed mechanically by means of a push-pull cable between the stator actuation linkage and the hydromechanical control.

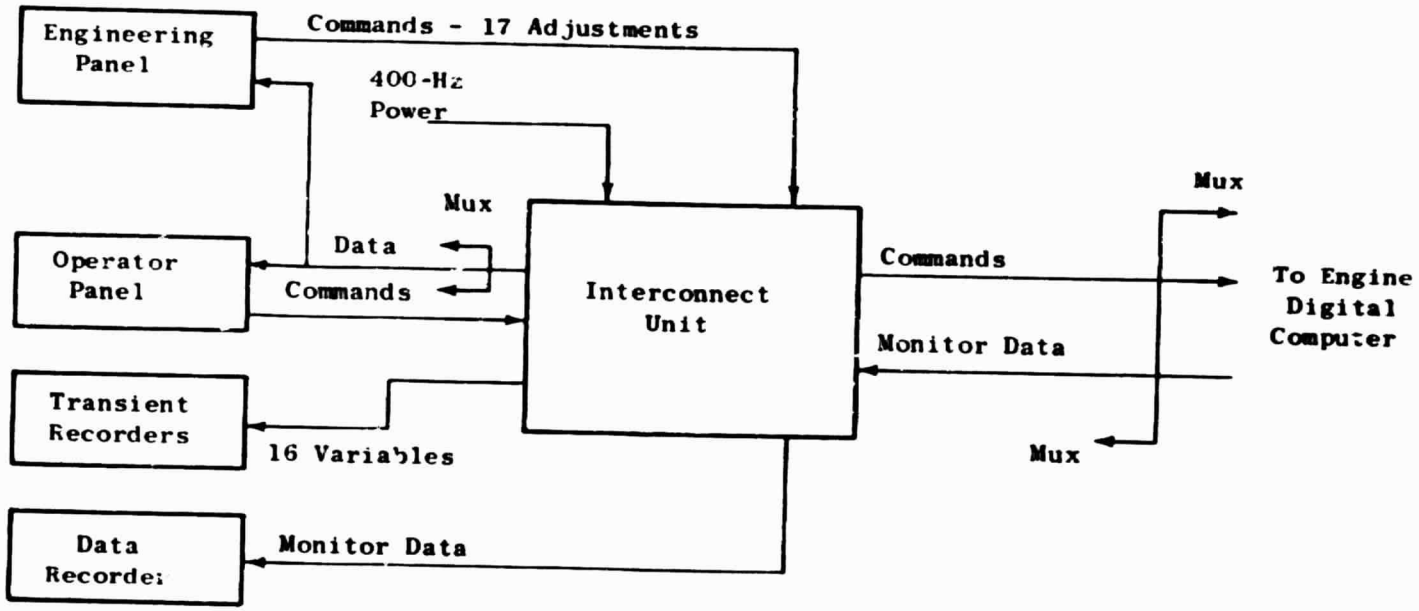

Figure 38. Control Room Elements of QCSEE Digital Control.

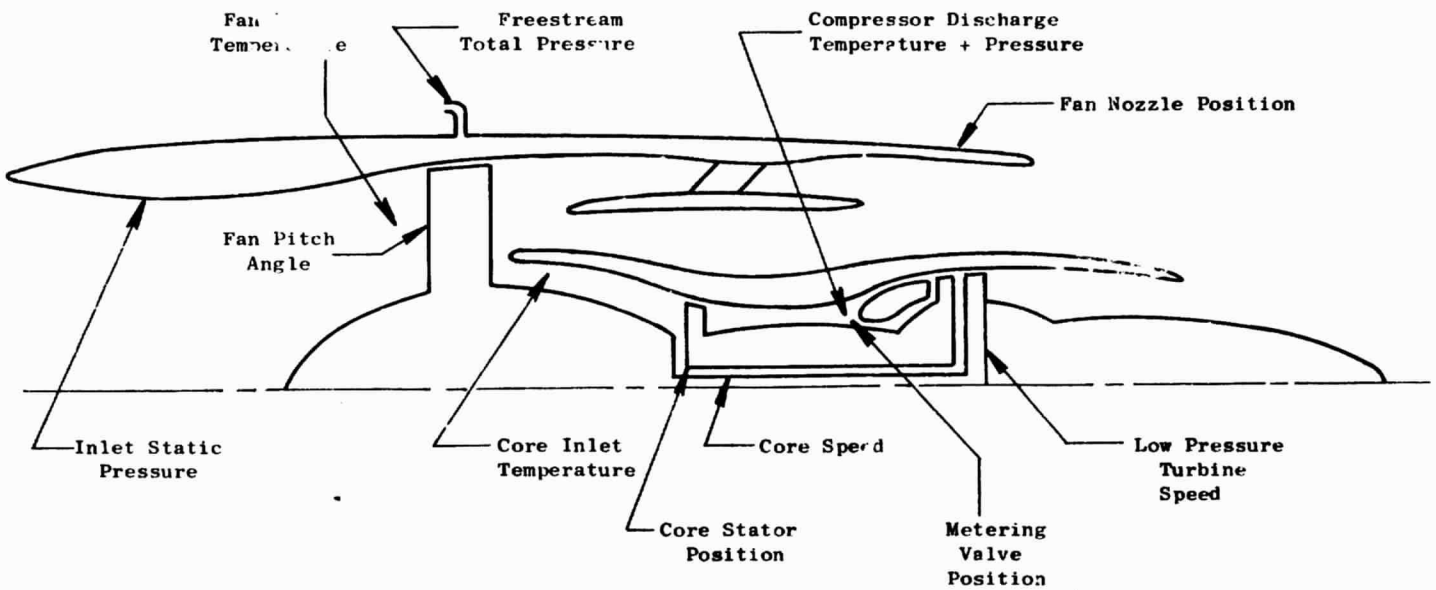

Figure 39. Sensed Engine and Control Variables.

Compressor Discharge Pressure - Sensed through a static pressure tap in the entrance to the engine combustor and piped to a pressure-to-electrical transducer in the digital control and to a sensing servomechanism (fuel) in the hydromechanical control.

Compressure Discharge Temperature - Sensed by a chromel-alumel thermocouple at the entrance to the core combustor.

Metering Valve Position - Used as a measure of fuel flow by the digital control and sensed with a transducer (rotary differential transformer) in the hydromechanical control.

Engine Inlet Static Pressure - Sensed through two static taps in the inlet duct wall and piped to one side of a differential pressure transducer in the digital control. The taps were located in a position near the inlet throat at an X/L position of 0.4.

Fan Inlet Temperature - Sensed by an electrical resistance temperature detector protruding through the inlet wall into the airstream.

Freestream Total Pressure - Sensed at the digital control as ambient total pressure for this static engine testing. A pressure-to-electrical analog transducer provided the signal to the digital control.

Fan Pitch Angle - Sensed by means of electrical position transducers (linear differential transformers) in the fan pitch actuation system. Because fan pitch angle was critical to satisfactory engine operation, two sensors were used. They were averaged by the digital control and protection was provided against the failure of one unit.

Fan Nozzle Position - Sensed by means of an electrical position transducer (linear differential transformer) in one of the nozzle actuators.

9.2 MANUAL CONTROL MODES

The manual control modes employed during engine test are shown in Figures 40, 41, and 42.

In the all-manual mode, the system operated in response to four basic inputs from the control room: three potentiometer inputs to the digital control computer and the manual power lever input to the hydromechanical control.

One of the potentiometer inputs served as a fan speed demand, causing fuel flow to be manipulated to set and maintain the desired fan speed. All of the fuel control loop limits shown in Figure 40 remain in effect to protect the engine and provide manual PLA control of core speed if desired (or necessary due to an electrical malfunction).

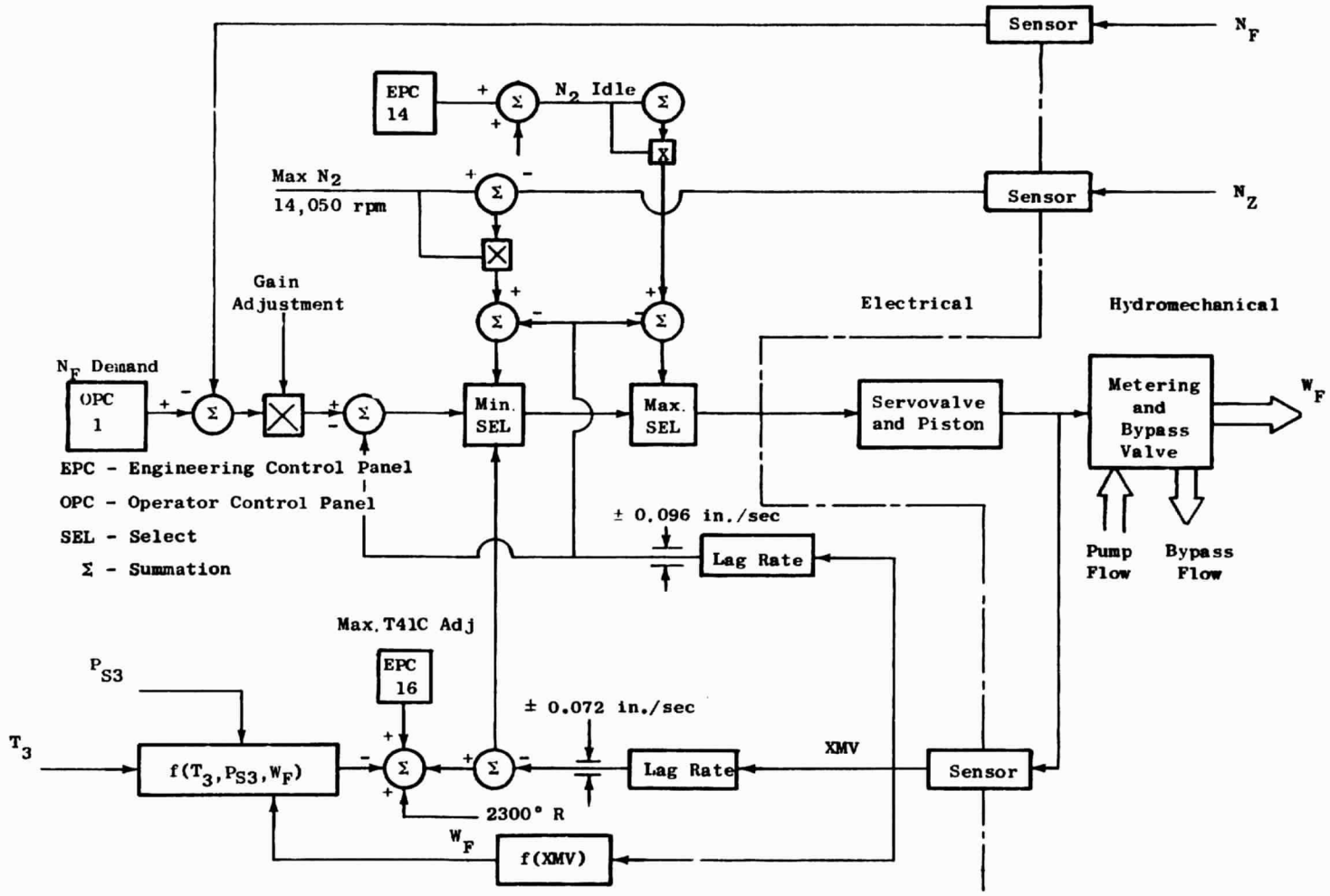

Figure 40. Manual Fuel Control System.

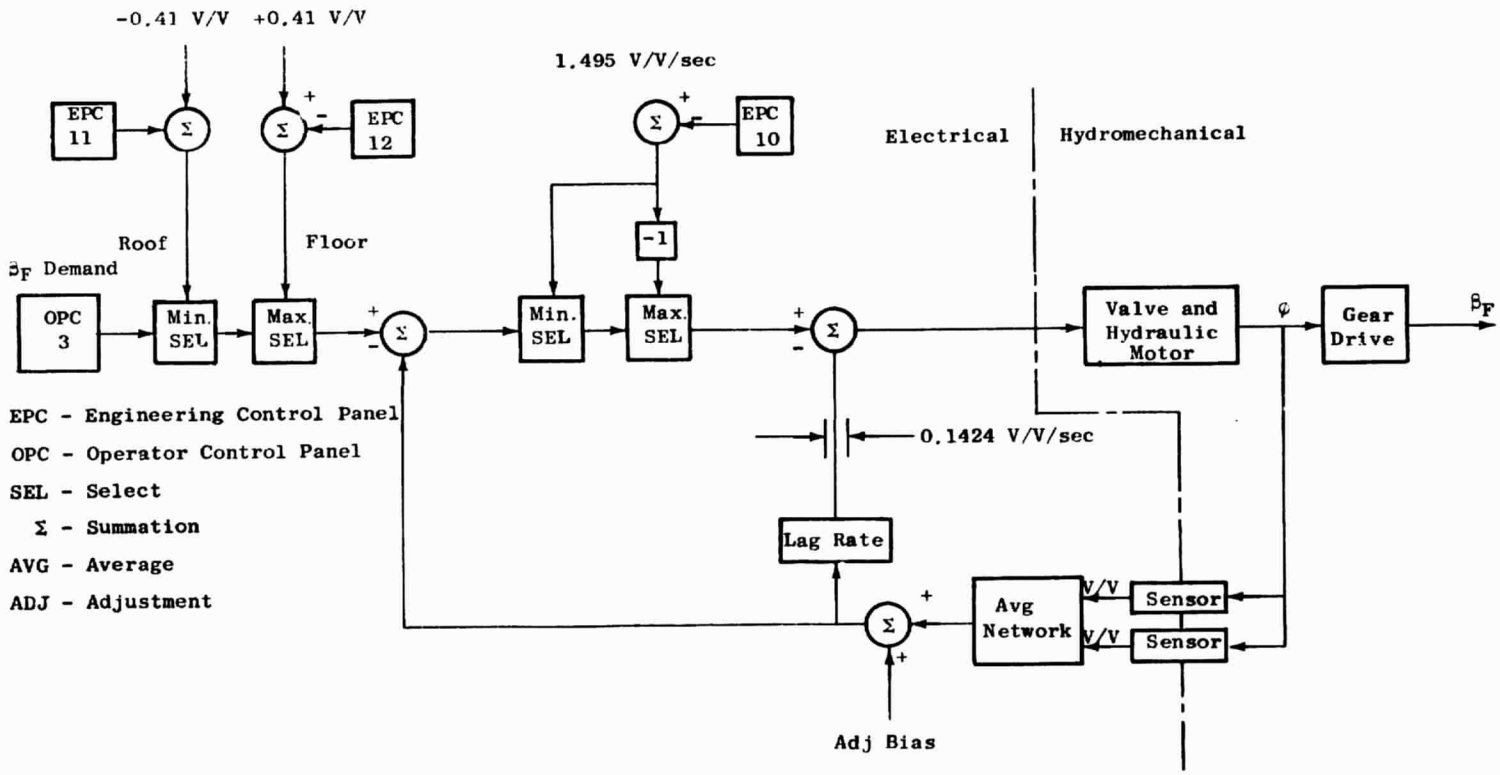

Figure 41. β_F Manual Control Variables.

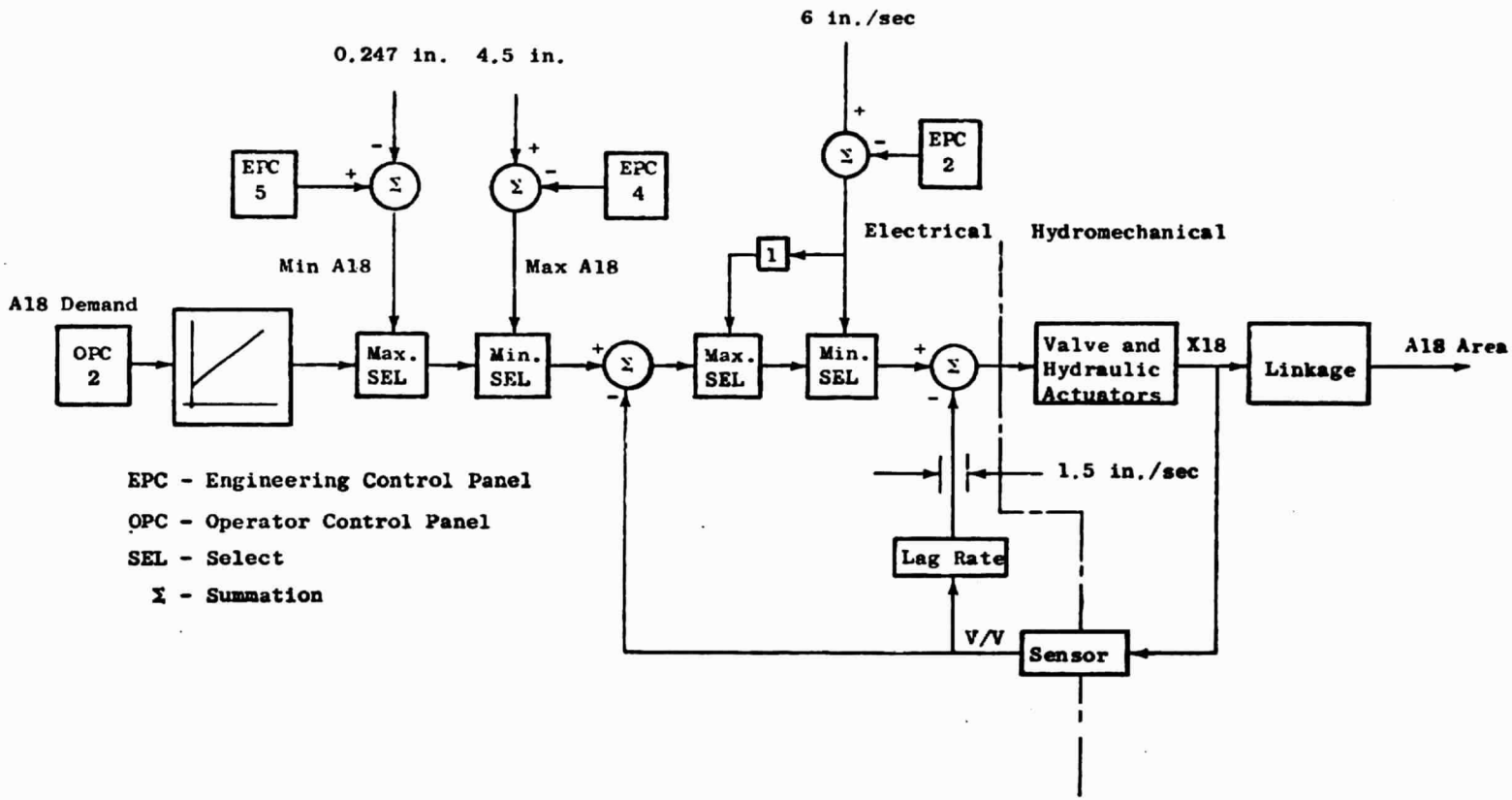

Figure 42. A18 Manual Control System.

The other two potentiometers serve as inputs to the digital control for operation of independent position control loops for fan pitch and fan exhaust area. Thus, in the all-manual mode, fan speed, fan pitch, and fan exhaust area could each be controlled independently.

9.3 FAILURE DETECTION AND CORRECTION

One objective of the QCSEE Program digital control technology development was to utilize the inherent abilities of a digital computer to record and compare large amounts of data for engine condition monitoring and fault detection.

The UTW control system incorporated several active fault detection features which are listed below. A fault light on the operator panel indicated when one or more of the faults had occurred, and a digital indicator on the engineering panel identified the fault or faults. A switch was available on the engineering panel to deactivate each of the features except the fan overspeed emergency shutdown.

Engine Vibration - Engine horizontal and vertical vibrations were sensed and if either exceeded 40 mils, fuel flow was reduced to set-idle core speed. This feature reduced the engine to idle when the A18 exhaust flap failed.

Loss of Command Data Link - A test word was among the set of digital commands that was transmitted respectively in series from the control room to the engine-mounted digital control computer. An error in this word at any time caused the control to revert to the last valid set of commands received and to continue operation at this condition until the fault was corrected.

Computer Fault - The program memory in the digital control computer included test elements which, if found to be incorrect for two successive iterations through the program, would interrupt the control outputs and cause fuel flow to drift downward, fan exhaust area to drift open, and fan pitch angle to drift open (increased pitch).

Fan Overspeed Emergency Shutdown - If the LP turbine (fan) speed signal exceeded an absolute maximum limit, or if it increased at a rate indicating a loss in turbine load, an electrical signal from the digital control to the hydromechanical control caused flow to be shut off immediately. All elements of this feature were isolated electrically from the remainder of the system so that it also protected against digital control system faults which might cause overspeed.

LP Turbine Speed Sensing Fault - Loss of the LP turbine (fan) speed signal can result in overspeed to the emergency shutdown level under certain conditions when operating on the automatic mode. To prevent this, the digital control would reduce fuel flow to set idle core speed if the LP turbine speed signal was lost. This function is ineffective below 45% core speed so that it will not interfere during starts.

Fan Pitch Transducer Failure - The signals from the two-fan-pitch-position transducers normally are averaged by the digital control. However, if the signals differ by 2.5° or more, the control uses the signal with the largest voltage level, discarding the other on the premise that the transducer producing the lower voltage may well have failed because the predominant failure mode for such transducers is loss of signal.

Lube Supply Temperature - If this temperature exceeds 356 K (180° F), the engineering panel fault light illuminates. This function also was demonstrated during during engine test.

Gearbox Bearing Temperature - If this temperature exceeds 395 K (250° F), the engineering panel fault light illuminates. This function also was observed during engine test.

Hydraulic Pump Pressure - If this pressure falls below 1724 N/cm^2 (2500 psia) with core speed above 45%, the engineering panel fault light illuminates. This function was demonstrated during subidle operation with the hydraulic pump depressurized.

Computer Timing Failure - The digital control includes redundant oscillators for timing in both the engine-mounted computer and in the control room portion of the control. An oscillator failure in the former will illuminate the fault light on the engineering panel, and a fault in the latter will illuminate a light on the interconnect unit in the control room.

9.4 MONITORING CONTROL AND ENGINE VARIABLES

The digital control system also included provisions for monitoring control and engine variables. Core speed, fan speed, power demand, exhaust nozzle area, fan pitch angle, inlet Mach number, engine pressure ratio, and calculated turbine inlet temperature were displayed continuously on the operator panel. Other parameters were provided for continuous recording on transient data recorders and all transmitted data were recorded on an automatic printer. The purpose of this monitoring function was to demonstrate the digital control's capability to incorporate an integrated engine condition-monitoring system.

9.5 FAN PITCH ANGLE (β_F) AND FAN EXHAUST NOZZLE CALIBRATION

9.5.1 Fan Pitch Angle Calibration

Calibration on the engine was accomplished using a 2000 psig slave hydraulic power source for the hydraulic motor power and an Elgar electrical power supply for the digital control. The pitch angle was set from the control room by movement of the βF fan pitch control potentiometer on the operator control panel. Blade angle was measured with an inclinometer held on a molded tool which fit over the fan blade tips. All calibration measurements were made on blade No. 8. This blade was positioned horizontally with

the blade stacking axis aligned with an accurate pin hole in the fan frame. Prior to taking measurements, it was established that the fan frame was level in both axial and radial directions. Measurements on the opposite blade No. 17 agreed with blade No. 8 within seven minutes of arc.

The plot of demand position versus measured βF position was as shown in Figure 43. The plot of measured pitch position versus engineering panel readout EPMI/05 is shown in Figure 44. From these data the following equations were derived to display the fan pitch angle (βF) on the operator control panel readout.

x = digital readout at EPMI/05

for $x < 1042$ $\quad -116 \text{ deg} < \beta F < -91 \text{ deg}$

$$\beta F = -135.667 + .0463676X - 3.647718E\text{-}6X^2$$

for $1042 \leq X \leq 3077$ $\quad -91 < \beta F < -10.3$

$$\beta F = -120.5679 + 1.46247E\text{-}2X + 1.59933E\text{-}5X^2 - 2.95709E\text{-}9X^3$$

for $3077 < X$ $\quad -10.3 < \beta F < +11.4$

$$\beta F = 638.918 + .517737X - 1.48361E\text{-}4X^2 + 1.51093E\text{-}8X^3$$

The calibration process was repeated in the closed-to-open direction by setting the fan-pitch-position command potentiometer to the No. 1 run position. Except for a hysteresis loop in the extreme closed position, the measured blade position over the full range agreed within 40 minutes. In the critical ranges (±5° and -95° to -105°) the agreement was 30 minutes or better. With respect to sensitivity, pitch angle readout on the operator panel could be set within 0.2°. The minimum hydraulic pressure required to move the blades was 850 to 900 psig.

The Beta regulator was opened and the limit switch adjusted to 12° 47' in the closed position and to -116° 7' in the open direction.

9.5.2 Fan Exhaust Nozzle (A18) Calibration

Engine calibration was accomplished using a 1379-N/cm^2 (2000-psig) slave hydraulic power source for the nozzle actuators and the Elgar electrical power supply for the digital control. A18 exhaust nozzle position was set from the control room by movement of the A18 control potentiometer on the operator control panel. The nozzle was rigged by making drop measurements from the tip of the nozzle flaps to the core plug and then adjusting the turnbuckles between the actuator and flaps to achieve a desired dimension. After final adjustment, flaps 1, 2, 3, and 4 agreed within 0.0076 cm (0.003 in.). The difference between the right and left sides was 0.0559 cm (0.022 in.).

The plot of demand position versus calculated A18 area is shown in Figure 45. A plot of calculated A18 area versus engineering panel readout EPMI/04 is shown in Figure 46. From these data the following equation was

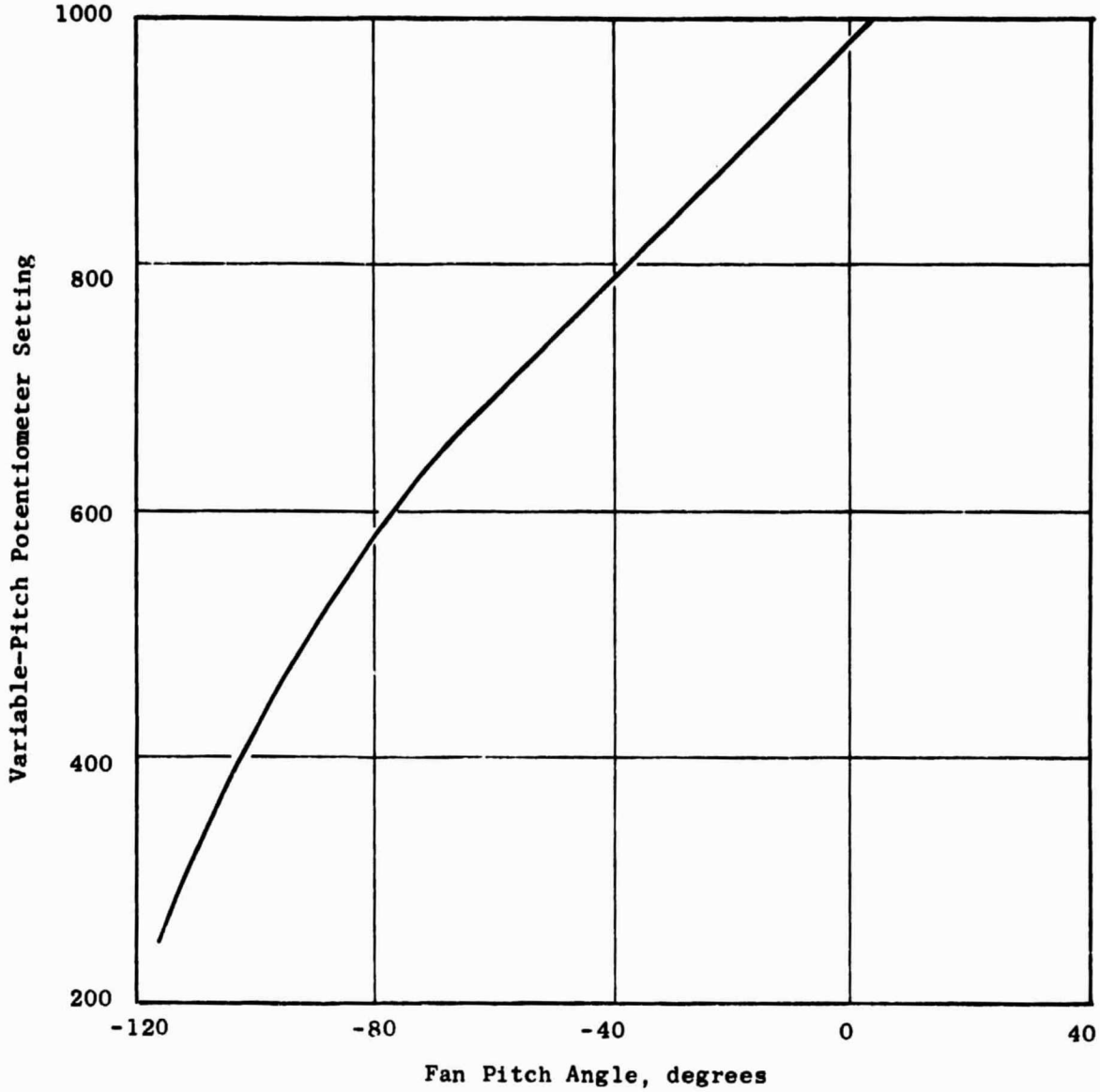

Figure 43. β_F Position Versus Demand Potentiometer Setting.

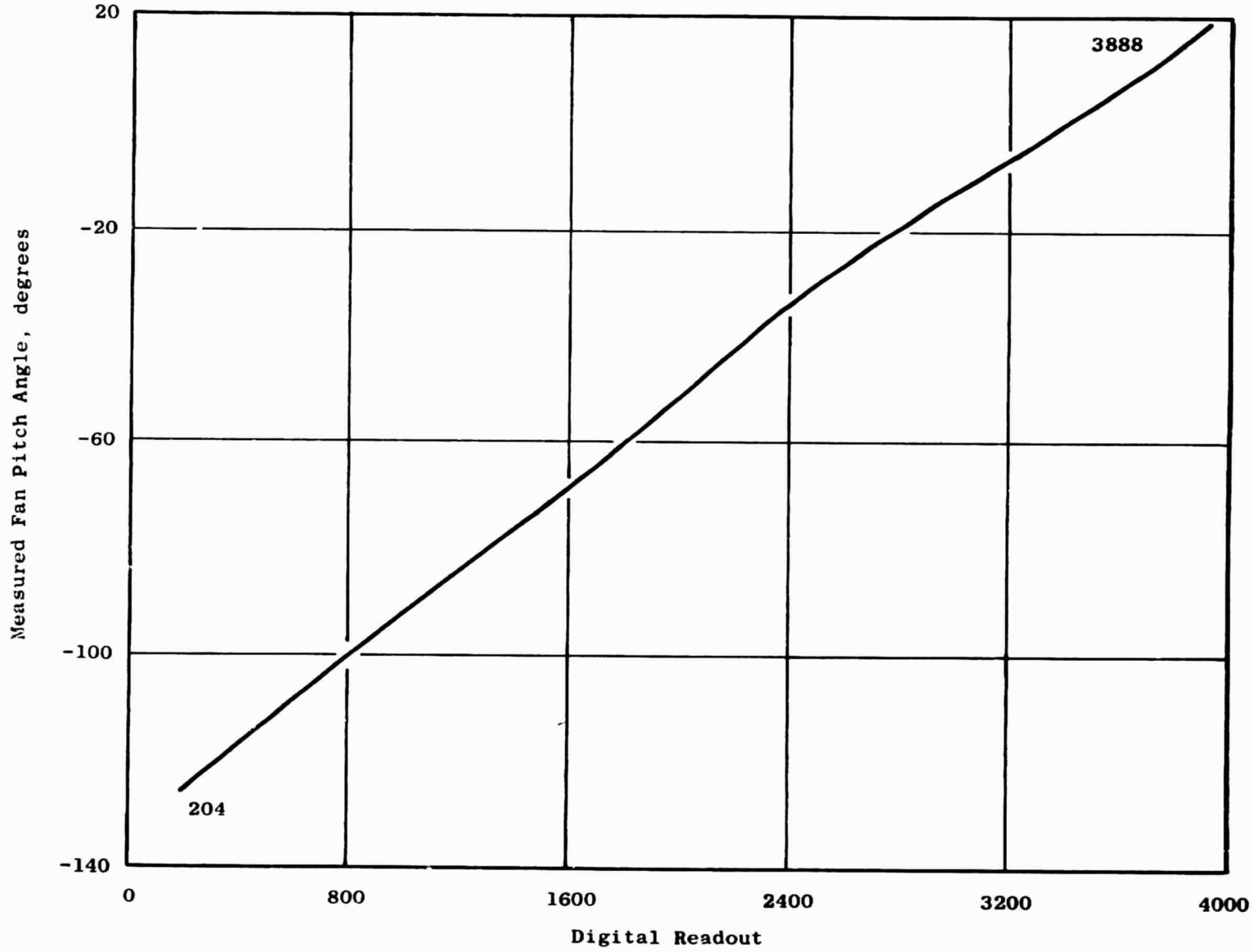

Figure 44. Fan Pitch Angle Versus Digital Readout.

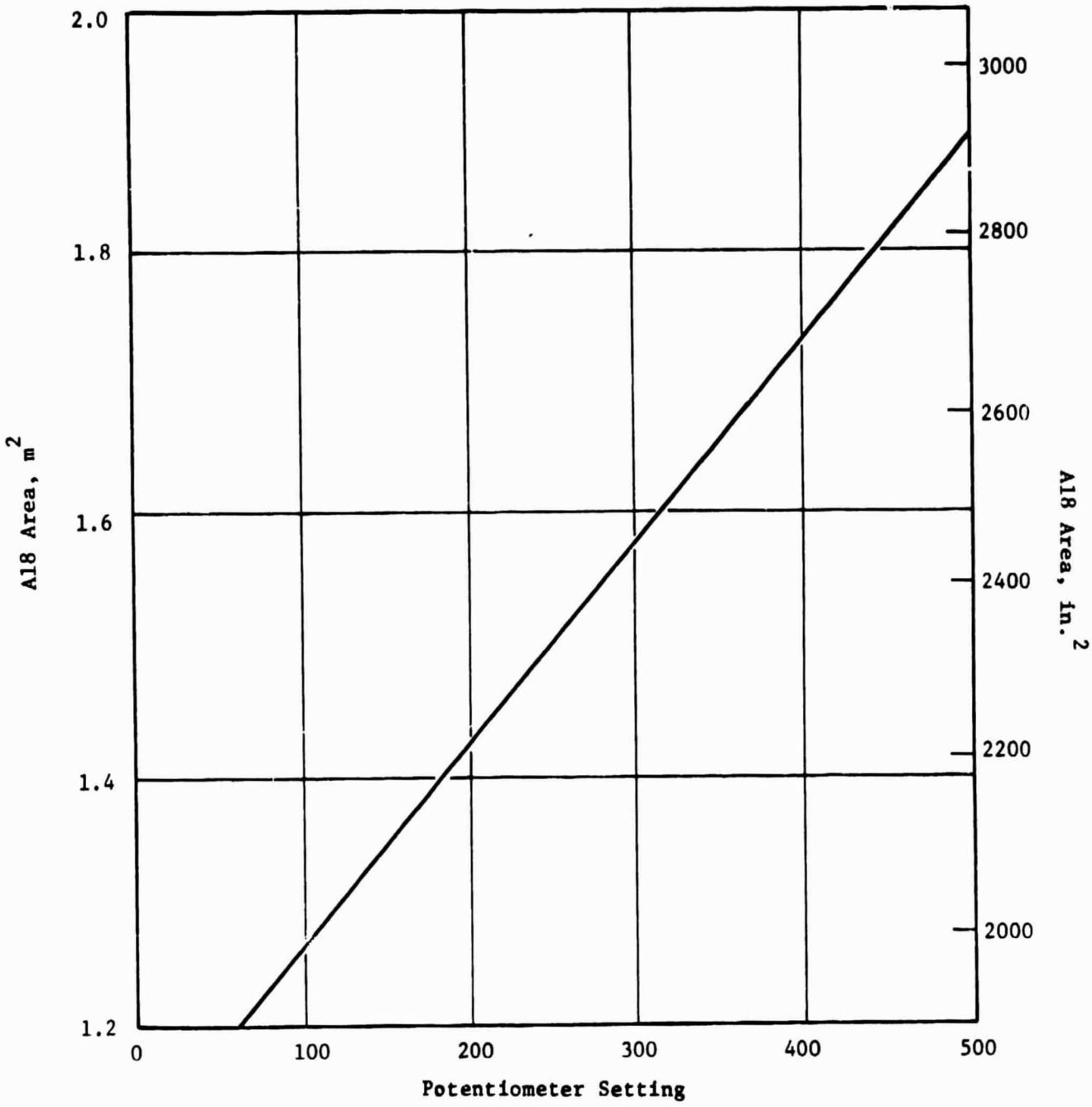

Figure 45. Fan Nozzle Area Versus Demand Potentiometer Setting.

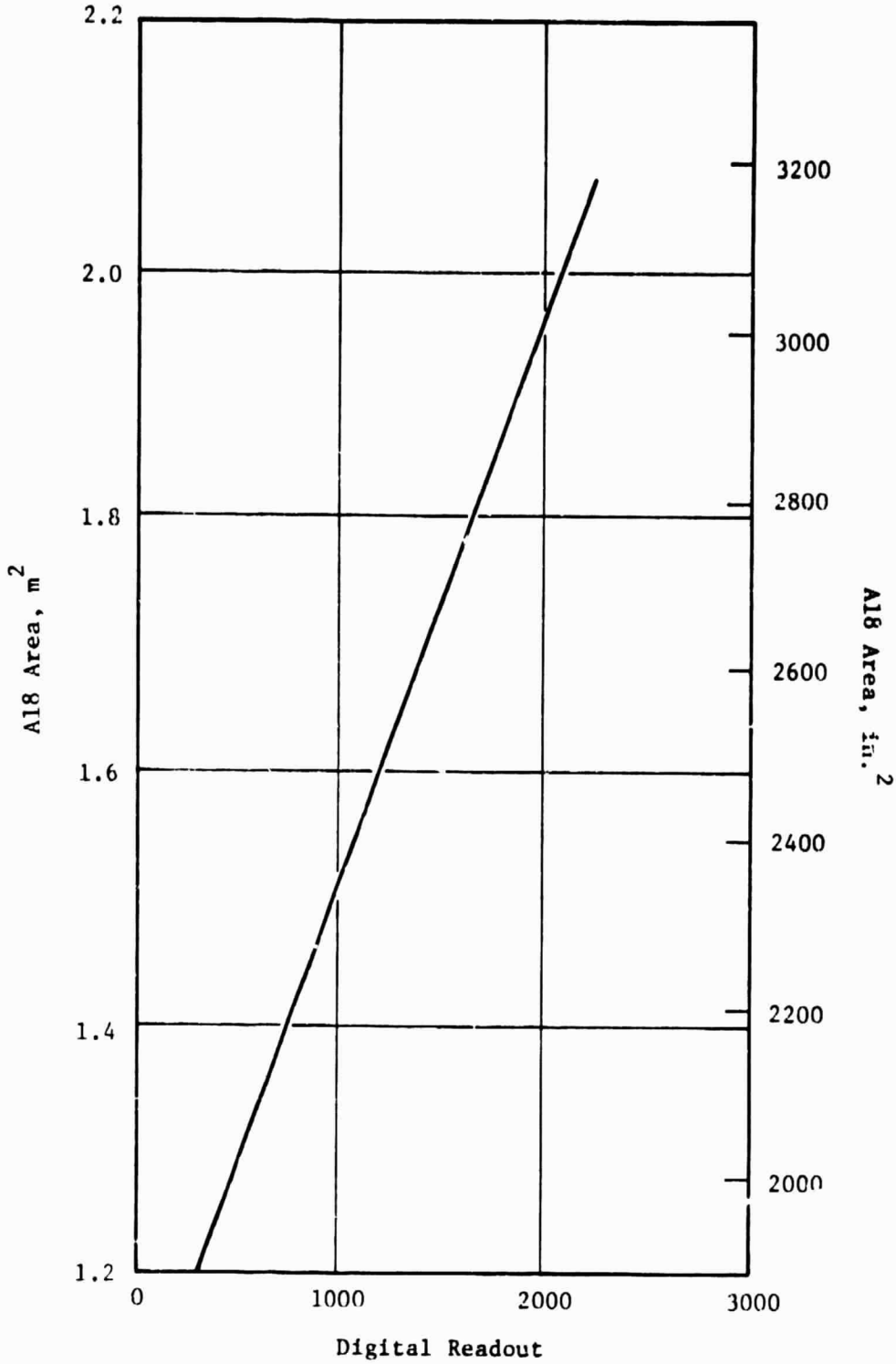

Figure 46. Fan Nozzle Area Versus Digital Readout.

derived to display A18 area on the operator control panel readout.

$$x = \text{digital readout at EPMI/04}$$

$$A18 = 0.66759X + 1681$$

The minimum hydraulic pressure required to move the exhaust nozzle was 138 N/cm^2 (200 psig). Resolution of the system was such that the area could be set within 12.9 cm^2 (2 $in.^2$).

9.6 ENGINE/CONTROL SYSTEM TESTING

The engine was started successfully and operated to takeoff power under control of the digital control system operating in the full-manual mode. The three electically controlled variables (fuel flow, fan pitch, and fan exhaust area) were stable and accurate.

9.6.1 Fuel Control System

On starting, the engine was motored-up in speed on the air starter until the digital control was in electrical regulation. Observation of operator control panel data indicated that the control went into electrical regulation at approximately 3000 rpm (20.7%) core speed versus a component requirement of 25% core speed. After achieving control regulation, the hydraulic pump was allowed to pressurize, and the engine was motored to approximtely 4000 rpm at which time the stopcock was opened and the ignition was energized. Idle speed, initially 10,900 rpm of the core, 1484 rpm fan, was reached in 19 seconds under core speed control. Figure 47 shows a typical start from the 4000-rpm core speed motoring point.

To allow exploration of the engine characteristics at low speeds, an idle speed adjustment was incorporated on the control system engineering panel. Movement of the adjustment reset the core speed idle reference point. Figure 48 shows a range of core speed operating points. In this control mode, core speed was stable within 4 rpm.

Operation in the fan speed control mode was accomplished by movement of the power demand potentiometer on the operator panel. The transfer from core-speed control to fan-speed control and vice versa on deceleration was smooth and without any observable discontinuities. Recorded data showing physical fan speed as a function of power demand is shown in Figure 49. In this control mode, fan speed was stable and held the desired operating point within 2 rpm. To avoid certain fan critical speeds, rapid accelerations and decelerations were made between 2100 and 2500 fan rpm. This transient operation accounts for the break in data points on Figure 49. The control system successfully accelerated and decelerated the engine through this critical region. A typical transient is shown in Figure 50.

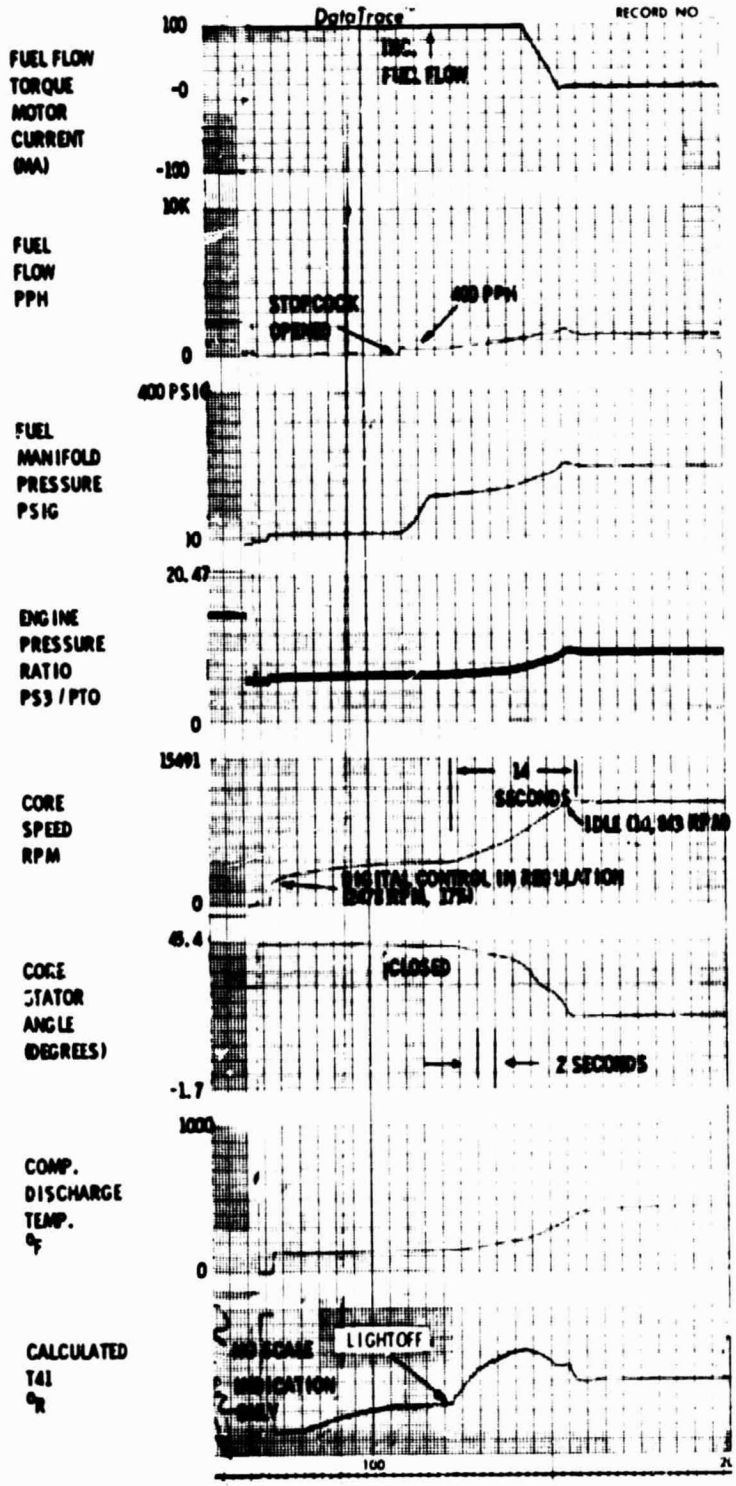

ORIGINAL PAGE IS
OF POOR QUALITY

Figure 47. QCSEE UTW Typical Start.

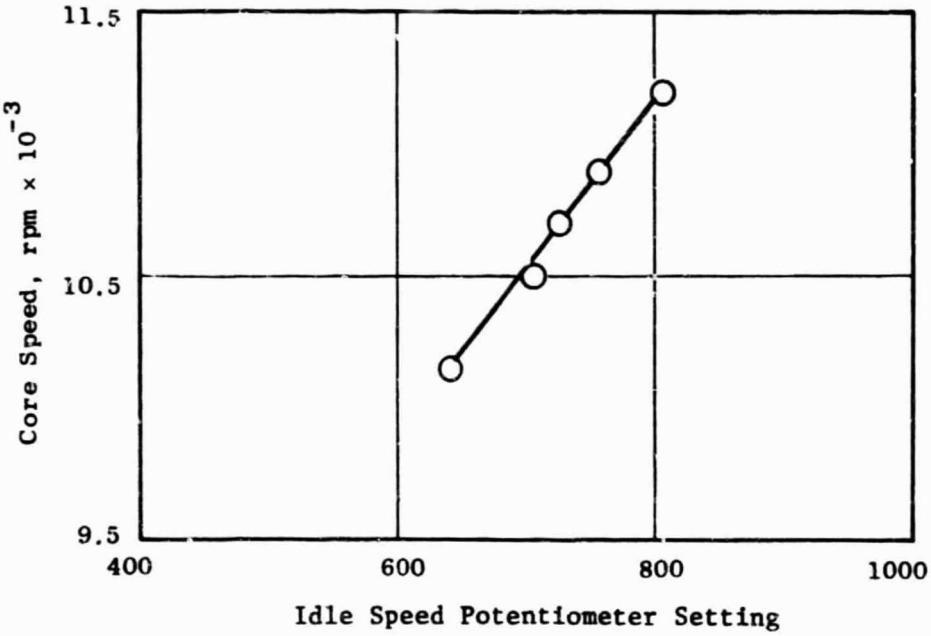

Figure 48. Core Idle Speed Ranges.

C-2

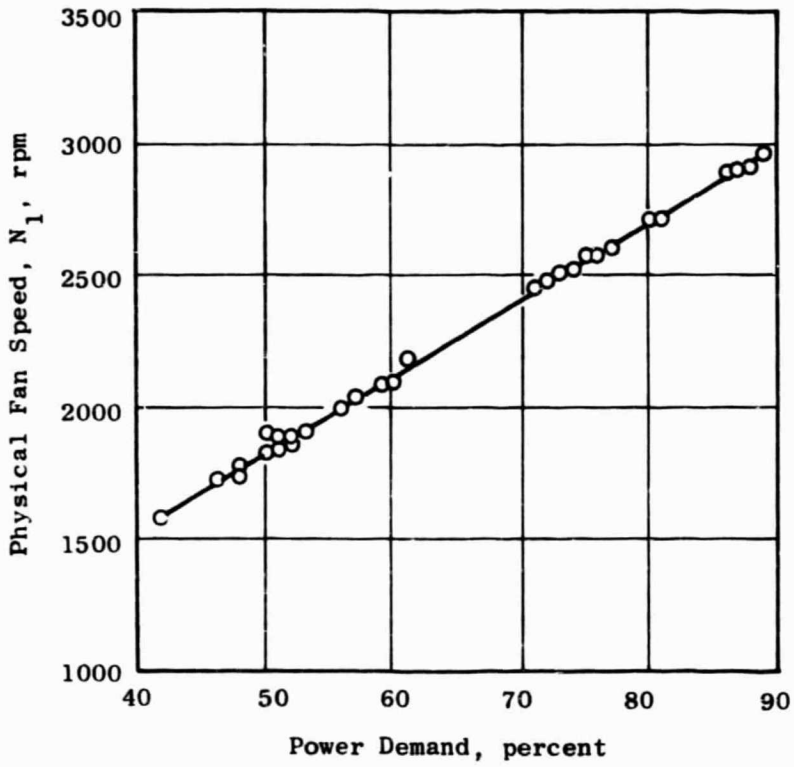

Figure 49. Fan Speed Vs. Power Demand.

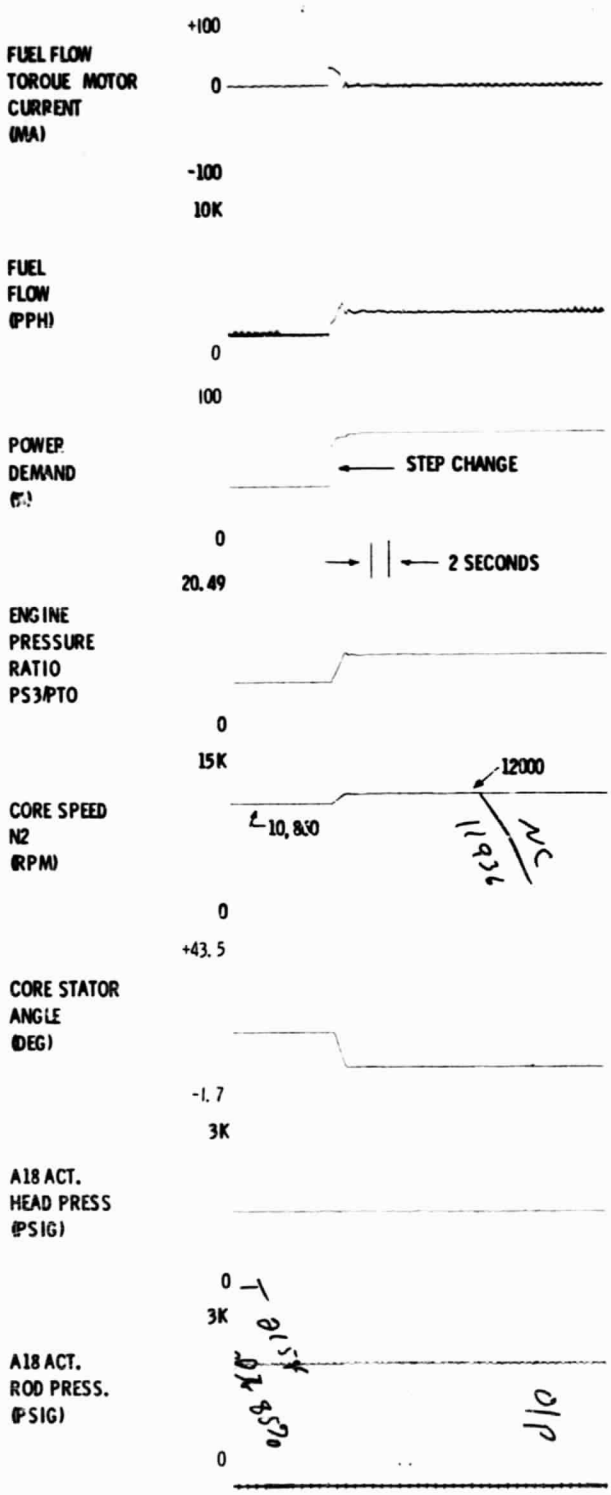

Figure 50. QCSEE UTW Power Change, Idle to 12,000 rpm.

In addition to demonstrating successful operation on core and fan speed control, two control system safety features were demonstrated: T_{41C} limiting and PLA override. To demonstrate the T_{41C} limit, the calculated temperature reference level was adjusted downward until fan speed was suppressed by the temperature limit. The engine and control system operated stably on the limit. The PLA override was demonstrated by retarding the hydromechanical power level until the core speed demand suppressed the core speed at the existing operating point. Operation at this point was stable as expected since a developed hydromechanical control was used.

The digital control calculates turbine inlet temperature (T_{41}) as a function of compressor discharge temperature (T_3), compressor discharge static pressure (PS_3), and fuel metering valve position (XMV), which is proportional to fuel flow, per the following equation:

$$T_{41C} = -14.6 + 1.0657T_3 + 23.585 \frac{W_F}{PS_3} \quad 1.245$$

where fuel flow (W_F) is a function of XMV as noted below.

$$W_F = 15981.5\ (XMV)^2 + 4098.59\ (XMV) - 342.87$$

The above equations are incorporated into the digital control program memory and the sensed parameters are a part of the engine control system as noted above. A comparison of T_{41C} as calculated by the digital control using the above equations and a time-share calculation of T_{41C} using the input data to the digital control is shown in Table 7. The data tabulation indicates that the control is calculating the temperature accurately from the input data.

Figure 51 compares T_{41C} calculated by the digital control with T_{41} from engine performance data. This curve indicates that the digital control is calculating a high-value turbine inlet temperature. Variation with engine data is from 30° to 80° F. This variation apparently is due to a high fuel flow measurement by the control system, Figure 52 compares fuel flow as calculated by the digital control with fuel flow measured during engine performance testing. This error in fuel flow measurement appears to account for the error in the T_{41} calculation. Further development in fuel flow measurement/calibration is required before the calculated temperature concept can be utilized.

The hydromechanical control positioned the core stators as a function of corrected core speed from a three-dimensional cam. Figure 53 compares measured data with the scheduled value. Most data points in the forward mode are within one degree of schedule which is within the accuracy of the control. The data for the reverse mode indicate that the stators are on the closed side of the schedule. The most probable cause of this error is an error in the measurement of core inlet temperature (T25). A low temperature measurement would result in a high corrected speed and result in an apparent schedule shift in the closed direction.

Table 7. Comparison of Turbine Temperature Calculations.

T_{41C*}, ° R	T_{41C**}, ° R	Difference
1088.36	1097.51	-9.15
1705.21	1702.44	2.77
1809.99	1806.95	3.04
2044.90	2041.39	3.51
1892.80	1884.81	7.99
2012.79	2009.13	3.66
2240.94	2237.94	3.00
2043.21	2035.76	7.45
2360.93	2355.97	4.96
2670.20	2672.81	-2.61
2269.67	2264.64	5.03
2396.42	2393.56	2.86
2431.91	2433.03	-1.12
2504.58	2510.41	-5.83
2585.70	2577.91	7.79
2600.67	2605.07	-4.40
2732.73	2727.99	4.74
2923.70	2916.16	7.54
2874.69	2873.38	1.31
2832.44	2826.53	5.91
2575.56	2573.13	2.43
2898.35	2898.96	-0.61

* As calculated by the Digital Control.

** As calculated by time-share from Digital Control input data.

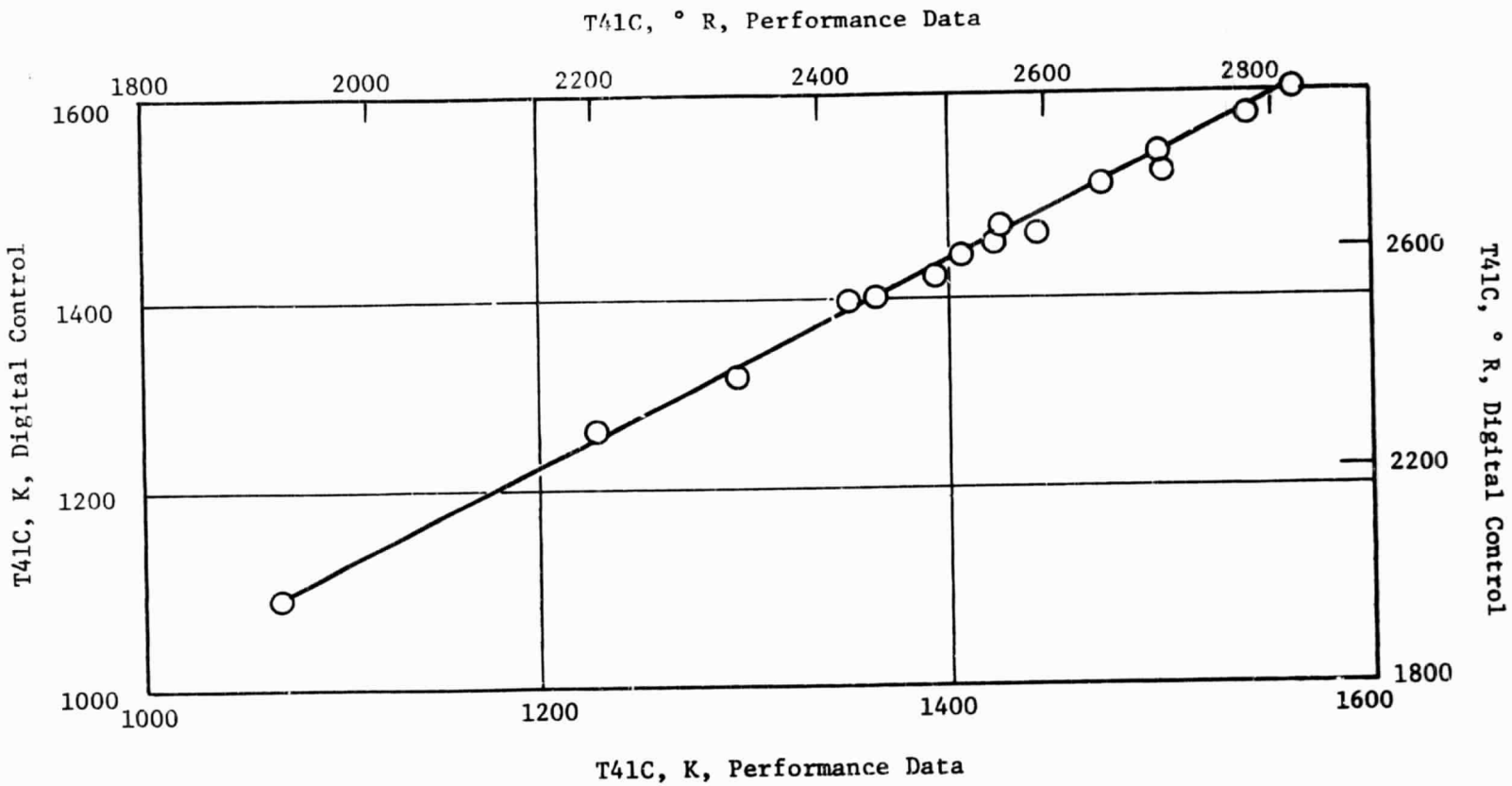

Figure 51. T41C Calculated Temperature Comparison.

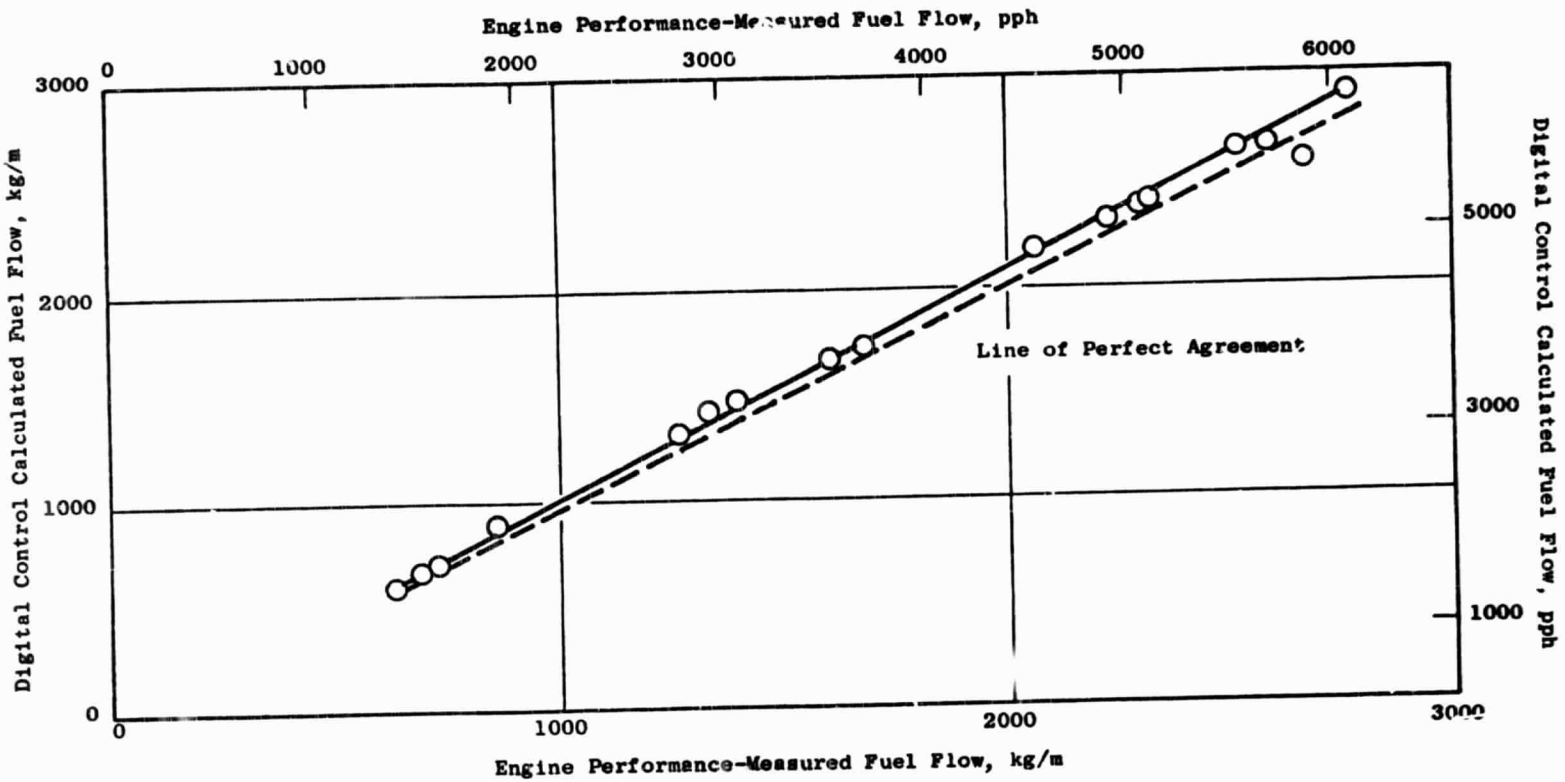

Figure 52. Fuel Flow Comparison.

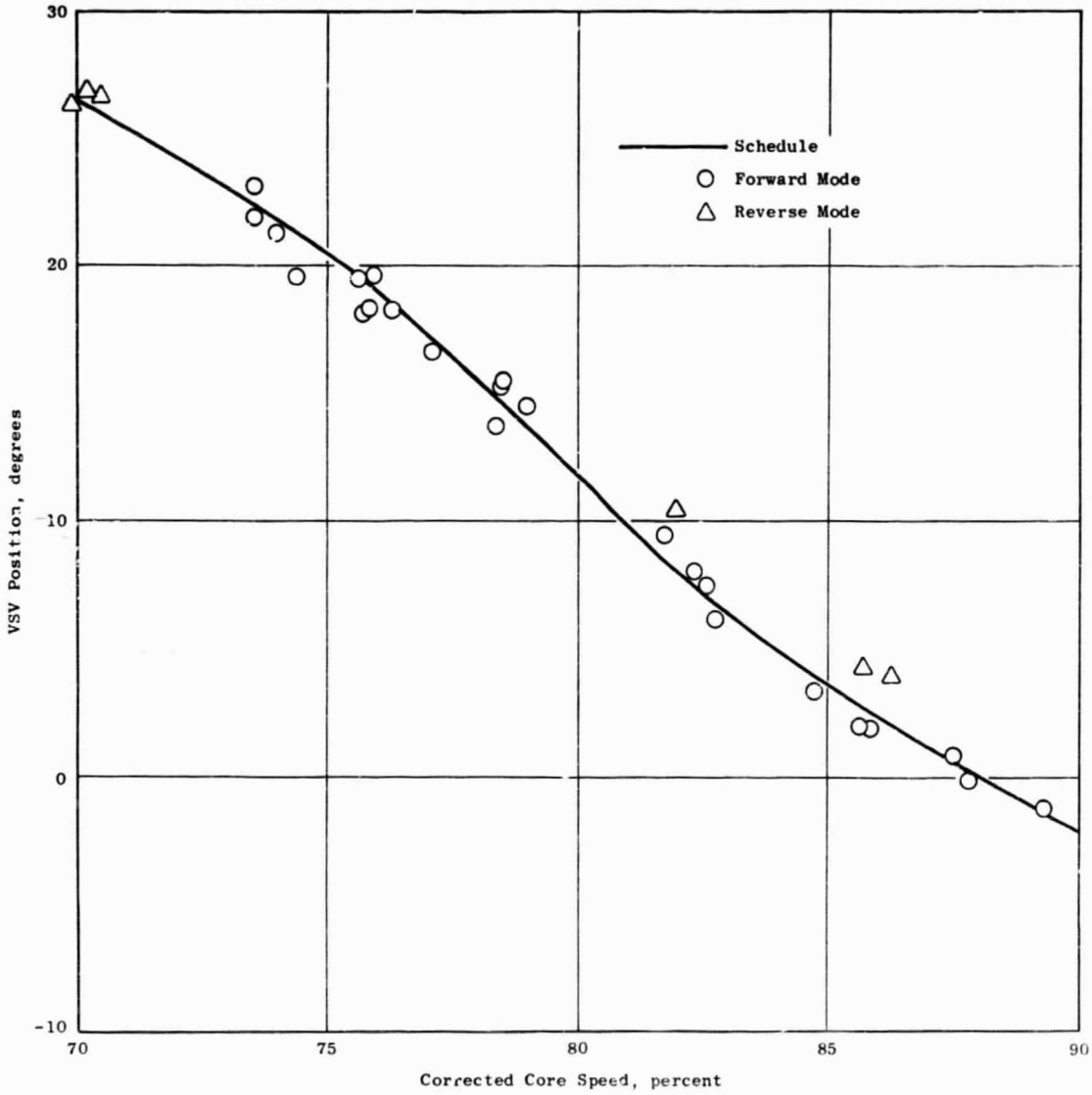

Figure 53. QCSEE UTW Core Stator Schedule.

9.6.2 Nozzle Control System

Prior to starting, the fan exhaust nozzle was in the full-open (flared) position because the digital control went out of regulation in the subidle coast down region (< 3000 core rpm), and the head end of the actuators was larger than the rod end. Prior to the engine starting sequence, the nozzle position command potentiometer was positioned to demand a 1.6-m^2 (2500-in.^{2}) area. During the starting sequence the nozzle would close to the commanded position when the core engine reached approximately 3500 rpm. Figure 54 shows the nozzle closure to the desired position during the start sequence.

During the engine test program, the A18 exhaust nozzle was varied from 1.35-2.03 m^2 (2100-3150 in.^{2}) while in the forward mode of operation. The nozzle was stable and could be set within 13 cm^2 (2 in.^{2}). No problems were experienced.

Prior to the reverse mode of operation while operating at idle power, the nozzle was opened to a maximum area of 2.65 m^2 (4112 in.^{2}). At approximately 2.58 m^2 (4000 in.^{2}), a limit cycle of $\pm$580 cm^2 ($\pm$90 in.^{2}) at 10 Hz was experienced as shown in Figure 55. This area was avoided for the remainder of reverse testing by limiting A18 to 2.51 m^2 (3900 in.^{2}) where no oscillations existed. Further investigation is planned during Build No. 2 of the engine to determine the cause of the oscillation.

One function of the digital control system is to display and to control the average engine inlet Mach number at the inlet throat for noise suppression. The inlet Mach number display is accomplished by measurement of free-stream total pressure (PTO) and the differential pressure between the inlet static and free-stream total pressure (PTO-PS11). Division of these two measurements produces a function which is proportional to local Mach number at the static pressure measurement point. Static pressure was measured at an X/L of 0.4, where L is the distance from the inlet highlight to the fan blades and X is the distance from the inlet highlight to the static pressure measurement plane. This static measurement point was chosen from experimental data on an inlet model which indicated that measurements at this plane were free of crosswind effects and were high enough to provide a good signal level. Figure 56 shows the experimental model data where inlet wall Mach number is a function of X/L with and without crosswinds. An empirical equation was used to convert the measured pressures to average inlet Mach number. The equation which was developed during testing with the accelerating inlet is:

$$XM11 = 1.99 * \frac{(PTO-PS_{11})}{PTO} + 0.2182$$

This equation was programmed into the minicomputer located in the operator display panel. The pressure measurements were transmitted from the engine-mounted digital control to the operator panel and were converted to an average inlet Mach number display. Figure 57 compares the displayed inlet Mach number calculated from engine performance data measurements.

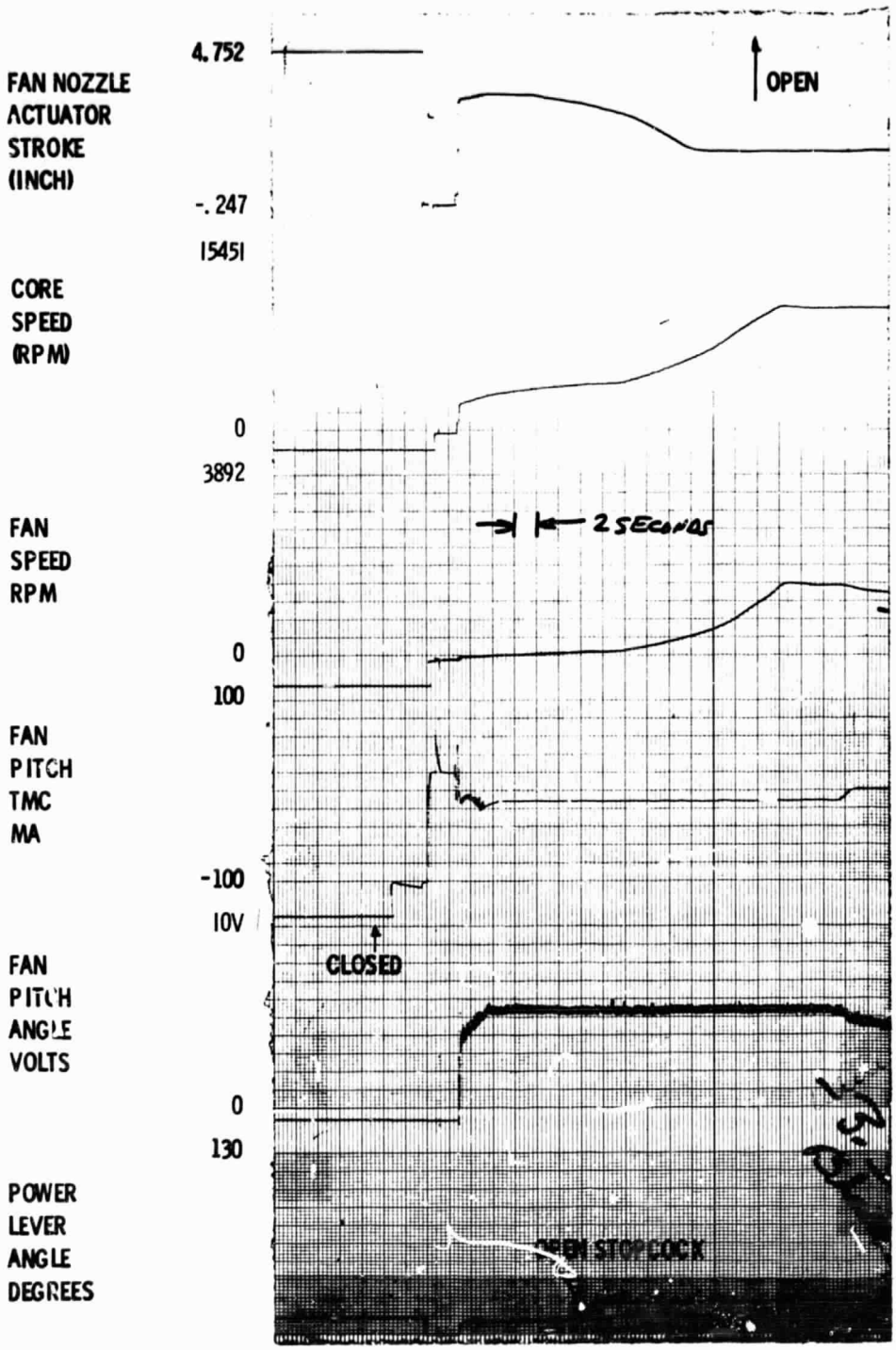

Figure 54. Fan Nozzle Closure On Start.

ORIGINAL PAGE IS
OF POOR QUALITY

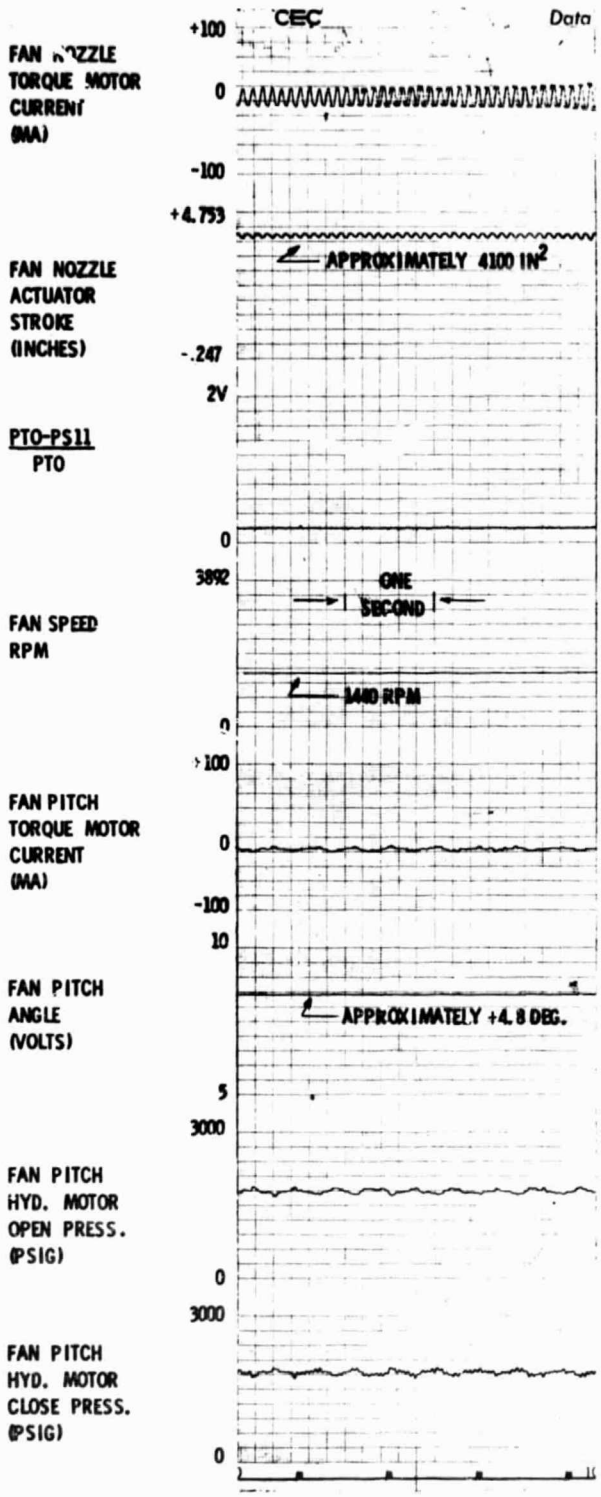

ORIGINAL PAGE IS
OF POOR QUALITY

Figure 55. QCSEE UTW Fan Nozzle Oscillations.

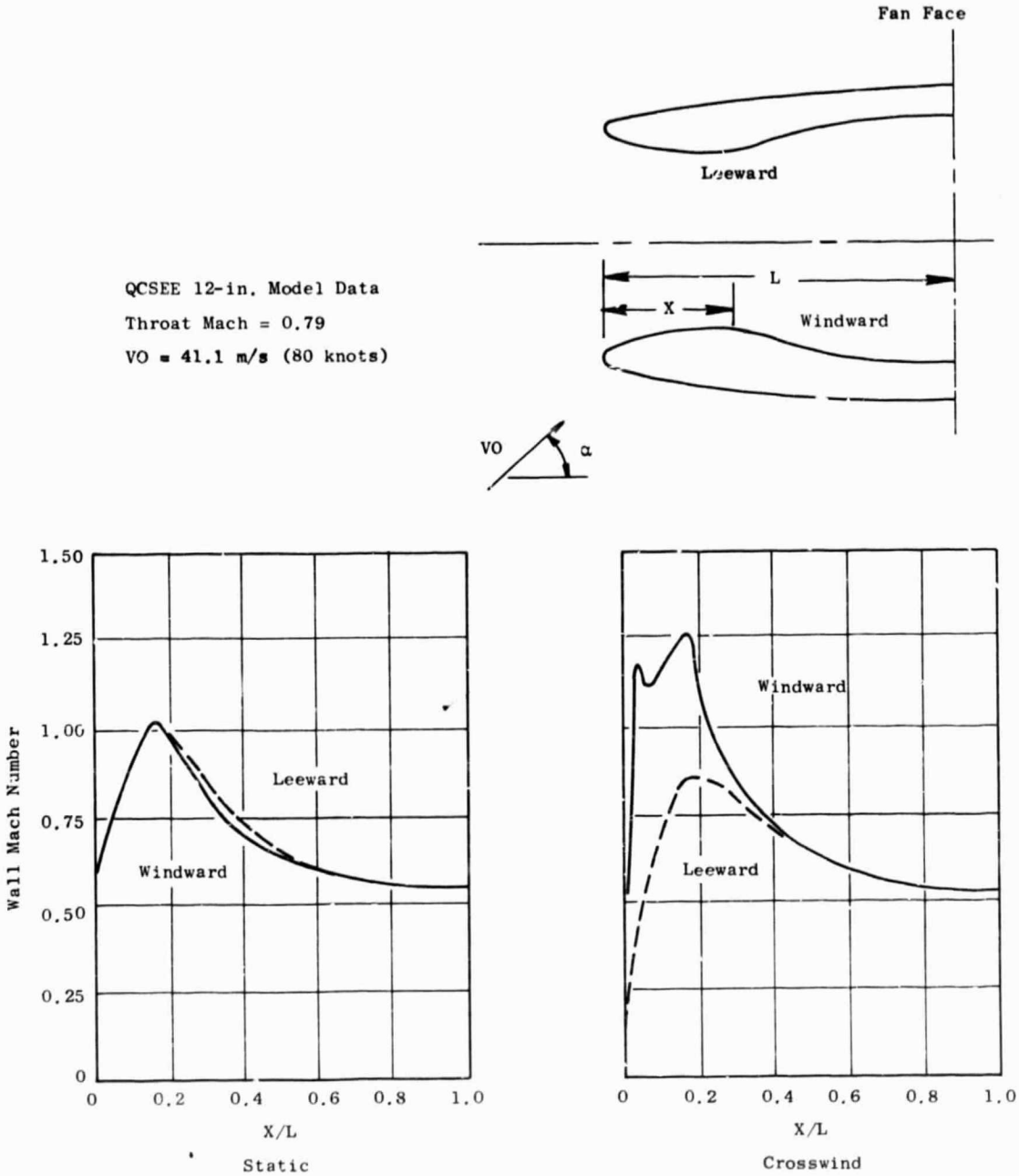

Figure 56. Experimental Mach Number Data.

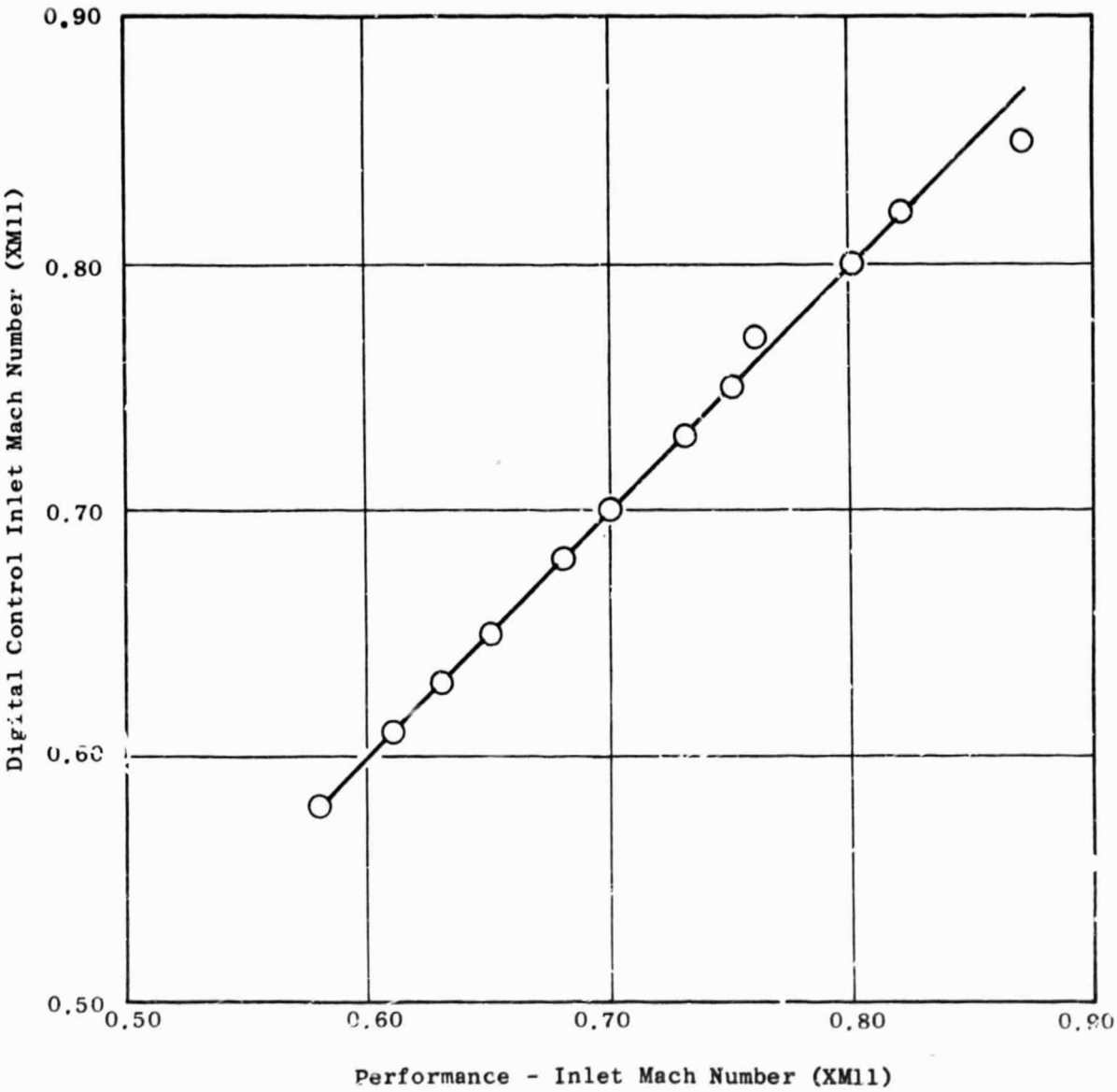

Figure 57. Inlet Mach Number Comparison.

In the automatic mode of operation the control system modulates fan exhaust nozzle area to hold a desired inlet Mach number. Operation in this mode of operation was not demonstrated during Build No. 1 of the engine; however, Figure 58 provides an insight to expected performance.

Figure 59 shows experimental engine data on fan nozzle actuator loads as a function of nozzle area with a constant fan speed and fan pitch angle. The data indicate that the zero-load point is in the 1.55-161 m^2 (2400-2500 $in.^2$) range. Further measurements are required to define fully the nozzle load effects with various fan speeds and fan pitch angles.

9.6.3 Fan Pitch Control System

Prior to the engine starting sequence, the fan pitch position command potentiometer was positioned to command a fan pitch angle of +5°. After reaching idle speed the fan pitch command potentiometer was varied to set various fan pitch angles as required by the basic engine test plan. Because of excessive fan-pitch hydraulic motor leakage there was a high deadband effect when a fan pitch change was requested from closed to open in the forward operating mode (against the load). To overcome this problem, an operating procedure was developed wherein the fan pitch was set from the open-to-closed position (i.e., load pulled fan pitch when no-back was unlocked by control action). After development of this procedure, the fan pitch could be set within 0.2° of the desired position. Throughout the operation, the fan pitch control was stable. During the engine test program, the control system positioned the fan pitch between ±10° in the forward mode of operation, automatically moved the fan pitch from the forward operating mode to the reverse mode on command, and positioned the pitch from -105° to -100° in the reverse operating mode. Figure 60 shows a typical fan pitch movement in the forward operating mode.

The absolute value of the fan pitch angle could not be measured during engine operation. To determine how accurately the fan pitch control was setting the fan pitch angle, the fan pitch was set from the open-to-closed direction with the engine at idle prior to shutdown. After engine and fan coast down, physical fan pitch measurements were made and compared with the operator panel fan pitch angle recorded at the idle power setting prior to shutdown. Table 8 shows the results of this experiment. From this evidence, it is concluded that the control system was accurately positioning the fan pitch angle.

During engine/fan pitch control operation, four problems associated with the fan pitch system occurred. The problems, analyses, and corrective actions are outlined in Table 9. The first three problems fall into the nuisance category, and successful corrective action was, or will be, developed. The fourth problem, fan pitch closure during engine operation, was of major significance because it could cause fan overspeed. A history of this fan pitch closure event, and the action to date, is outlined below.

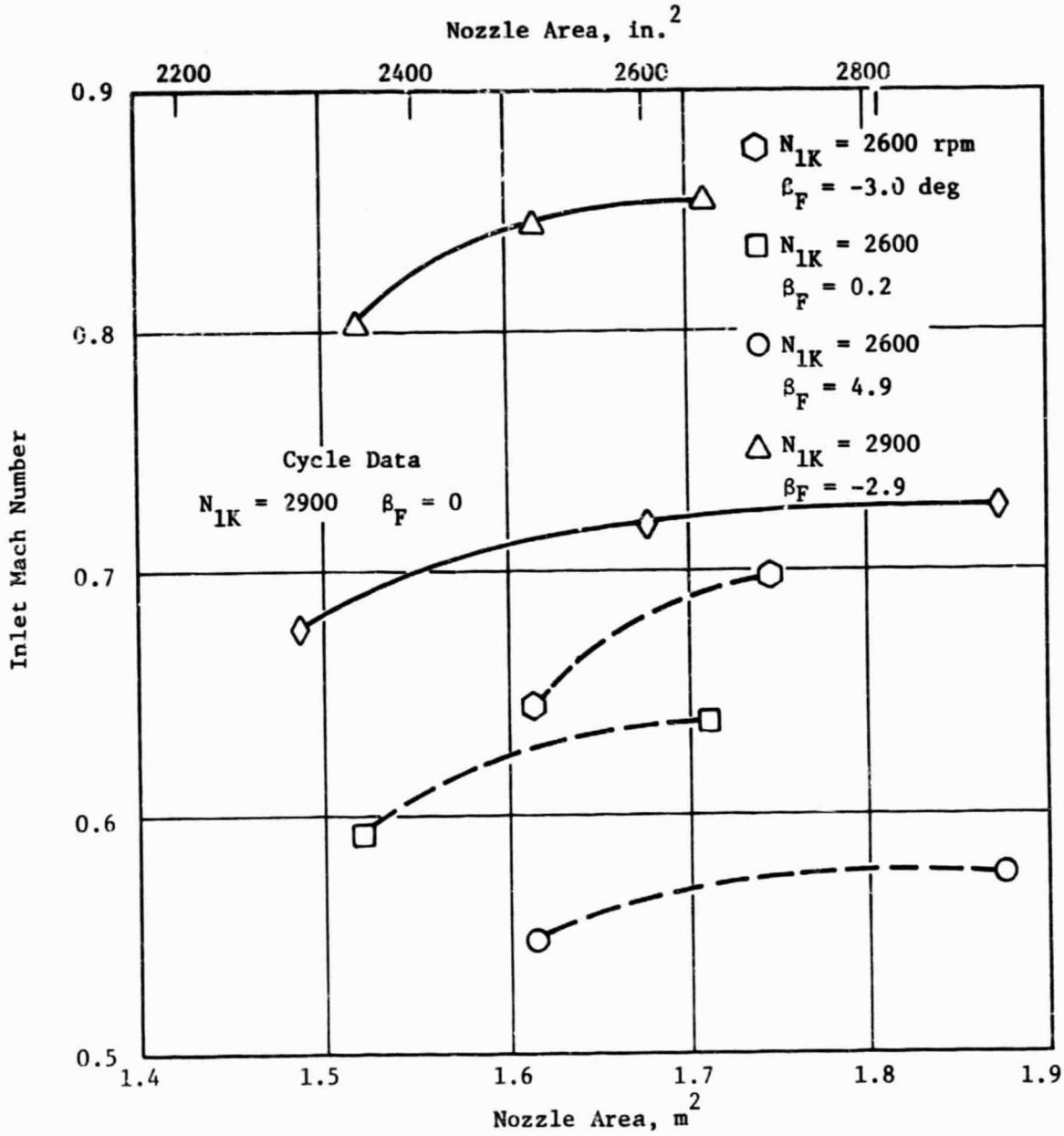

Figure 58. Inlet Mach Number Variations.

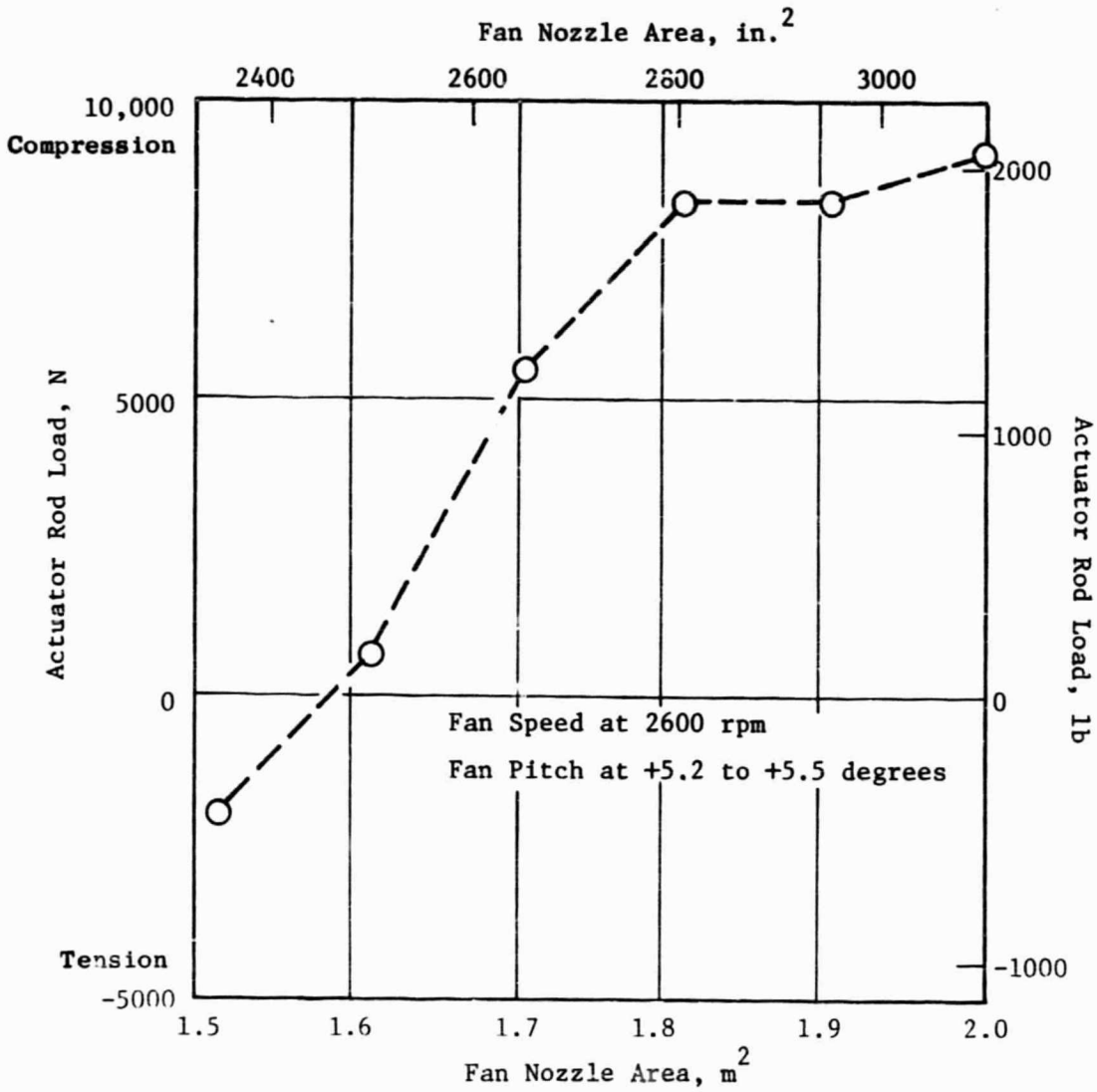

Figure 59. Fan Nozzle Load Data.

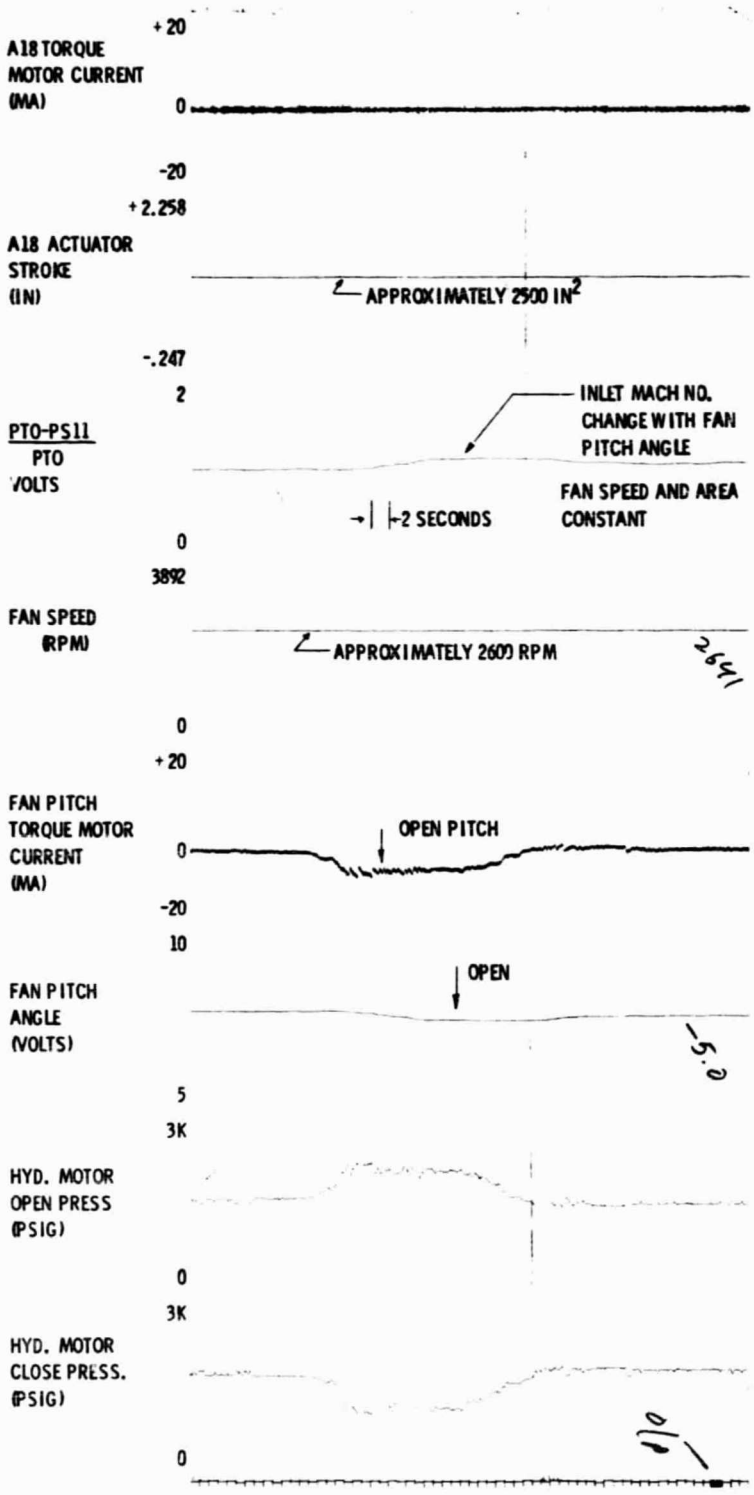

Figure 60. Fan Pitch Movement in Forward.

Table 8. Comparison of Set and Measured Fan Pitch Angles.

Date	Operator Panel Fan Pitch Angle	Measured Angle	Delta
10-77-6	+4.9	+4° 41'	+13'
9-17-76	+5.2	+4° 58'	+14'
10-19-76	-0.1	-23'	-17'

Table 9. Fan Pitch Control System Problems.

Problem No.	Engine Symptom	Problem Analysis	Corrective Action
1	Fan pitch moved in closed direction on coast down when core speed was less than 3200 rpm.	Hydraulic pressure ported to fan pitch closed motor port when digital control went out of regulation at core speed <3200 rpm.	Added slave control room switch to force a zero electrical null on fan pitch torque motor during coast down. Corrective action was effective.
2	Fan pitch moved in closed direction through fan pitch limit switches on start at core speeds of less then 3200 rpm.	A mechanical null shift in fan pitch servovalve at low pump pressures allowed pressure to be ported to close pitch port on fan pitch motor.	Added slave solenoid between open and closed port on fan pitch motor to produce zero delta pressure on motor during starting sequence. Corrective action was effective.
3	Hydraulic oil leaked at pump depressurizing solenoid.	The leak occurred between solenoid body and bulkhead fitting into solenoid. Improper seal compression or shifting of seal allowed hydraulic leak.	Tightened fitting or replaced seal as required; added backup seal. Action not totally effective. Will replace bulkhead fitting with standard MS- and B-nut arrangement on Build 2.
4	Experienced intermittent fan pitch closure from -3° to 0° and from +7° to +14° on several occasions while operating at high fan speed.	Analysis to date indicates that fan pitch feedback No. 2 was sensitive to voltage level. Problem suspected in analog-digital-multiplexer.	Module containing fan pitch feedback demodulator replaced - action not effective. Continue test and analysis to isolate cause so corrective action can be implemented before engine Build 2.

While operating at high fan speed, the fan pitch twice closed from -3° to 0°. On both occasions, the fan pitch was reset and the test continued. On subsequent engine test within a period of 55 minutes, the fan pitch made two unscheduled blade closures from +7° through the limit switch to 14.7°. Data from Sanborn traces at slow speeds were inconclusive. The digital control was removed from the engine and returned to the laboratory for investigation. Testing indicated possible noise problems and the fan pitch LVDT demodulator module (A6) was replaced.

The digital control was returned to engine test, this time was pertinent parameters being recorded on magnetic tape. After less than one and one-half hours of running, the fan pitch again went from +7° to +14.7°. Time traces from the tape, Figure 61, showed the closed-transient to be initiated by a step change in the averaged βF feedback signal that persisted for one iteration period, 0.0075 sec. The initial current response can be seen to be in the open blade direction but not to produce sufficient motor pressure drop to move the pitch against the load. Upon removal of the step input, the torque motor current went far in the closed direction, subsequently unlocking the no-back and starting the blades in the closed direction. As seen by the open and closed pressure traces, the load became overhauling and drove the hydraulic motor. Analysis of the lag-rate-feedback program in the digital control showed that, for a pulse input that exceeded the normal rate limits, the response would be just as observed on the time trace; i.e., upon removal of the step-input, the current could reverse in sign, then latch onto the lag circuit and decay to zero current as determined by the lag time constant. Had the magnitude of the pulse been within the normal rate limits, the current would have barely overshot zero upon removal of the step input and would have returned to zero current in a short period of time. The fan pitch position would have twitched, then returned to +7°.

As seen on the trace in Figure 61, the one-iteration pulse was in the βF average calculations. βF 1, which was instrumented, showed no movement. Since βF 1 showed no movement but the βF average went high, it was apparent that the problem was in the βF 2 channel in the form of noise. This was subsequently verified when another fan pitch failure from +7° to +14.7° occurred, this time with βF 2 instrumented on tape instead of βF 1. As seen in Figure 62, both βF 2 and βF average show the one-iteration pulse.

Further engine testing was accomplished with βF 2 disconnected. When Build No. 1 testing was terminated, due to the loss of the A18 exhaust panel, no fan pitch failure to the closed position had occurred. The noise spike problem is still unexplained, but a malfunction in the analog-to-digital converter is suspected. A modification to the lagged-rate-feedback network which will prevent the large sign reversal has been implemented in the QCSEE QTW and will be implemented on UTW Build No. 2.

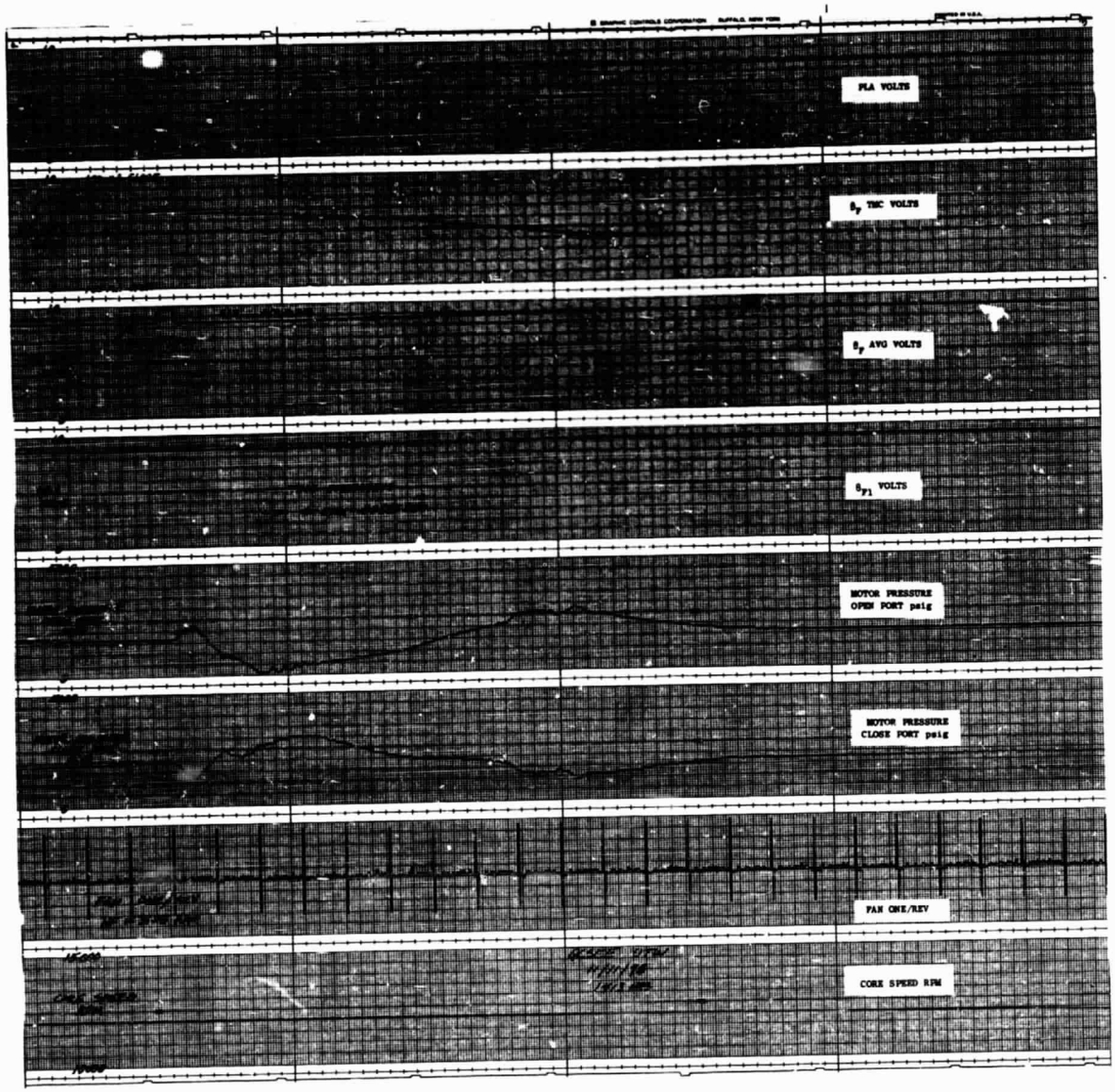

Figure 61. Fan Pitch Closure.

ORIGINAL PAGE IS
OF POOR QUALITY

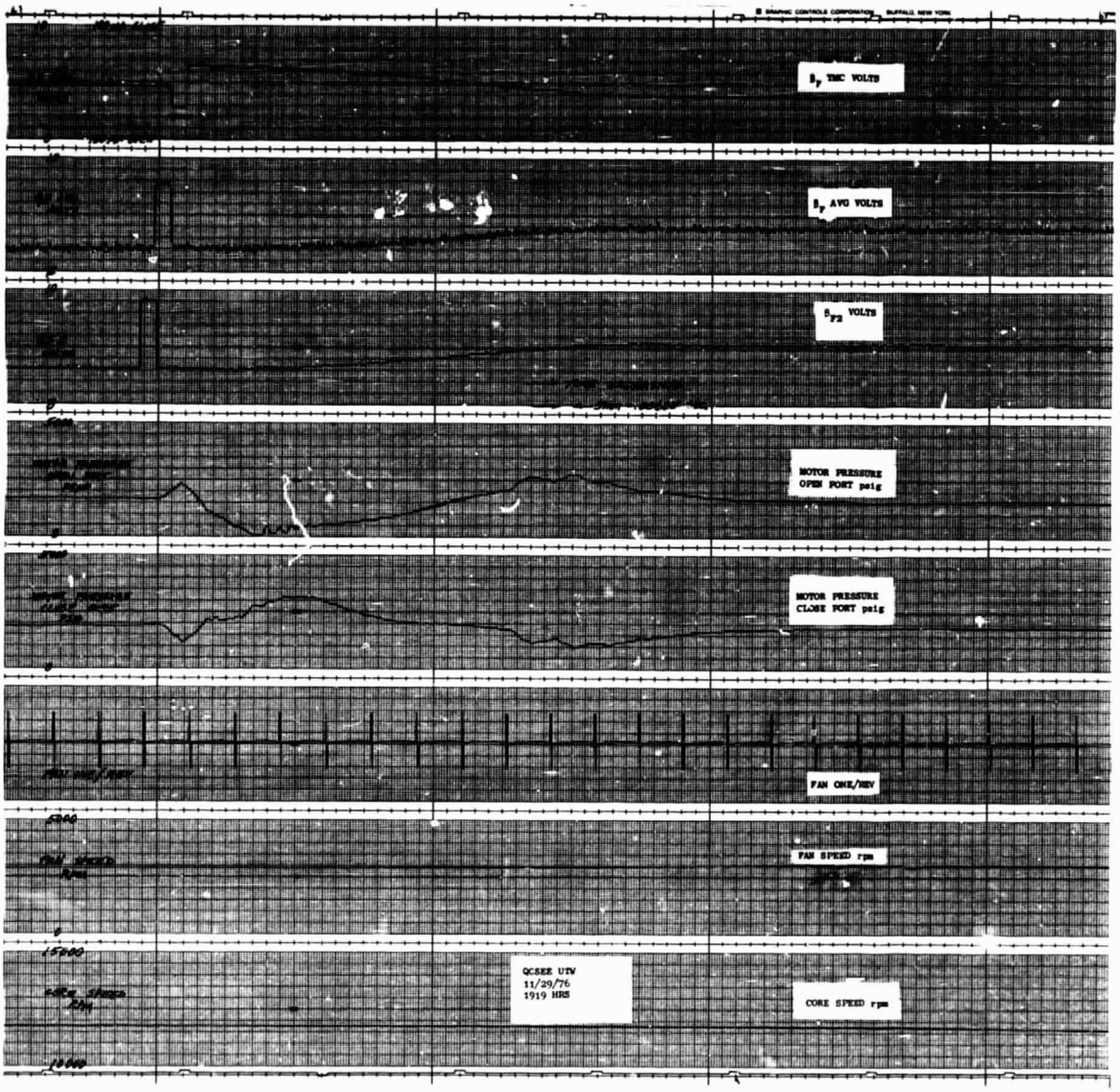

Figure 62. Fan Pitch Closure.

ORIGINAL PAGE IS
OF POOR QUALITY

10.0 VARIABLE-PITCH ACTUATION SYSTEM

All UTW Build No. 1 engine testing used the Hamilton Standard variable-pitch mechanism. The cam/harmonic drive system, illustrated in Figure 63, was developed by the Hamilton Standard Division of United Technologies Corporation under subcontract to the General Electric Company. (See Reference 3.)

The Beta Regulator module, consisting of two hydraulic gear motors, a speed increaser, and two linear-variable differential transformers, mounted in the core cowl area provided rotary mechanical input to the differential gear train through a flexible cable. The rotary motion then was transmitted through a no-back, harmonic drive, rotating spherical cam, and cam follower arms to the blade trunnion. The overall gear ratio from the blades to the flexible shaft varied from 725 to 1050 as a function of blade position due to the spherical cam ratio variations as shown in Figure 64. Most of the gear ratio (201/1) was provided by the harmonic drive. The planetary differential gear train provided a 5/1 ratio, and the speed increaser gear ratio was 1/1.2. A bidirectional, spring-type no-back locked the fan blades in position in the absence of a pitch change command. The two LVDT's, driven by the hydraulic motor output, provided a blade angle feedback signal to the engine digital control system for closed-loop operation.

All testing on the UTW engine was in the manual mode of control described in Section 9 and shown in block-diagram form in Figure 41. Whenever the digital control detected an error between the demanded and actual position of the blades, it sent an electrical signal to a hydraulic servovalve which in turn ported hydraulic fluid to the hydraulic motors to correct the pitch angle.

10.1 ENGINE TEST RESULTS

Figure 65 shows representative breakaway pressure differentials across the hydraulic motor which were required to move the fan pitch mechanism more open from initial steady-state positions shown. Exhaust nozzle and fan speed conditions were as indicated. As noted on Figure 65, with fan speed at 2654 rpm, A18 at 1.871 m^2 (2900 $in.^2$), and βF at +9.2°, the pitch could not be moved in the open direction.

Sanborn traces from which motor pressure drops were obtained also showed a six-milliamp deadband in the pitch mechanism system. The six-milliamp deadband (the servovalve current change required to change the direction of the pitch) was six times the design intent as seen in Figure 66.

10.2 DISCUSSION OF TEST RESULTS

An analysis was made of engine test data taken at a representative condition: NF = 2642 rpm, A8 = 1.613 m^2 (2500 $in.^2$), βF = 0°. The analysis

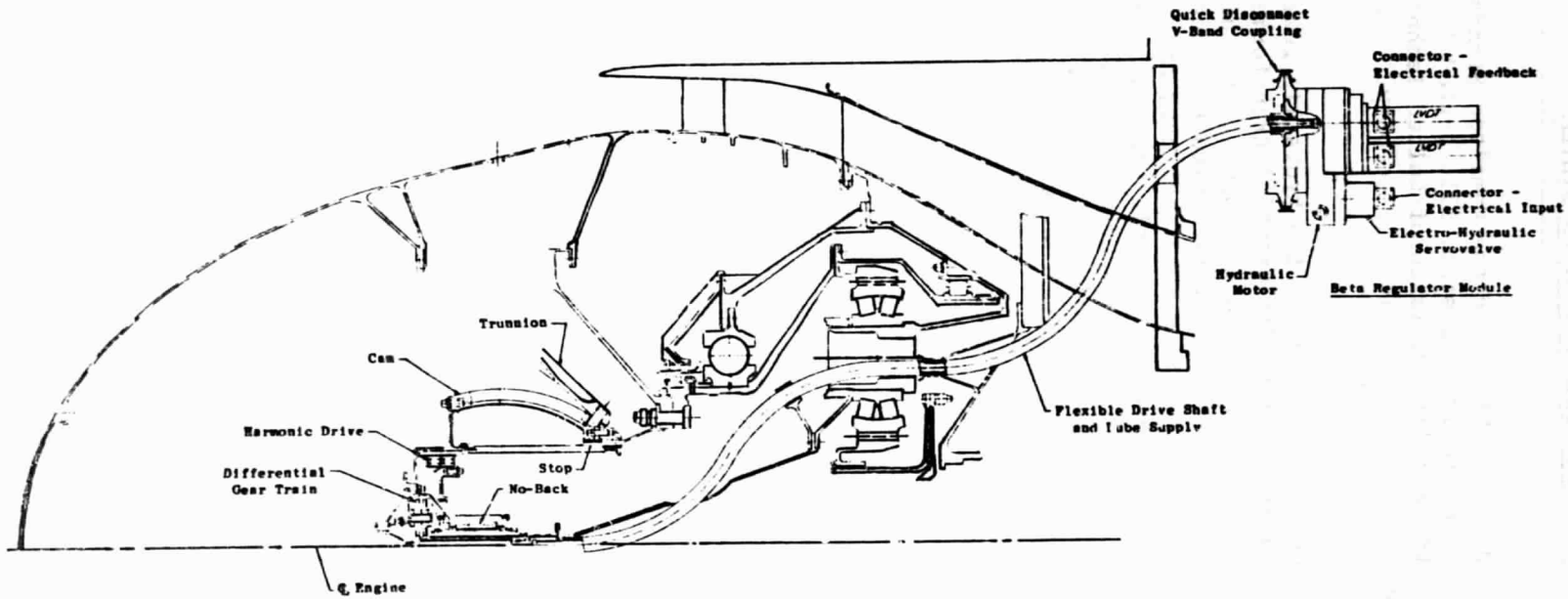

Figure 63. QCSEE UTW Build 1 Variable-Pitch Actuation System.

ORIGINAL PAGE IS
OF POOR QUALITY

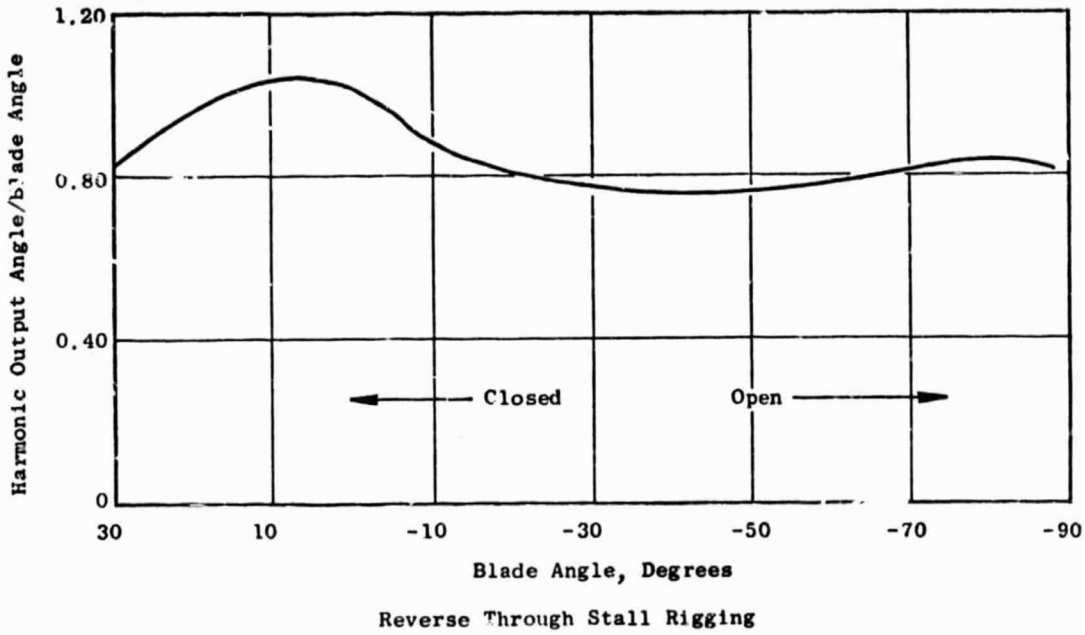

Figure 64. Spherical Cam Gear Ratio Effect.

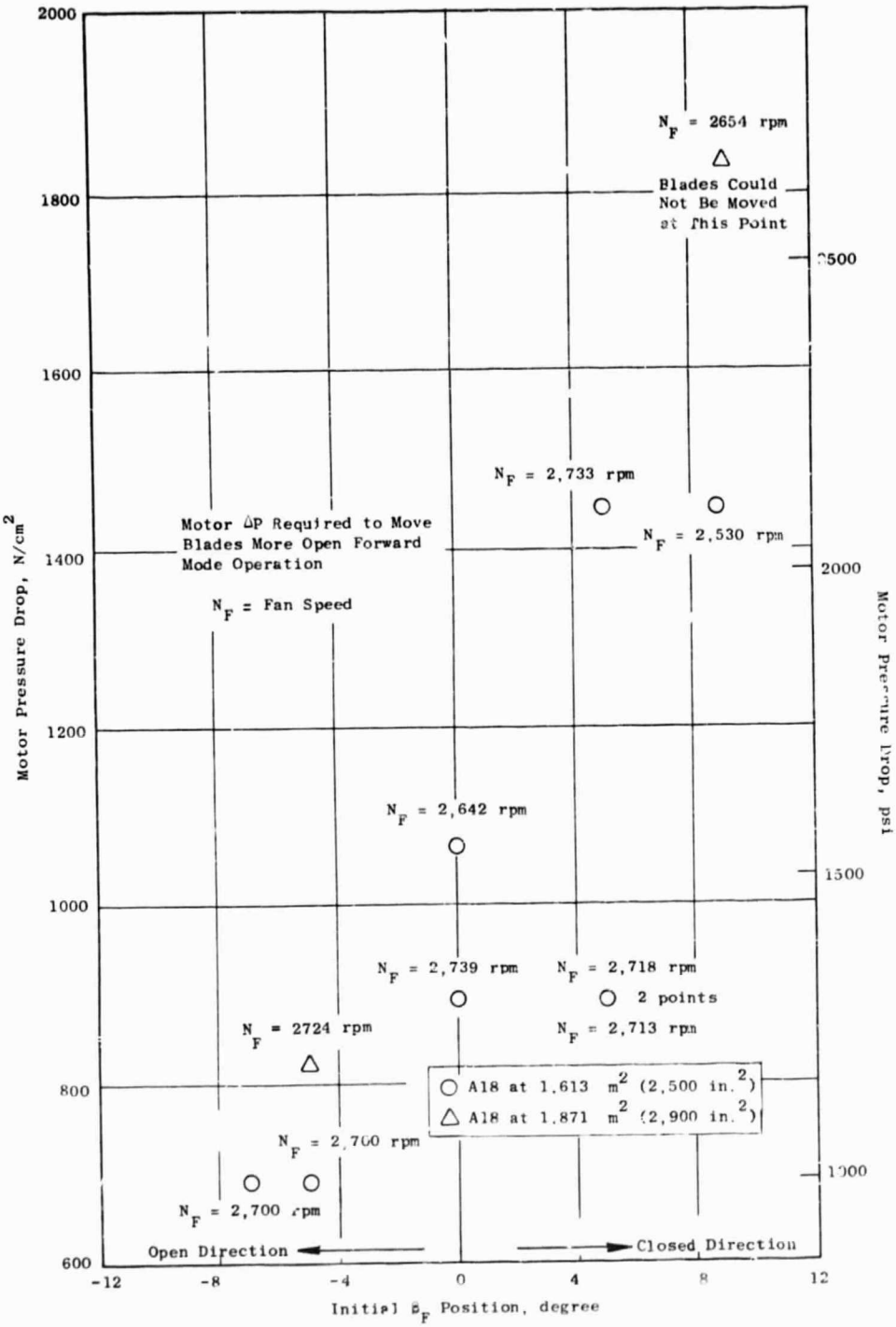

Figure 65. Breakaway Motor Pressure Drops.

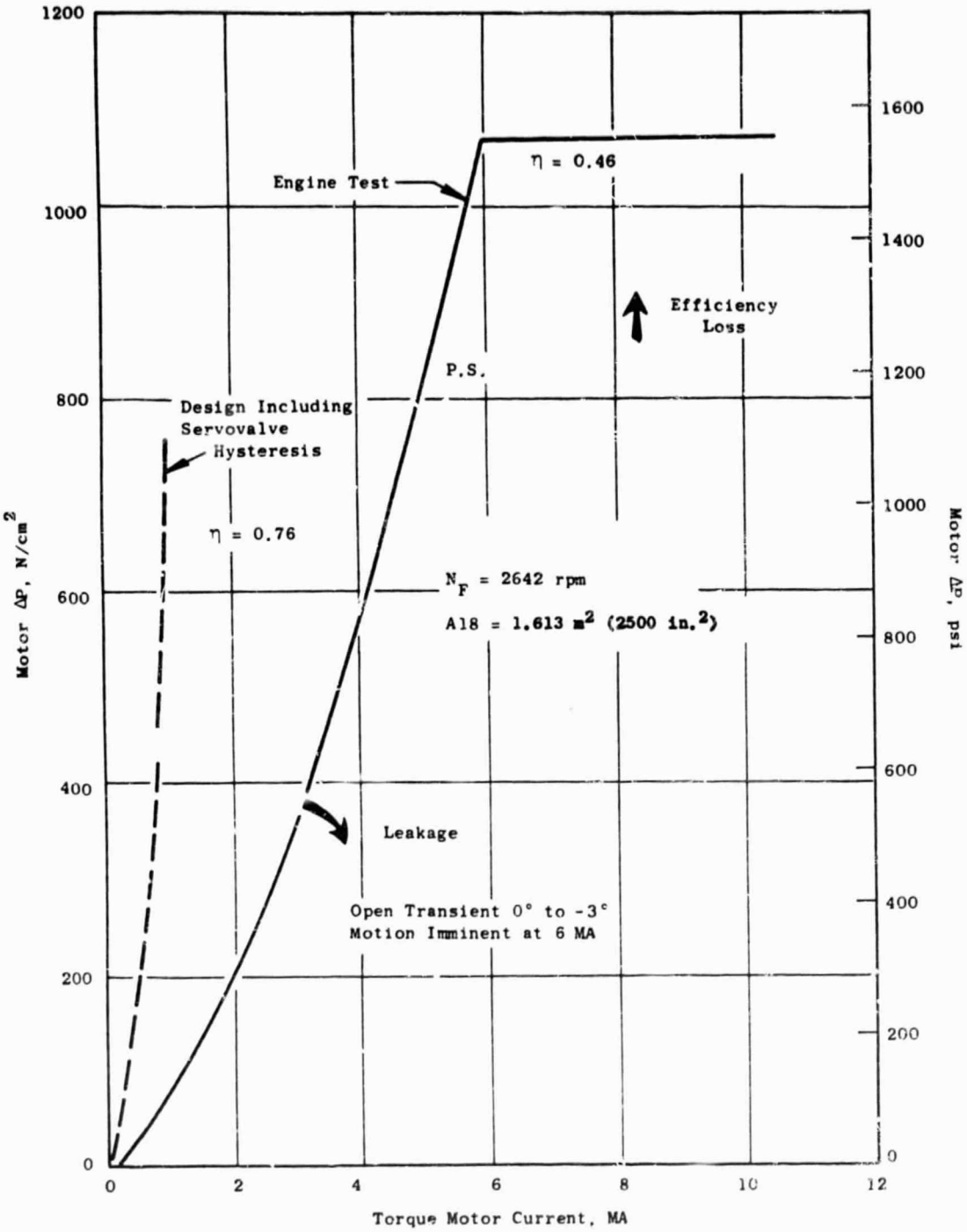

Figure 66. Hydraulic Motor Pressure Drop Versus Torque Motor Current.

ORIGINAL PAGE IS
OF POOR QUALITY

was based upon the system description shown in Figure 67. It accounted for servovalve characteristics, motor leakage, known and assumed motor and flexible cable losses, and published blade loads defined in Figure 68. The results indicate:

1. The servovalve hysteresis accounts for 1.0 milliamp of the total deadband.

2. High motor leakage of 2.52 cm^3/sec (4 gpm) at 1379 N/cm^2 (2000 psi) pressure accounts for 3.5 milliamps of the total deadband.

3. The remaining 1.5 milliamps can be attributed to loads being higher than predicted, or pitch mechanism efficiencies being lower than predicted, or some combination of higher loads and lower efficiencies.

Although the blades could not be moved at high rotor speeds in the engine, the system had operated satisfactorily at full speed in whirl-rig tests (see Reference 4). Static torque wrench measurements agreed with the whirl tests; no evidence from inspection showed why more pressure should be required to move blades in the engine.

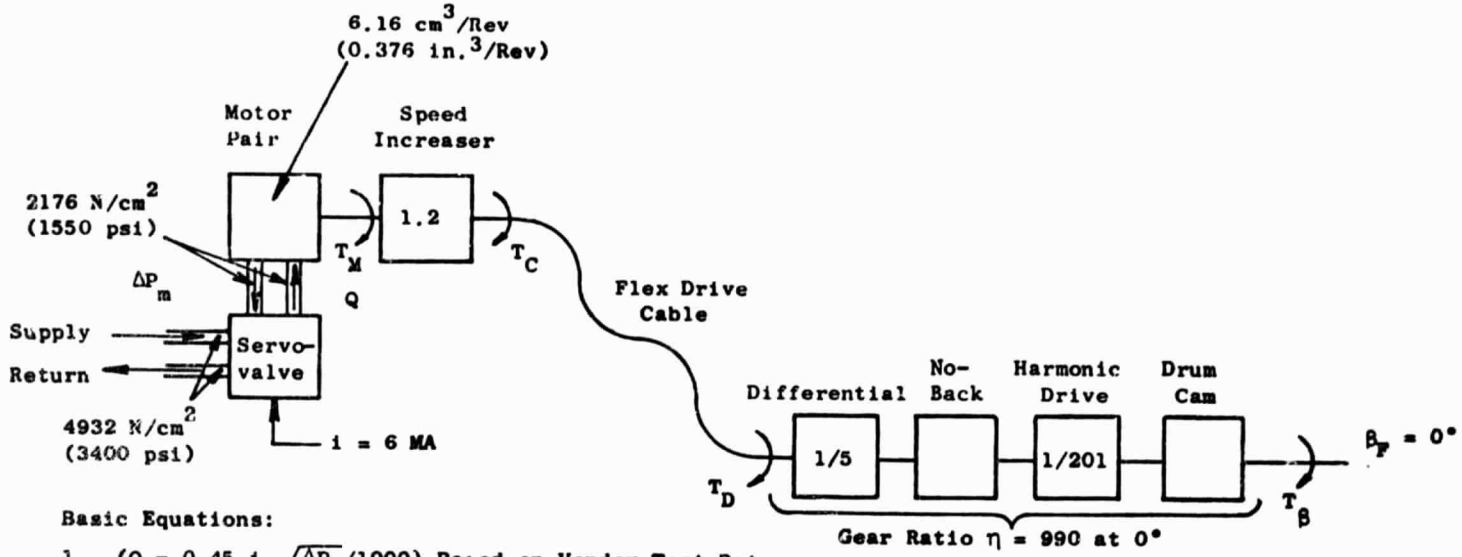

Basic Equations:

1. $(Q = 0.45\ i\ \sqrt{\Delta P_v}/1000)$ Based on Vendor Test Data

2. $(\Delta P_m = 3400 - \Delta P_v)$

3. $(Q = Q_o \sqrt{\Delta P_m}/2000)$

   Q_o = Motor Leakage at 1379 N/cm² (2000 psi) Pressure Drop from Test

4. $\left[T_M = (0.159)\ (0.376)\ \Delta P_m - 3.7 \times 10^{-6}\ \Delta P_m^{\ 2}\right]$ Loss Based on H/S Stalled Torque Data

5. $\left[T_C = T_M\ (0.99)/1.2\right]$ Assumes η of Speed Increaser $\approx$ 0.99

6. $(T_D = 0.889\ T_C - 6.44)$ Based on H/S Cable Test Data Plus No-Back Release Torque of 113 cm-N (10 in.-lb)

7. $(T_\beta = 990\ \eta\ T_D)$

Figure 67. Description of V-P Mechanism Used in Analysis.

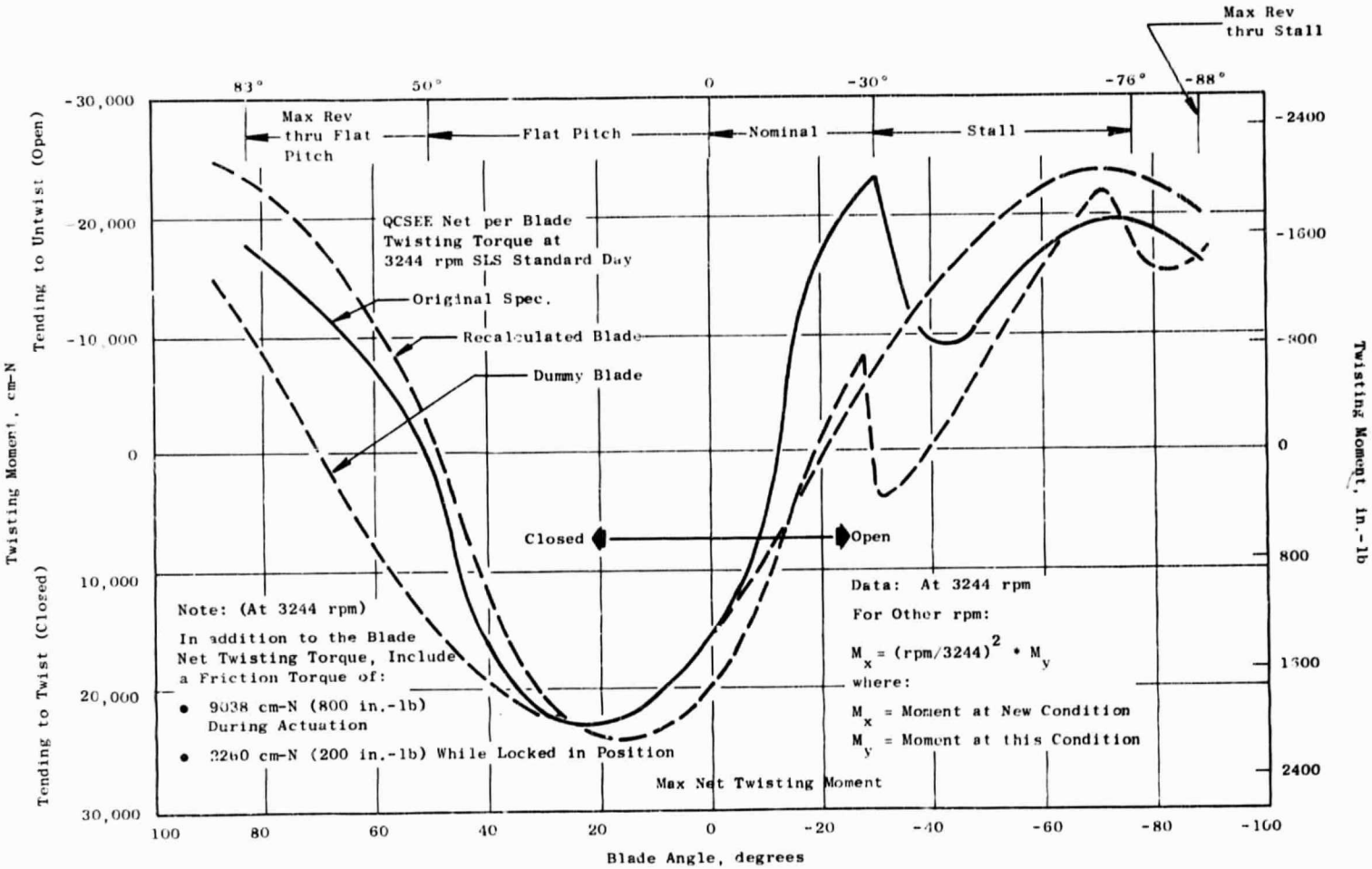

Figure 68. Predicted UTW Blade Loads.

ORIGINAL PAGE IS OF POOR QUALITY

11.0 REFERENCES

1. The General Electric Company; "QCSEE UTW Engine Composite Fan Blade Design," NASA CR-134840, May 1975.

2. The General Electric Company; "QCSEE UTW Engine Composite Fan Blade Final Design Test Report," NASA CR-135046, February 1977.

3. Hamilton Standard Division of United Technologies Corp.; "QCSEE Hamilton Standard Cam/Harmonic Drive Variable-Pitch Fan Actuation System Detail Design Report," NASA CR-134852, October 25, 1977.

4. Hamilton Standard Division of United Technologies Corp.; "QCSEE Hamilton Standard Cam/Harmonic Drive Variable-Pitch Fan Actuation System Whirl-Rig Test Report," NASA CR-135140, to be Published.